Assessment of Capacitor Voltage Transformer Affect On Distance Relay

A dissertation submitted to

THE UNIVERSITY OF MANCHESTER
INSTITUTE OF SCIENCE AND TECHNOLOGY

For the degree of

MSc

By

Nursyarizal MOHD NOR

September 2001

CONTENTS

DEDICATION.

I dedicated this dissertation to my parents and family for the everlasting loves and concerns.

ACKNOWLEDGEMENTS.

First and foremost I would like to thank my supervisors, Dr. Peter Crossley and Dr. H. Li, for the supported and guided in bringing this dissertation to completion.

In this opportunity, I also wish special thanks to my friends either Ph. D. students or MSc students for the invaluable contribution are given in knowledge and materials.

Finally, I gratefully acknowledge to University of Technology Petronas (UTP), Malaysia for the financial support.

LIST OF TABLES.

LIST OF FIGURES.

ABSTRACT

A capacitor voltage transformer (CVT) comprises a capacitor voltage divider connected to an iron-core voltage transformer. The capacitor voltage transformer is used in the transmission and distribution circuit for stepping down voltages for metering or protection.

The performance of the capacitor voltage transformer described in this dissertation is assessed by computer simulation. The simulation tools MATLAB and PSCAD/EMTDC were used. Various types of fault have been made to investigate the transient response of the CVT. It can be seen that as the location of the fault becomes more remote the period of oscillation becomes longer. The results obtained indicate that the CVT transient behaviour is controlled by the sum of the stack capacitances, the shape and parameters of the ferroresonance suppression circuits and the point on wave at which the fault occurs.

Experiment results are presented in this dissertation. The objective of the experiment is to investigate the effect on the performance of a distance relay of the CVT transient response. From the results obtained we can see that the CVT transient will slow down the relay for in zone faults. The type of fault applied in this experiment is single phase to ground.

CHAPTER 1
BACKGROUND OF CAPACITOR VOLTAGE TRANSFORMER.

1.0 INTRODUCTION

In power systems the primary voltage and current signals are transformed to voltages of current for metering and protection purposes. These signals are required at adequately low level in order to suit the operation of instruments and relays. In order to obtain a low voltage level from high voltage source, a wound voltage transformer is normally used to step down the primary voltage. However, as the system voltage increases, the insulation cost makes this type of transformer inappropriate and other type of voltage sensing units are needed. The most commonly used voltage sensing unit is the capacitor voltage transformer (CVT). CVT is commonly used in electricity distribution and transmission systems at high and extra high voltages.

1.1 LITERATURE REVIEWS

Theoretical study and tests carried out with CVT model and system protective relays show that it is possible to study the performance of protective relays fed by capacitor voltage transformers systematically [1]. This will enable the limits of the load for this particular type of CVT to be fixed before feeding the relays. Some examples are given in [1].

The results described in [1] show that a load represented by the parallel connection of a resistance and an inductance has a very harmful effect on the

transient voltages of CVT. The amplitudes of the transient voltages are not sufficient to characterise the risk of disturbance in the performance of the relay.

It is not possible to find the values for transient voltages, which are identical and valid for all system protective relays fed by capacitor voltage transformer. Whereby it can be achieved by determine the characteristics of the permissible transient voltage, i.e. frequency and amplitude from a given time subsequent to the appearance of the fault, for each of the relay [1]. It is because these values rely upon the rapidity of operation as well as the type of relay and the sensitivity of its measurement.

Protective relays fed by CVT do not operate correctly if the secondary side voltage is not a direct replica of the primary side voltage [2]. In order to ensure correct operation of the relay, it is necessary for the secondary side voltage to be operated as accurately as possible to the primary voltage when the latter falls rapidly. The other conditions that the CVT must fulfil have been given in [2].

1.2 CAPACITOR VOLTAGE TRANSORMER

Capacitive Voltage Transformers (CVTs) are predominantly used tool to measure the voltage signals on a transmission network. This is particularly important for distance relays in high voltage (HV) and extra high voltage (EHV) systems. Thus it is not appropriates to connect the voltage coils of protective devices direct to the system. We need to step down the voltage to a manageable value and to insulate the protective device from the power system. Therefore a suitable device should be designed to serve these purposes. Currently, there are voltage-transforming devices to serve these purposes in the power system.

Capacitance divider with a suitable matching or isolating potential transformer tuned for resonance condition, known as CVT, is often used in power systems for voltage measurements. CVTs provide a mean of deriving safe source of voltages from

a high voltage system. Under line fault conditions, when the voltage drops and there is no threat of exceeding the knee-point of the magnetizing characteristic of the step-down transformer, a CVT can be represented by the equivalent linear circuit as shown in Figure 1.1. It consists of a capacitive voltage divider, i.e. stack capacitor (Cs) and base capacitor (Cb), and a wound transformer. Tuning inductance, La, is usually connected in series with the transformer primary. Depending on the design and type of equipment, various impedances may be added to complete the circuit. Figure 1.2 shows the simplified circuit diagram of the CVT that provides more accurate information on the CVT characteristics. The capacitor, C in Figure 1.2 is the sum of Cs and Cb in Figure 1.1. The inductance, L, comprises the leakage inductance of the transformer together with the tuning inductance, La, in Figure 1.1. Resistance, R, in Figure 1.2 represents the sum of the equivalent core resistance (Rc), winding resistance (Rw), primary and secondary resistance (Rp and R2) and magnetising resistance in the transformer (R_m), refer to Figure 1.1. Load, Z, represents the total load of CVT that is including the impedance of the burden in Figure 1.1, referred to the primary of the transformer, together with the iron losses and magnetisation impedance of this transformer.

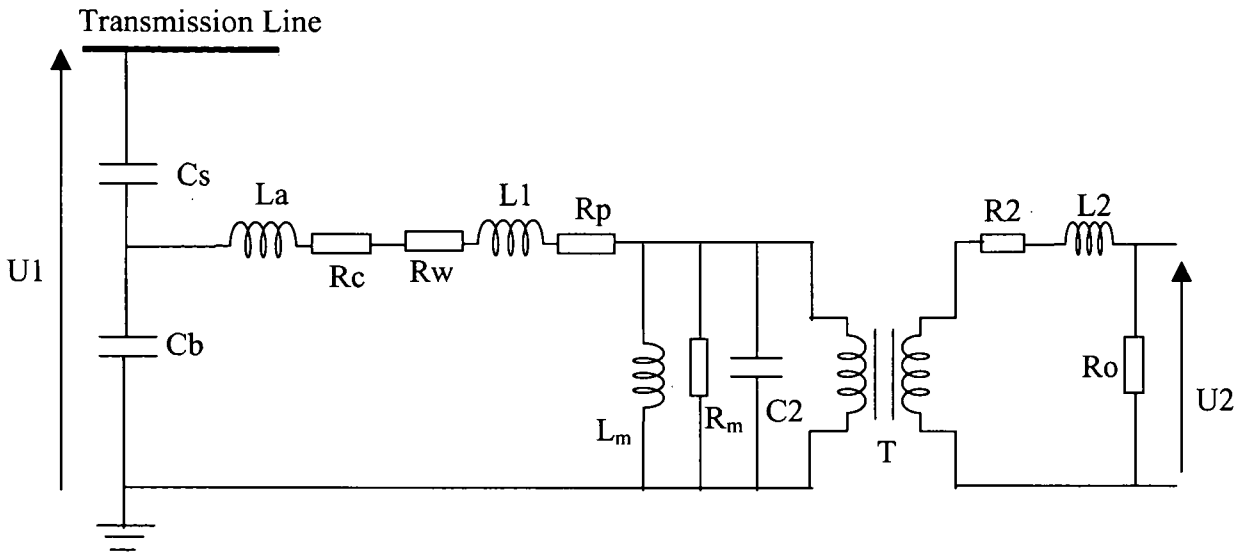

Figure 1.1: Outline diagram of a capacitor voltage transformer the burden being represented by connecting three circuits in parallel.

Descriptions:

Cs : *Stack capacitance*
Cb : *Base capacitance*
La : *Tuning inductance*
L1 : *Primary Leakage inductance*
Rc : *Equivalent Core resistance*
Rw : *Winding resistance*
Rp : *Primary resistance*
R2 : *Secondary resistance*
L2 : *Secondary inductance*
Ro : *Burden resistance*
L_m : *V.T. Magnetising inductance*
R_m : *V.T. Magnetising resistance*
C2 : *Lumped Stray capacitance*
U1 : *Primary voltage*
U2 : *Secondary voltage*
T : *Transformer*

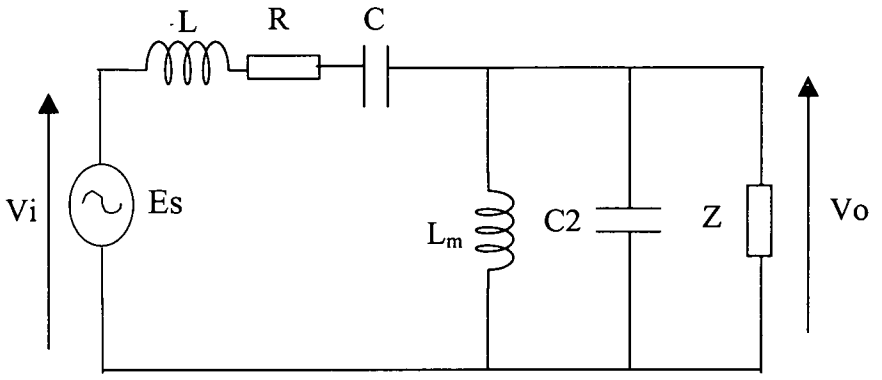

Figure 1.2: Simplified model of a CVT from Figure 1.1.

Descriptions:

C : *Sum of the capacitive voltage divider*
L : *Equivalent inductance*
R : *Equivalent resistance*
Z : *Load*

CVTs provide a cost-efficient way of obtaining secondary voltages for EHV systems. They create however, certain problems for distance relays. During line faults, when the primary voltage collapses and the energy stored in the stack capacitors and the tuning reactor of a CVT needs to be dissipated, the CVT generates severe transients that affect the performance of protective relays.

A capacitor voltage transformer must necessarily give rise to transient phenomena during a short-circuit, and these make it necessary to take certain precautions when using the transformer with relays. Several precautionary methods have been described in [2].

The transient caused by the CVT are of significant magnitude and relatively long duration. This becomes particularly important for large Source Impedance Ratios (SIR - the ratio of the system equivalent impedance and the relay reach impedance)

when the fault loop voltage can be as low as a few percent of the nominal voltage for faults at the relay reach point. Such a small signal is buried beneath the CVT transient making it extremely difficult to distinguish quickly between faults at the reach point and faults within the protection zone.

Currently, the transient performance of CVTs is not covered by any standard. In addition to that, transient behaviour of CVTs is relevant for the application in protection relaying and an analysis of their transient response is needed. The purpose of this project therefore, is to investigate the transient responses of CVTs and the affect of CVTs to the distance relay performance.

In order to investigate the performance of the CVT, MATLAB was used. It is also possible to investigate by experiment. Apart from the economical point of view, computer simulation technique also enables us to study the performance of the device and the relays connected to it under a number of fault conditions in a very short time.

Figure 1.3 shows the simplified circuit diagram for this project. Once the MATLAB program is completed, the program has to be downloaded into a model of distance relay, OMICRON, to investigate the performance of distance relay while using CVT.

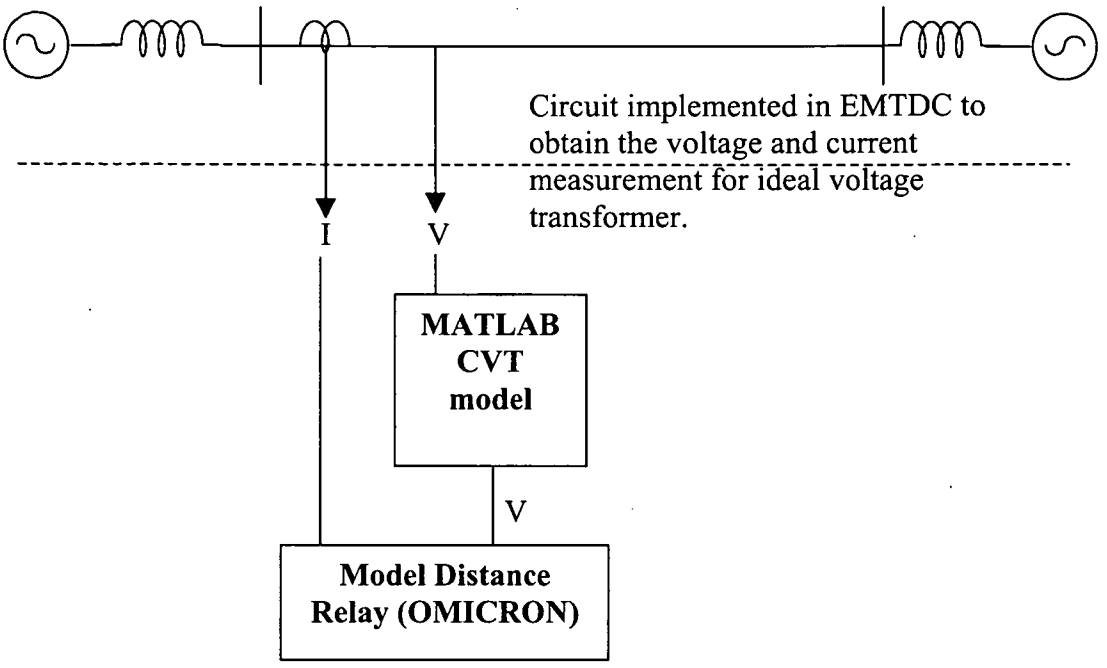

Figure 1.3: Simplified circuit diagram.

A summary of the contents of the various chapters and appendices in this dissertation are:-

- Chapter 2 describes the mathematical method used to calculate the output to input voltage ratio, H(ω), of the CVT circuit.
- Chapter 3 describes the voltage response of the CVT when various faults were applied to the system. Two circuits can be used to represent the CVT. These circuits will be used to analyse the type of CVT transient. The circuits represent the transformer with a suppressing circuit connected and one circuit disconnected.
- Chapter 4 describes how the performance of distance relay varies while using the model of the CVT described in Chapter 3. In this chapter the experiment will be established to observe the performance of distance relay. The single phase to ground fault is applied in this experiment.
- Chapter 5 describes the conclusions and discussions.

- Appendix A provides a programme listing for the Capacitor Voltage Transformer written in MATLAB format.
- Appendix B provides a programming listing for the Capacitor Voltage Transformer while various faults were applied to the system written in MATLAB format.
- Appendix C provides Technical Data of OMICRON CMC 56 Test Set.
- Appendix D describes the calculations of positive and zero sequence impedance for the transmission line used in this dissertation.
- Appendix E provides Technical Data of OPTIMHO LFZP 111.
- Appendix F provides the report of all results obtained in Chapter 4.

CHAPTER 2

MATHEMATICAL ANALYSIS.

2.0 MATHEMATICAL ANALYSIS

Several methods can be used to solve the electric circuit, shown in Figure 1.2. In this thesis, the inverse method is used. Table 1 shows the parameters of the CVT circuit, shown in Figure 1.1.

Table 1: Circuit parameters of CVT shown in Figure 1.1.

SYMBOL	NAME OF COMPONENT	VALUES
Cs	*Stack capacitance*	2000 pf
Cb	*Base capacitance*	0.084 μf
La	*Tuning inductance*	1.056 H
L1	*Primary Leakage inductance*	79.832 mH
Rc	*Equivalent Core resistance*	2000 Ω
Rw	*Winding resistance*	239 Ω
Rp	*Primary resistance*	1050 Ω
R2	*Secondary resistance*	0.162 Ω
L2	*Secondary inductance*	0.168 mH
L_m	*V.T. Magnetising inductance*	27050 H
R_m	*V.T. Magnetising resistance*	5.8 M Ω
C2	*Lumped Stray capacitance*	1060 pf
Ro	*Burden resistance*	103997 Ω

2.1 STEADY STATE ANALYSIS

As shown in Chapter 1, the linear circuit in Figure 1.1 can be further simplified as shown in Figure 1.2. All the components are referred to the intermediate voltage level and capacitors Cs and Cb are group together to form a Thevenin equivalent voltage source. Refer to Figure 1.2,

- The resistor R is the total resistance of the primary, core and winding resistance.
  R = Rp + Rc + Rw = 1050 + 2000 + 239 = ***3289 ohms.***
- The capacitor C is the total capacitance of the base and stack.
  C = Cb + Cs = 0.084e-06 + 2000e-12 = ***86 nF.***
- The inductor L is the total inductance of primary leakage inductance, tuning inductance and secondary inductance.
  L = L1 + La + L2 = 79.832e-03 + 1.056 + 0.168e-03 = ***1.136 H.***

Using Figure 2.1, the output and input voltage ratio can be calculated. The impedance Z1, Z2 or Z3 represents the combination of resistance, capacitance and inductance in series or in parallel, where,

$$\mathbf{Z1 = (1/j\omega C) + j\omega L + R} \quad \mathbf{.....(2.1)}$$

$$\mathbf{Z2 = (j\omega L_m) \,//\, (1/j\omega C2)} \quad \mathbf{.....(2.2)}$$

$$\mathbf{Z3 = Ro} \quad \mathbf{.....(2.3)}$$

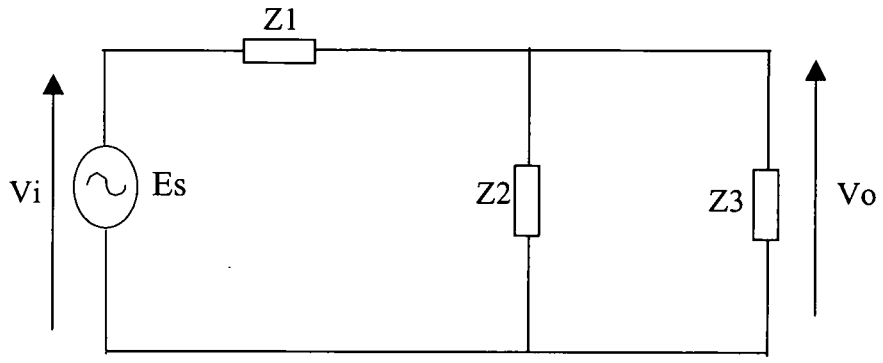

Figure 2.1: Simplified equivalent circuit.

Figure 2.1 can be further simplified as shown in Figure 2.2. The impedance Z4 represents the combination of Z2 and Z3 in parallel. The output voltage Vo therefore can be written as:

$$\mathbf{Vo = i_T Z4 \ldots\ldots\ldots\ldots\ldots (2.4)}$$

According to Ohm's Law, the total current i_T can be written as:

$$\mathbf{i_T = Vi/(Z1+Z4) \ldots\ldots\ldots (2.5)}$$

By substituting Equation 2.4 into Equation 2.5, the output to input voltage ratio, referred to as H(ω) can be found:

$$\mathbf{H(\omega)} = \frac{Vo}{Vi} = \frac{Z4}{Z1+Z4} \ldots\ldots (2.6)$$

where,

$Z1 = (1/j\omega C) + j\omega L + R$

$Z4 = Z2 \,//\, Z3 = (j\omega L_m) \,//\, (1/j\omega C2) \,//\, Ro$

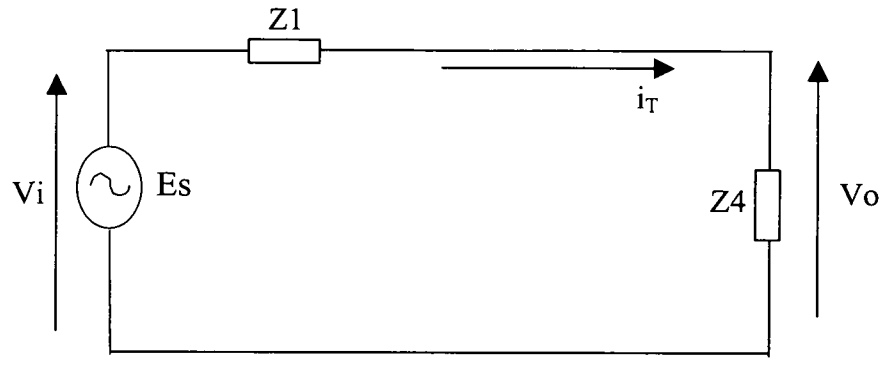

Figure 2.2: Further simplified circuit

MATLAB program was used to calculate H(ω) in frequency domain. The codes written in MATLAB are attached in Appendix A. By using the circuit parameters in Table 1, the bode diagram for H(ω) is created, shown in Figure 2.3. From Figure 2.3, the gain at 50 Hz is equal to 0 dB. Which is H(ω) at 50 Hz is equal to 1. Figure 2.4 shows the phase shift of H(ω). At 50 Hz, the phase shift is equal to 10 degree. Hence, using Equation 2.6, the output secondary voltage under steady state condition therefore is given by:

$$\mathbf{Vo = H(\omega) \times Es \sin(\omega t - \theta)} \quad \text{.....(2.7)}$$

At f=50 Hz, Vo is equal to Es sin $(\omega t - 10^0)$.

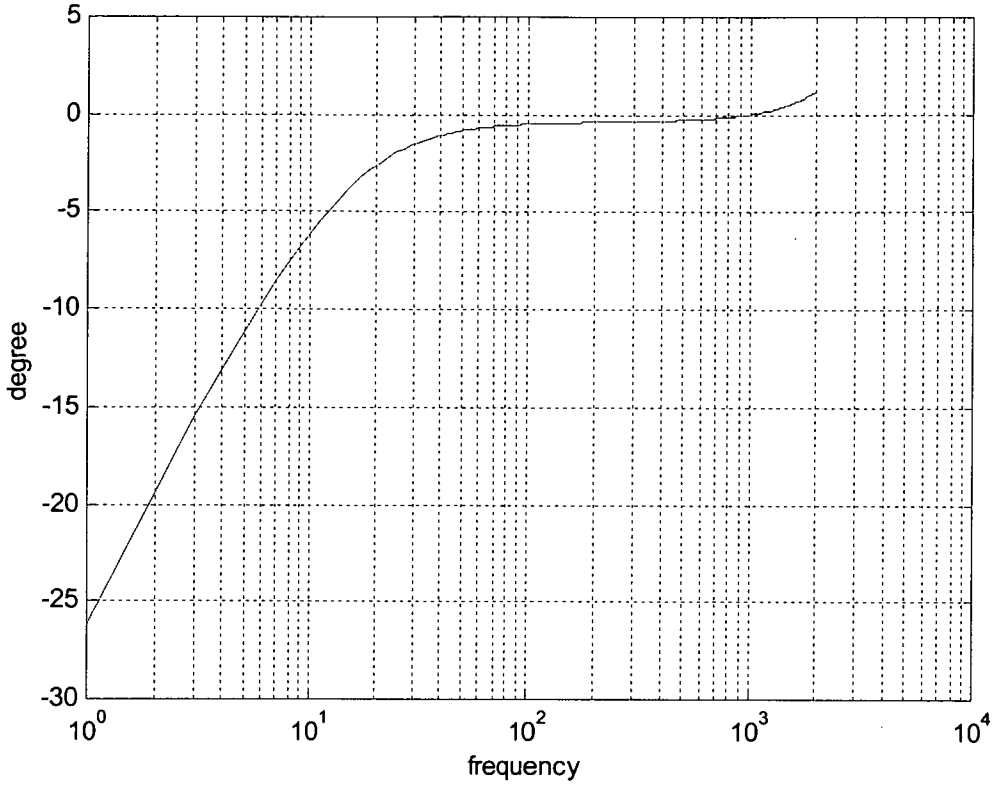

Figure 2.3: H(ω) Bode diagram (Amplitude in dB)

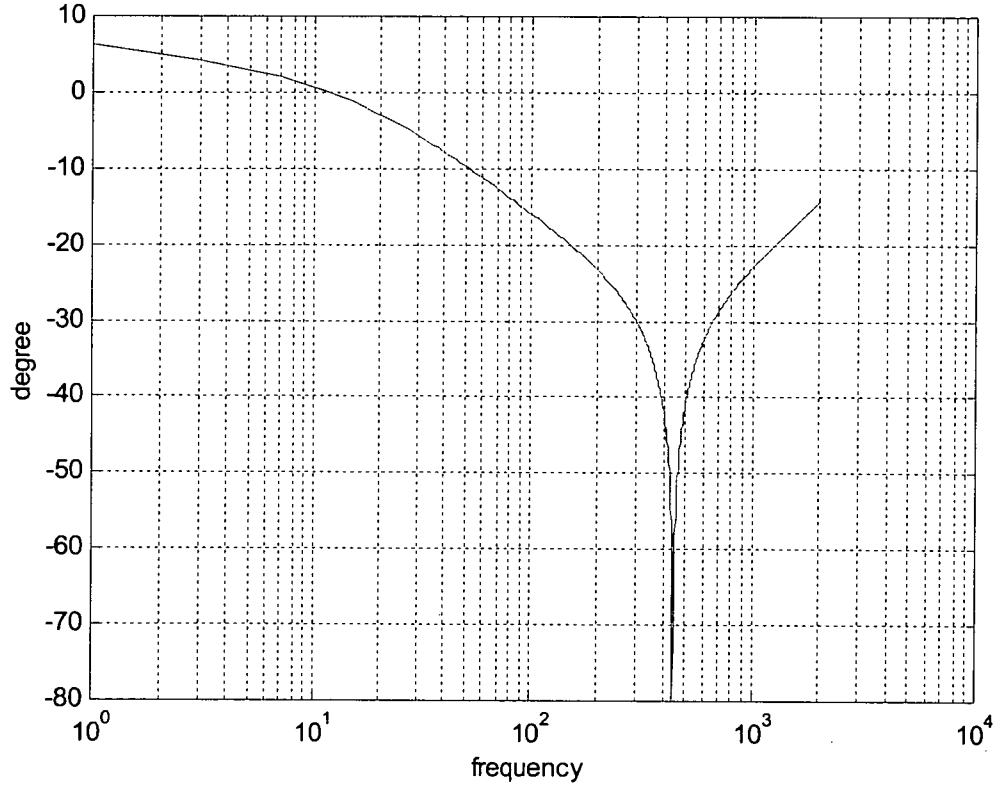

Figure 2.4: H(ω) Bode diagram (Phase shift)

H(ω) is a continuous complex frequency function and therefore can be written as real and imaginary parts of the frequency function. Figure 2.5 (a) illustrates the real part of the complex frequency. Figure 2.5 (b) shows remaining samples of frequency function. The gain at 50 Hz is approximately 0.9, based on Figure 2.5 (a).

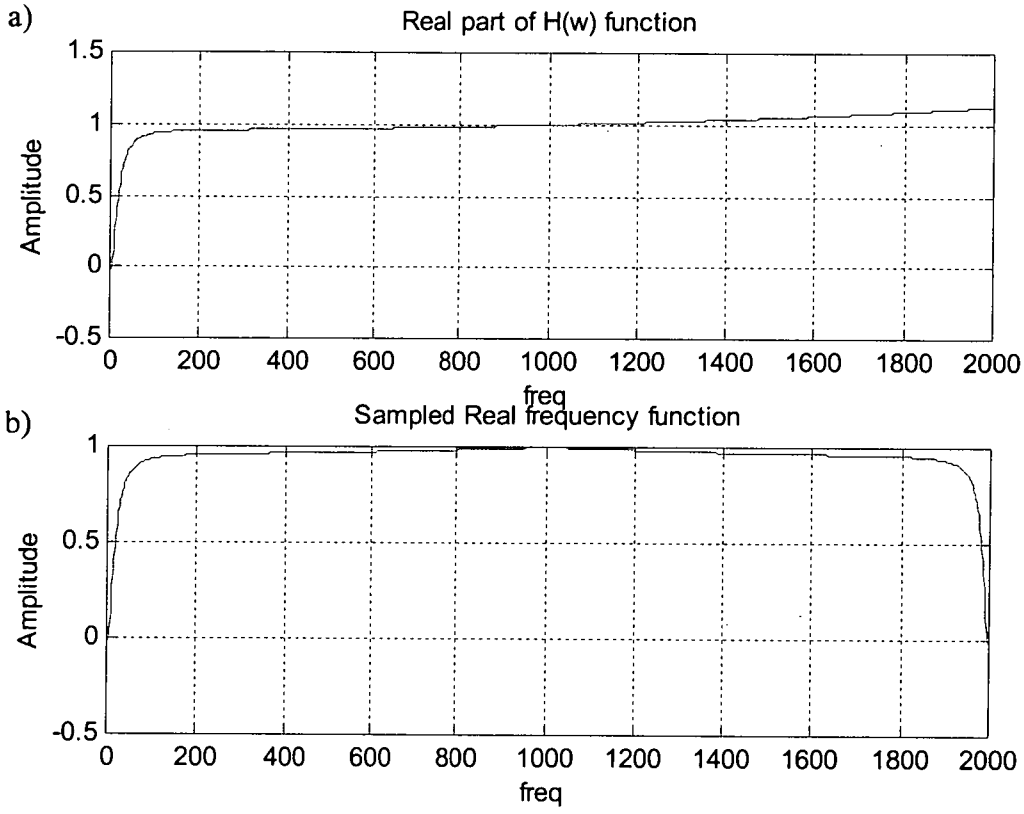

Figure 2.5: Real part of the H(ω)

The imaginary part of the complex frequency is illustrated in Figure 2.6. The imaginary part of the frequency at 50 Hz is approximately 0.2.

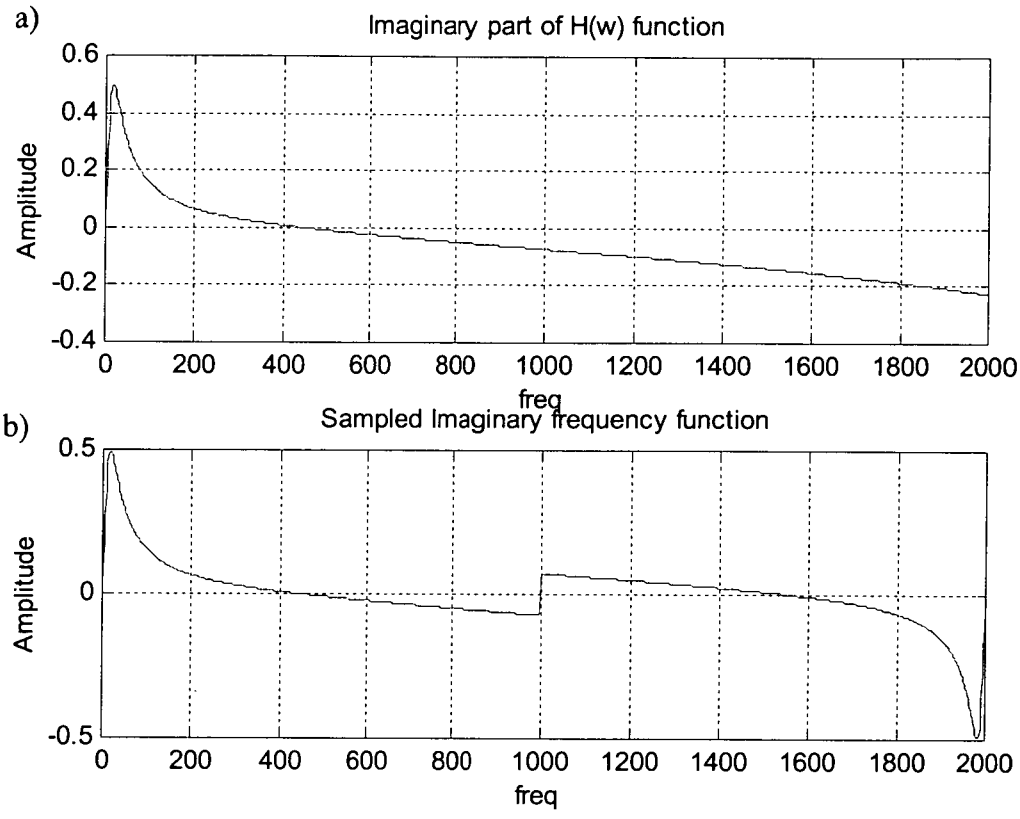

Figure 2.6: Imaginary part of H(ω)

To examine the transient CVT under various conditions, the ratio of the output and input voltage in discrete time domain is required. This is achieved by using inverse Fourier transforms method. Figure 2.7 shown the results of steady state analysis in discrete time domain (see Appendix A for MATLAB programming).

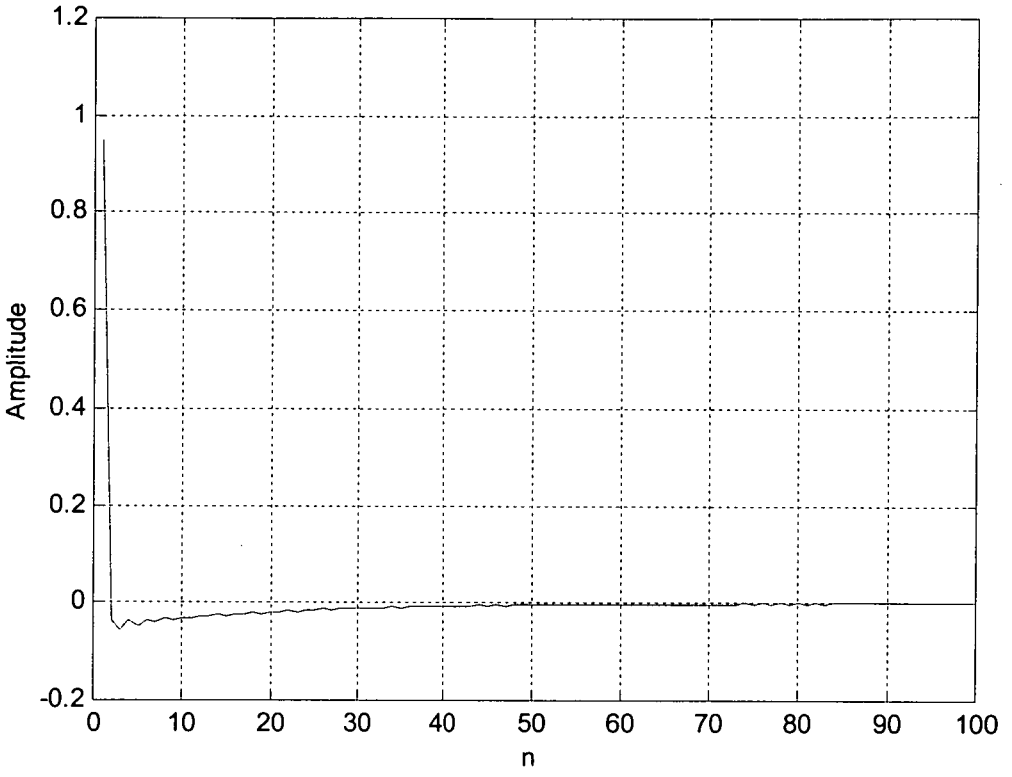

Figure 2.7: Time function graph

2.2 FERRORESONANCE SUPPRESION CIRCUIT

Sometime phenomena known as ferroresonance can be occurred in the CVT. Ferroresonance is a complicated non-linear electrical phenomenon, which can lead to transformer voltages being several times higher than the normal ratings. Ferroresonance, which causes overcurrent or overvoltage, occurs due to the change of operating point in the circuit, which composes of ac voltage source, capacitor and a saturable inductor. The change of operating point can occur due to the variation of the capacitance, the supply voltage and the operating frequency. In practice, the short-circuit on the secondary side of the transformer and the open circuiting of the fuse can cause ferroresonance in the capacitor voltage transformer, which results in the damage of the equipment.

A ferroresonance suppression circuit is designed to prevent sub-synchronous oscillations due to saturation of the core of a step-down transformer during overvoltage conditions. Generally, the ferroresonance circuit loads a CVT and creates an extra path (apart from the burden) for dissipating energy. Therefore, the damping circuit has significant impact of the characteristic of the CVT transients. Figure 2.8 shows the basic circuit of the CVT with ferroresonance circuit. Figure 2.9 shows the simplified circuit for the equivalent circuit illustrated in Figure 2.8.

As the circuit has a non-linear transient characteristic, three methods of damping are introduced to stabilise the ferroresonance phenomena. They are:

- Permanently connected resistive burden.
- Permanently connected tuned circuits.
- Switched damping circuits.

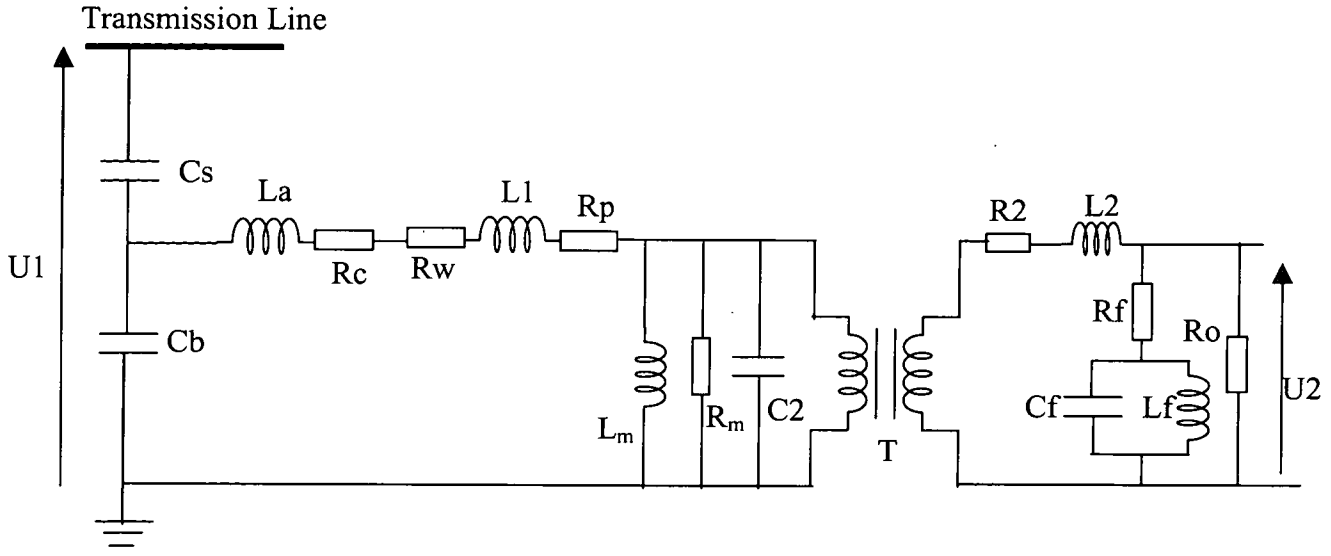

Figure 2.8: Outline diagram of a capacitor voltage transformer with Ferroresonance suppression circuit.

Descriptions:

Cs : *Stack capacitance*
Cb : *Base capacitance*
La : *Tuning inductance*
L1 : *Primary Leakage inductance*
Rc : *Equivalent Core resistance*
Rw : *Winding resistance*
Rp : *Primary resistance*
R2 : *Secondary resistance*
L2 : *Secondary inductance*
Ro : *Burden resistance*
L_m : *V.T. Magnetising inductance*
R_m : *V.T. Magnetising resistance*
C2 : *Lumped Stray capacitance*
Rf : *Suppression resistance*
Lf : *Suppression inductance*
Cf : *Suppression capacitance*
U1 : *Primary voltage*
U2 : *Secondary voltage*
T : *Transformer*

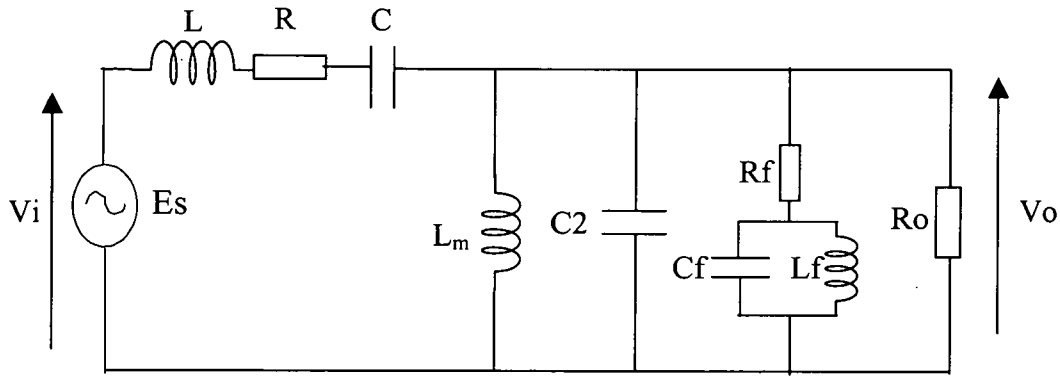

Figure 2.9: Simplified model of a CVT from Figure 2.8.

Descriptions:

C : *Sum of the stack capacitances*
L : *Equivalent inductance*
R : *Equivalent resistance*
Z : *Load*
f : *Subscript for parameters of the ferroresonance circuit*

2.2.1 Mathematical analysis.

Table 2 shows parameters of the active ferroresonance components in the CVT circuit diagram shown in Figure 2.9.

Table 2: Component values of ferroresonance circuit.

COMPONENT	VALUE
Suppression Capacitance, Cf	0.285 nF
Suppression Inductance, Lf	315.3 H
Suppression Resistance, Rf	77379 Ω

Using Figure 2.10, the output and input voltage ratio can be calculated. Equation 2.1 and 2.2 were used to calculate Z1 and Z2. Whereas Equation 2.8 and 2.9 were used for the calculation of Z3 and Z4.

$$\mathbf{Z3 = Rf + [(j\omega Lf)//(1/j\omega Cf)]} \quad \mathbf{.....(2.8)}$$

$$\mathbf{Z4 = Ro} \quad \mathbf{.....(2.9)}$$

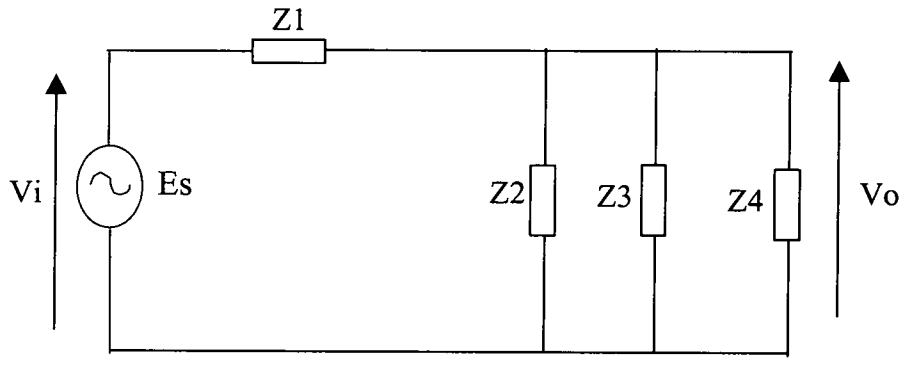

Figure 2.10: Equivalent circuit impedance representation

Figure 2.10 can be further simplified as shown in Figure 2.11. The impedance Z5 represents the combination of Z2 Z3 and Z4 in parallel. The output voltage Vo therefore can be written as:

$$\mathbf{Vo = i_T Z5} \quad \mathbf{.....(2.10)}$$

Using Ohm's Law, the total current i_T can be written as:

$$\mathbf{i_T = Vi/(Z1+Z5)} \quad \mathbf{.....(2.11)}$$

The output and input voltage ratio, H(ω), can be written as:

$$\mathbf{H(\omega) = \frac{Vo}{Vi} = \frac{Z5}{Z1 + Z5}} \quad \mathbf{....(2.12)}$$

where,

Z1(represent the primary impedance) = $(1/j\omega C) + j\omega L + R$

$Z5 = Z2 // Z3 // Z4$

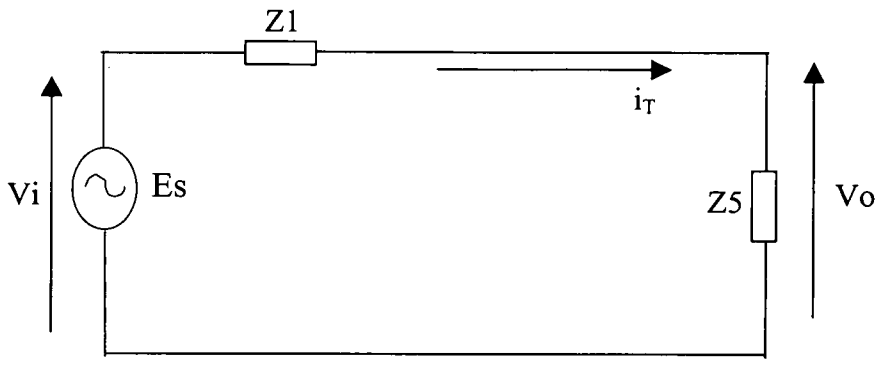

Figure 2.11: Further simplified circuit

Considering all above equations and using MATLAB programming (attached in Appendix A), the Bode diagram for this model of CVT is shown in Figure 2.12.

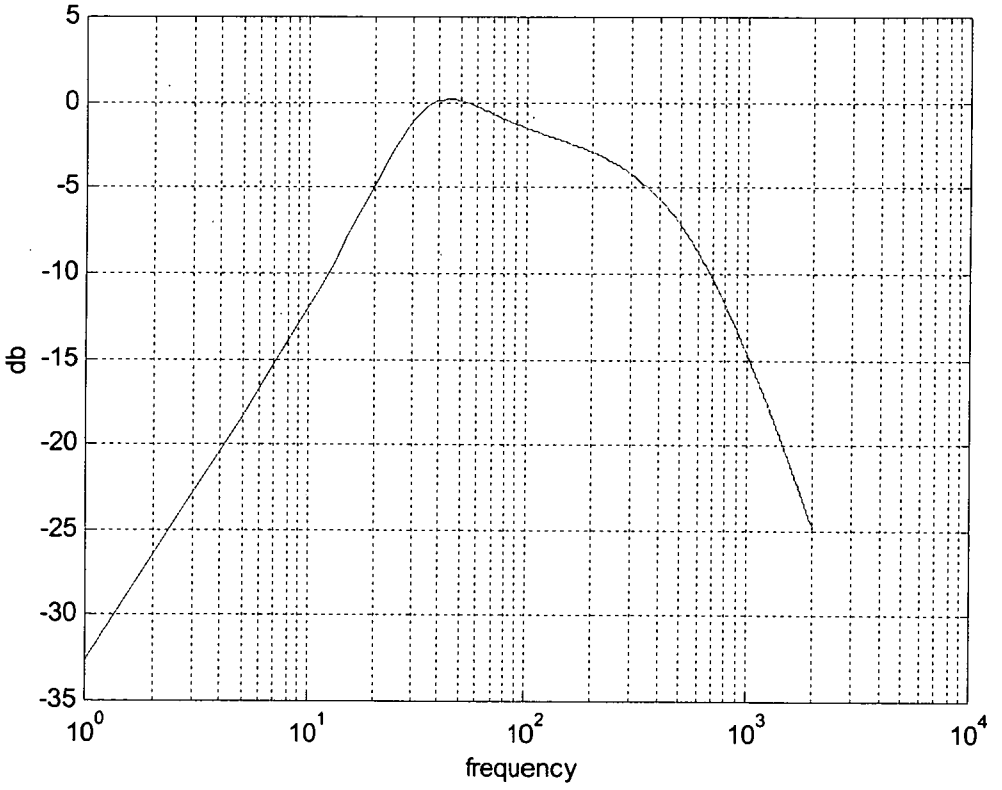

Figure 2.12: H(ω) Bode diagram (Amplitude in dB)

Figure 2.13 shows the phase shift of H(ω). At 50 Hz, the phase shift is equal to 42 degree. Hence, using Equation 2.7, the voltage output with ferroresonance circuit at 50 Hz is equal to

$$Es \sin (\omega t - 42^0)$$

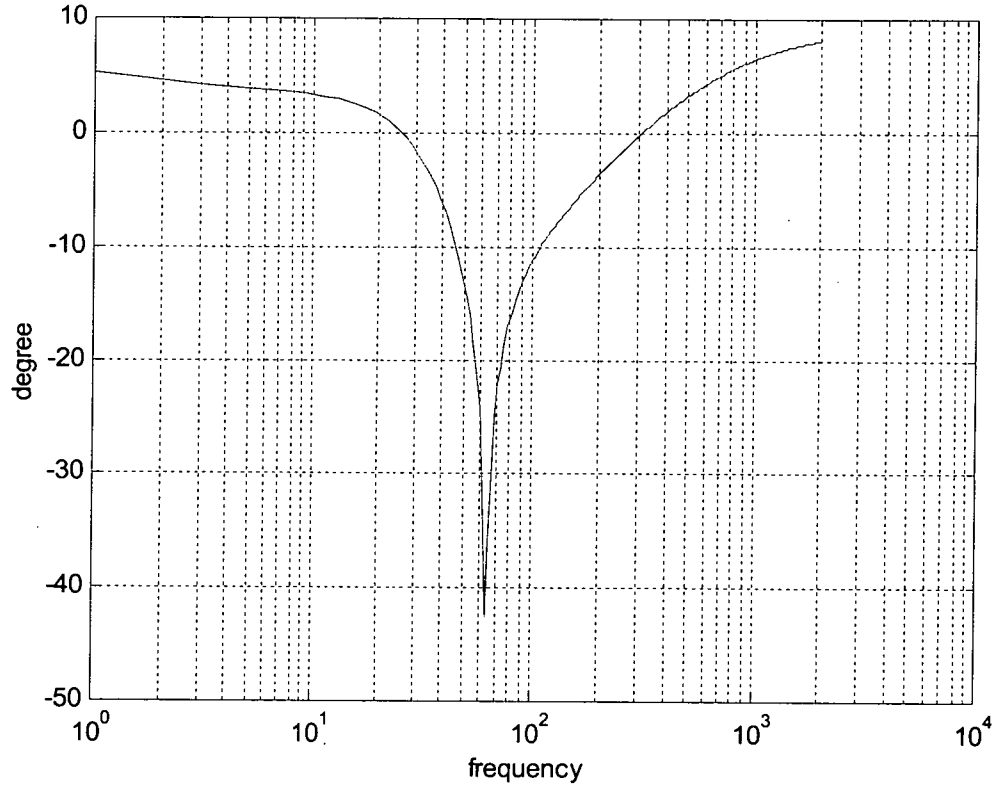

Figure 2.13: H(ω) Bode diagram (Phase shift)

Similar principle and explanation as in section 2.1, H(ω) is a continuous complex frequency function and therefore can be written as real and imaginary parts of the frequency function. Figure 2.14 (a) illustrates the real part of the complex frequency. Figure 2.14 (b) shows remaining samples of frequency function. The gain at 50 Hz is approximately 1, based on Figure 2.14 (a).

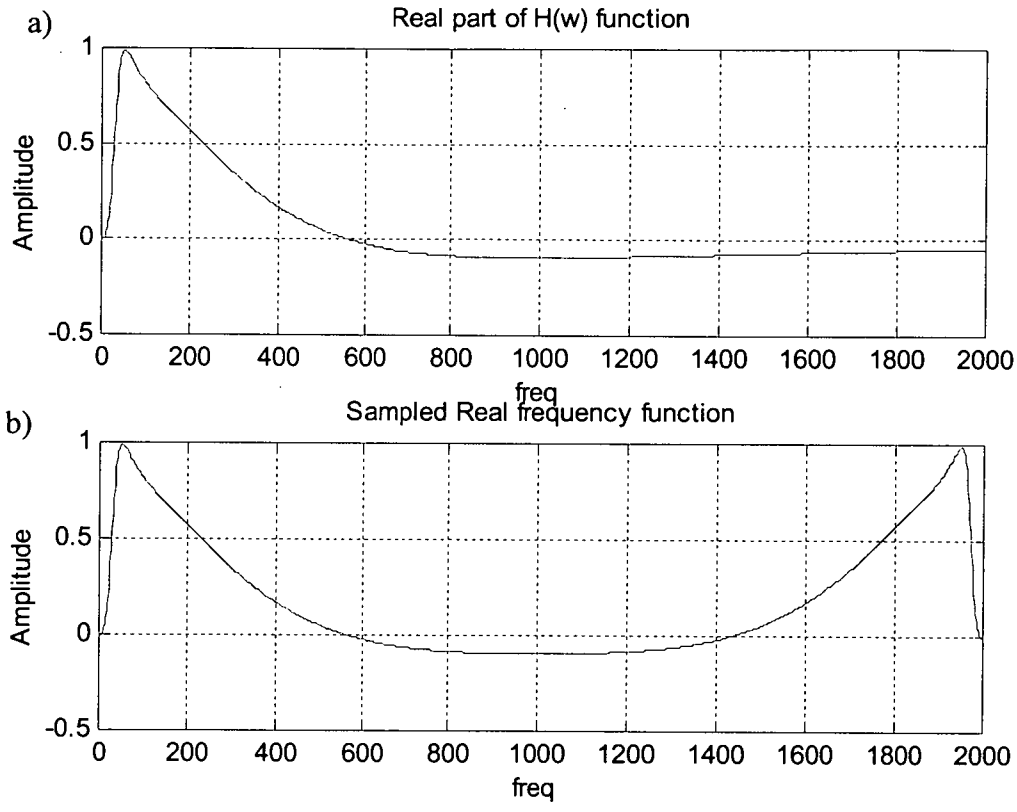

Figure 2.14: Real part of the H(ω)

The imaginary part of the complex frequency is illustrated in Figure 2.15. The imaginary part of the frequency at 50 Hz is approximately 0. Figure 2.16 shown the results of CVT with ferroresonance analysis in discrete time domain (see Appendix A for MATLAB programming).

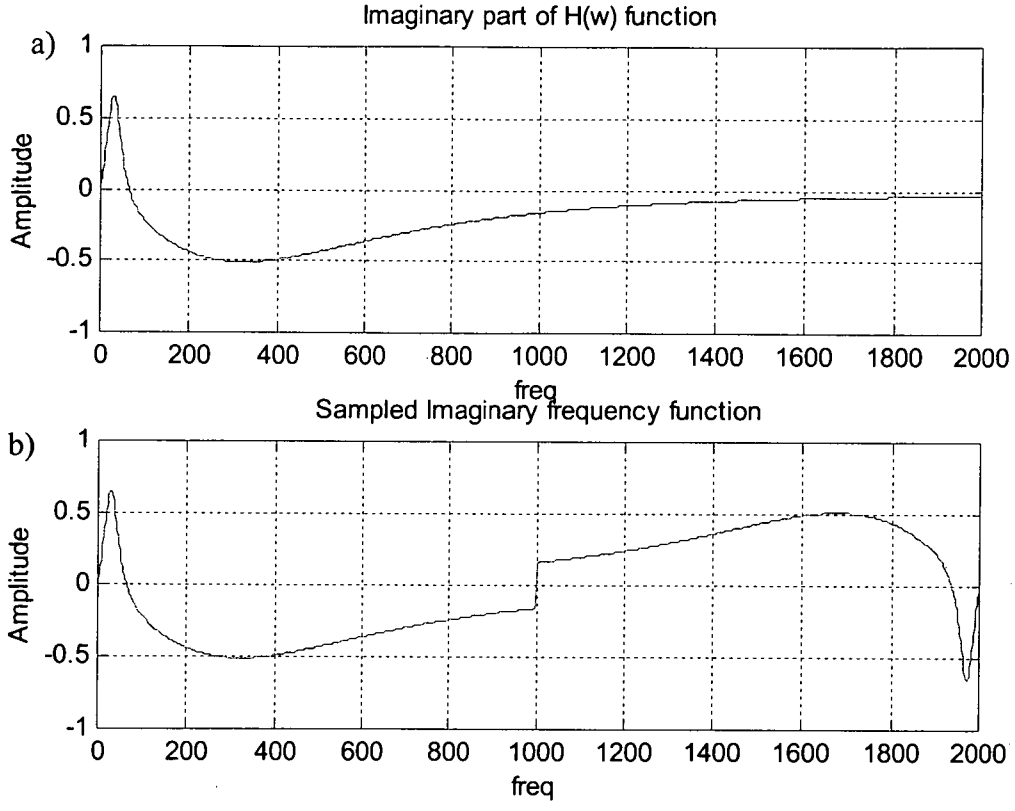

Figure 2.15: Imaginary part of the H(ω)

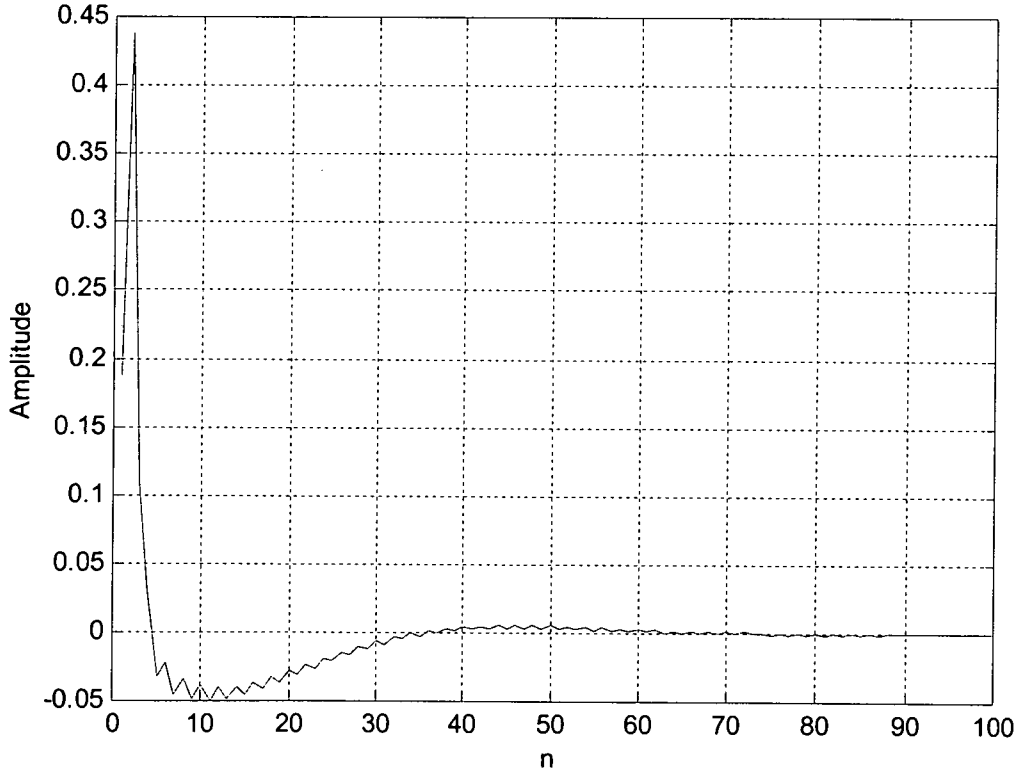

Figure 2.16: Time function graph

CHAPTER 3
VOLTAGE RESPONSE.

3.0 INTRODUCTION TO PSCAD/EMTDC

PSCAD/EMTDC and MATLAB v.5.3 simulation package was used for this project. PSCAD/EMTDC stands for Power System Computer Aided Design/Electro-Magnetic Transient of high voltage Direct Current converters and controls. It was developed for studying HVDC systems and performs the electromagnetic transient analysis on the user defined power system. It is used for examining the effect on complex circuits of over voltages and issues related to insulation co-ordination, current and voltage harmonics, surge arrester studies and the effectiveness of control and protection equipment.

PSCAD is a family of tools designed to help simulate power systems. Combination with EMTDC, i.e. PSCAD is the Graphical User Interface (GUI) for the EMTDC, these two software packages are referred as 'PSCAD/EMTDC'. The following are list of summary of the studies that can be conducted with PSCAD/EMTDC:-

- Designing power electronic systems and controls.
- Insulation co-ordination of AC and DC equipment.
- Sub synchronous oscillations, their damping and resonance.
- Incorporate the capabilities of MATLAB/Simulink directly into PSCAD/EMTDC.
- Power quality analysis and improvement.
- Effects of DC currents and geomagnetically induced currents on power systems, inrush effects and ferroresonace.

3.1 CONFIGURATION OF THE POWER SYSTEM

The power system used for the simulation in PSCAD/EMTDC is a typical 400 kV transmission line of 100 km length connected to various sources at the local and remote ends as shown in Figure 3.0. The fault was initiated at different distance, i.e. 20 km, 50 km, 80 km, from the S-end busbar. The sending end has a short circuit level of 10000 MVA and an X/R ratio of 30. The short circuit level of the remote end is 5000 MVA with an X/R ratio of 25.

3.2 TYPE OF FAULTS SIMULATED

This power system configurations was then used in the following fault study.

a) Phase to ground fault.
b) Phase to phase fault.
c) Impedance fault.
d) Phase angle fault.

The above fault conditions were initiated at different location of distance, i.e. 20 km, 50 km and 80 km of the transmission line.

The results of voltage signal obtained from this simulated protection are recorded. By using MATLAB program (attached in Appendix B), those data obtained were then convoluted with the impulse obtained from Chapter 2.

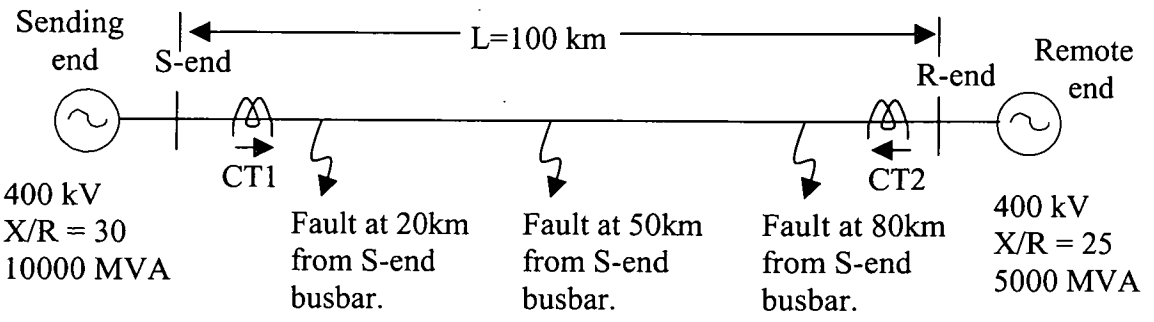

Figure 3.0 (a): Schematic diagram for 100 km transmission line.

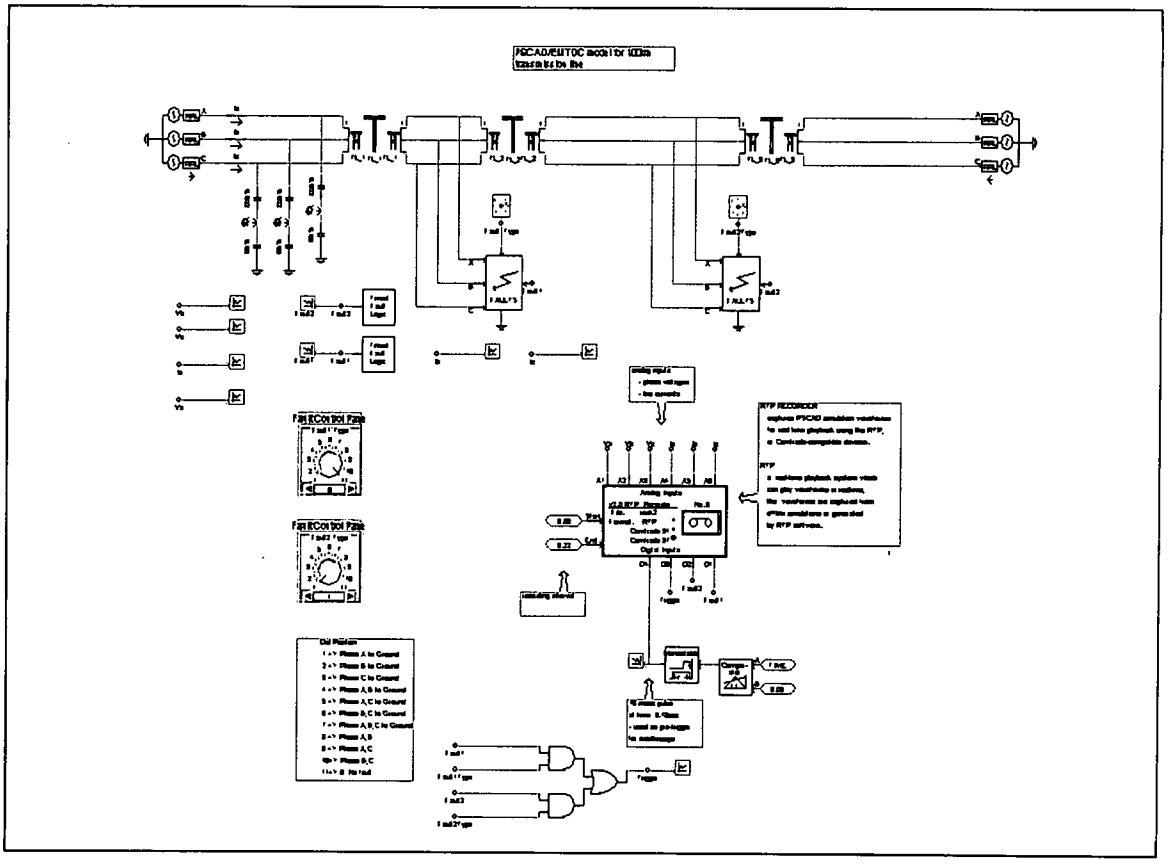

Figure 3.0 (b): PSCAD/EMTDC model for 100 km transmission line.

3.3 ANALYSIS

Analysis was observed by two conditions of circuit. It is with the suppressing circuit and without the suppressing circuit.

3.3.1 Phase A to ground fault.

The fault was applied at 0.1 second. The fault resistance is 0 Ω.

3.3.1.1 With the Suppressing circuit disconnected.

Figure 3.1 shows the response of voltage for a fault located 20 km away from S-end busbar, before convolution, i.e. response for ideal voltage transformer, and after convolution, i.e. response for CVT. The dotted line graph represents the response before convolution and the bold graph represents the response after convolution. As seen from the figure, the CVT transient response oscillates at around four to five cycles and reaches the magnitude of up to 20% of the nominal voltage. Generally, the CVT generate transients from the energy stored in the stack capacitors and the tuning reactor [7]. In other word we can say that the transients are basically controlled by the parameters of the CVT itself. Due to that reason we can see the different of transient between ideal and CVT response shown in Figure 3.1.

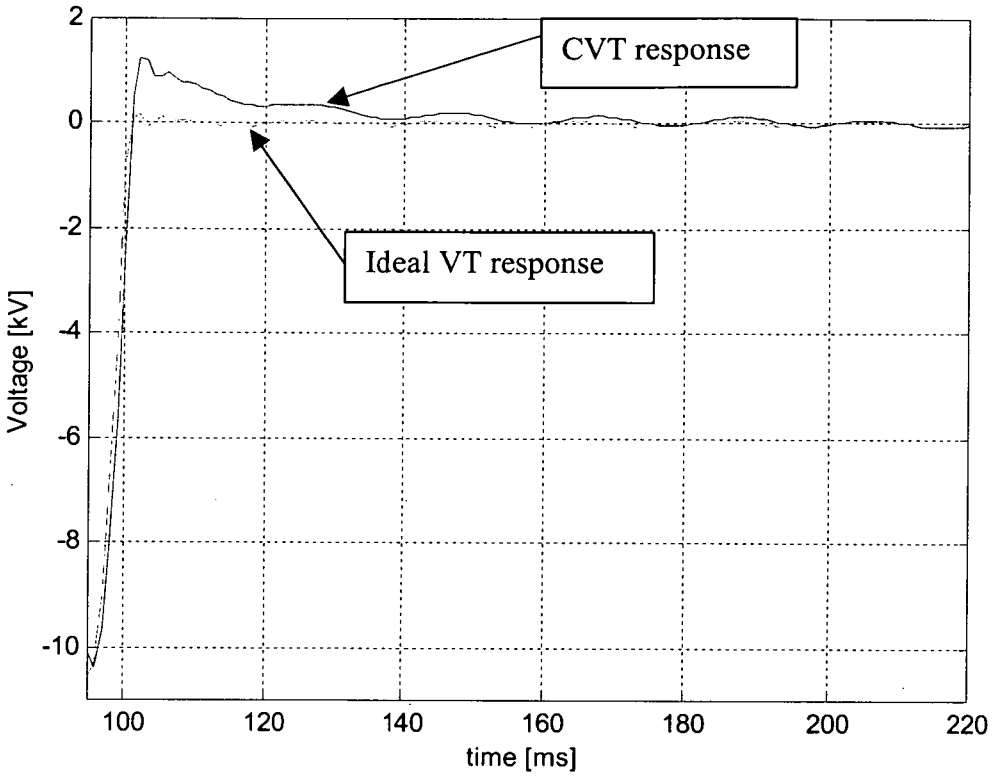

Figure 3.1: Voltage response for phase to ground fault. Fault location at 20 km from S-end busbar.

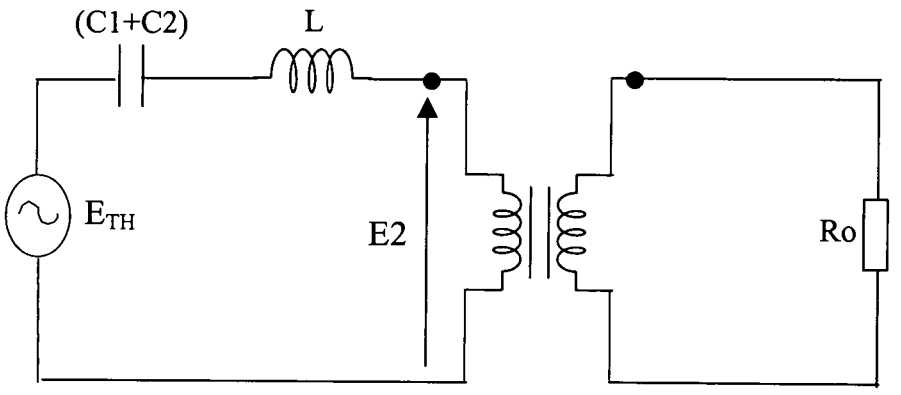

Figure 3.2: Simple CVT equivalent circuit.

However, there is a phase angle difference between the responses before and after the convolution. This is due to the error which exists in the transformer itself. Normally, the core of the intermediate transformer is usually operated at a low flux density at normal voltages resulting in difficulty to maintain the required accuracy at voltages above the nominal value. Let we consider the Thevenin equivalent circuit of the capacitive divider is shown in Figure 3.2. The Thevenin voltage is given by

$$E_{TH} = E_{pri}\frac{C1}{C1+C2} \quad \text{.....(3.0)}$$

The Thevenin source impedance is capacitive, C1 + C2. If the primary and secondary currents in the transformer are I_1 and I_2 respectively, therefore

$$E2 = E_{TH} - I_1\,(j\omega L + (1/j\omega(C1+C2))) \quad \text{.....(3.1)}$$

Thus from Equation 3.1 it is clear that the secondary voltage will have a phase angle difference.

Figures 3.3 and 3.4 illustrate the response for faults located at 50 km and 80 km from S-end busbar respectively. The further the fault is, the maximum amplitude of the voltage after the fault increases. The oscillation period also increases. Figure 3.5 is used as a reference to explain this.

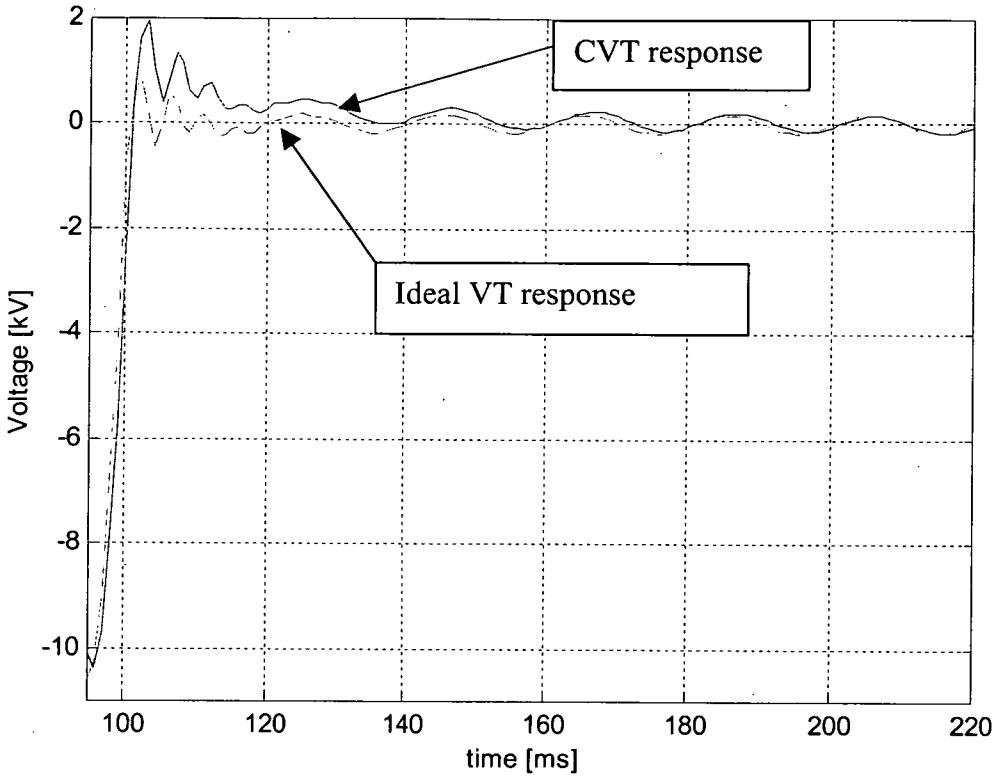

Figure 3.3: Voltage response for phase to ground fault. Fault location at 50 km from S-end busbar.

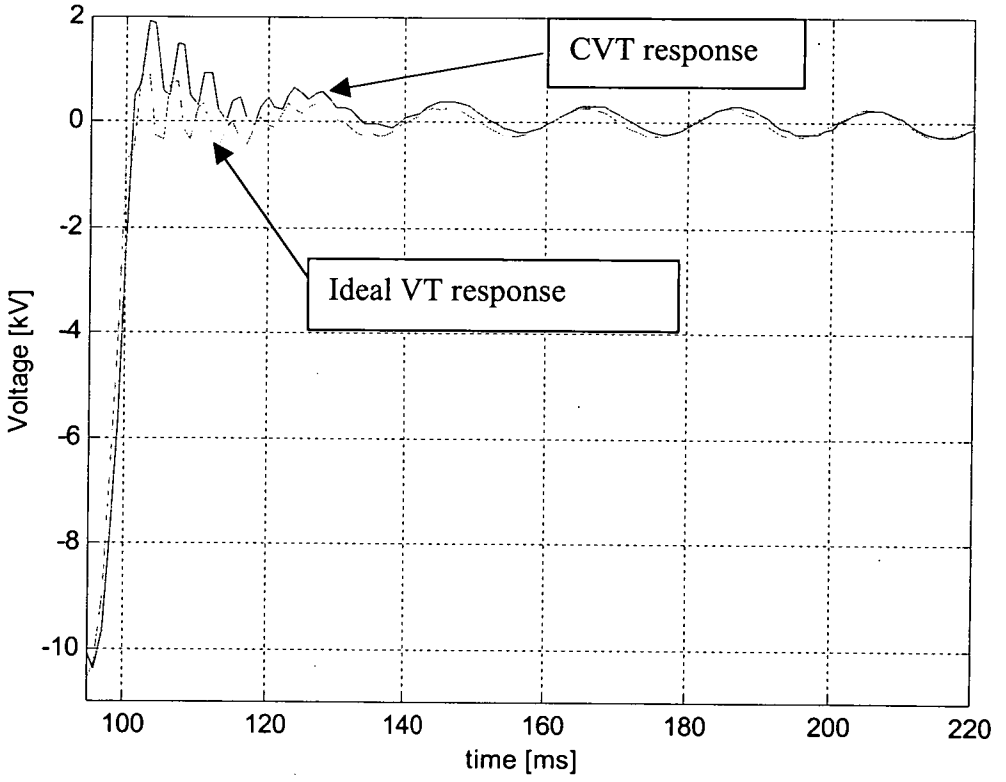

Figure 3.4: Voltage response for phase to ground fault. Fault location at 80 km from S-end busbar.

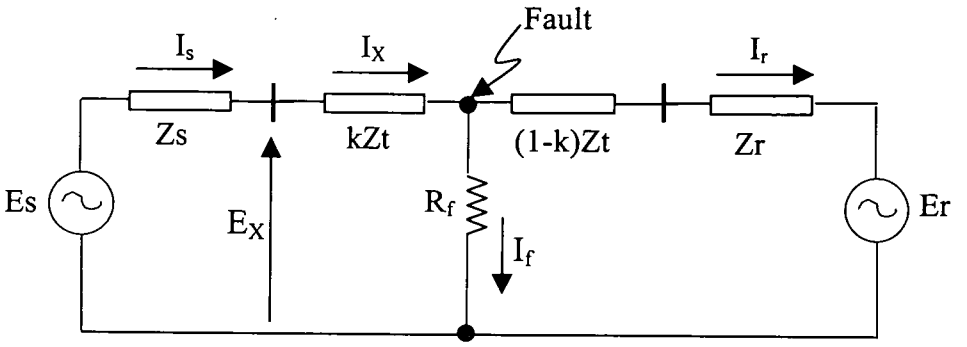

Figure 3.5: Ground fault through a resistance in a single phase circuit.

Let Zt represents the impedance of the transmission line, Zr and Zs represent the impedances of sources Er and Es respectively and Ex is the voltage at the relay terminal. The current at the relay terminal is indicated as Ix. If the fault current is If=(Is+Ir), the voltage at the relay location therefore is given by:

$$Ex = kZtIx + RIf \quad \text{.....(3.2)}$$

where k is the fractional distance to the fault and R is resistance in the fault path, which is normally very small (in this simulation R is equal to 0 Ω). The further the location of the fault, Zt will also increase. Therefore from Equation 3.2, it shown that Ex will increase when Zt increases. An increase in Zt will also effect the oscillation of transient (compare Figure 3.1, 3.3 and 3.4). It is because the series capacitive and inductive reactances are high in relation to the load impedance (referred to the intermediate voltage), particularly when power factor correcting capacitors which are employed to tune inductive load, are prone to exhibit oscillations in the secondary voltage when the primary voltage changes rapidly. Therefore increasing Zt, will result in a longer transient period.

3.3.1.2 With the Suppressing circuit connected.

Figure 3.6 shows the voltage response for a fault located 20 km away from S-end busbar with the suppressing circuit connected. When compared with Figure 3.1, the CVT transients lasts for up to two cycles and the magnitude is increased. It is because the series reactance in the intermediate voltage circuits, through which the exciting current, i.e. current flowing through suppressing circuit, is normally capacitive. Therefore any increase in exciting current with relative to the input voltage results in magnitude error and phase angle. In other word we can say that the shape and parameters of the ferroresonance suppression circuits is one of the factor that controls the transient behaviour.

Figures 3.7 and 3.8 illustrate the response for fault located at 50 km and 80 km away from S-end busbar. In general, the purpose of the suppressing circuit is to damp out both the subharmonic and high frequency oscillations. Therefore, when comparing Figures 3.7 and 3.8 with Figures 3.3 and 3.4, it can be observed that the subharmonic oscillation is reduced considerably.

3.3.2 Phase to phase fault.

The time to apply fault is set to 0.1 second. The fault resistance is 0 Ω.

3.3.2.1 With the Suppressing circuit disconnected.

Figure 3.9 and 3.10 illustrate the response for phase A-B fault and A-C fault respectively. It can be seen that the voltage when the fault occurred at 100ms is different for both figures. It is due to the different phase between the three phases, i.e. A, B and C.

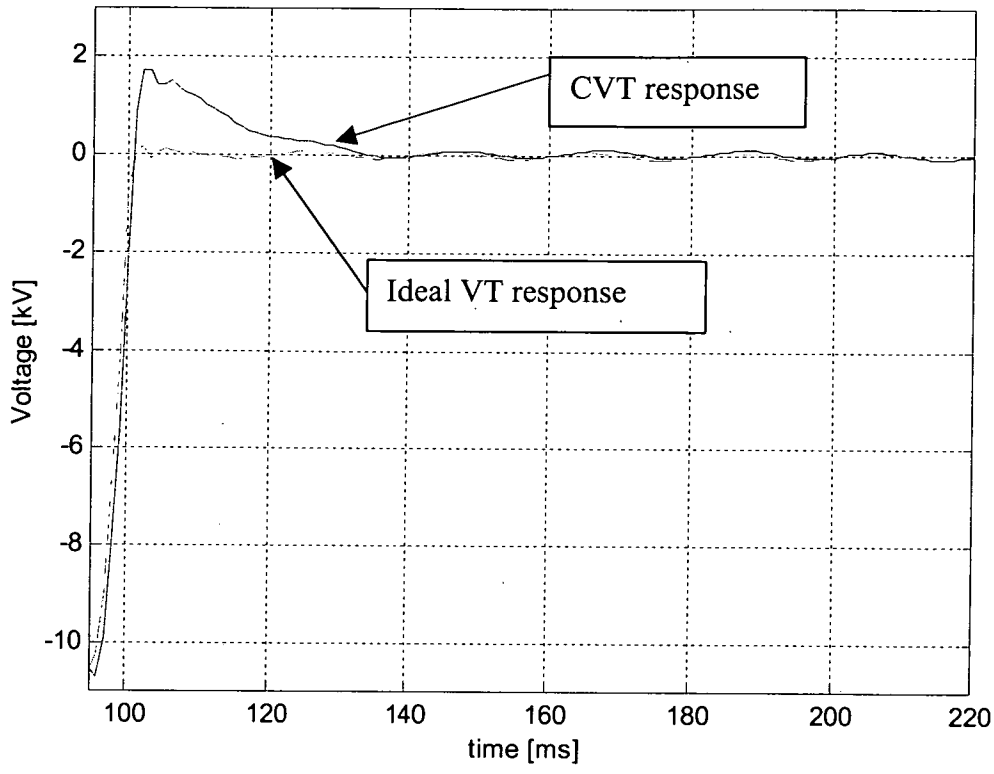

Figure 3.6: Voltage response for phase to ground fault. Fault location at 20 km from S-end busbar.

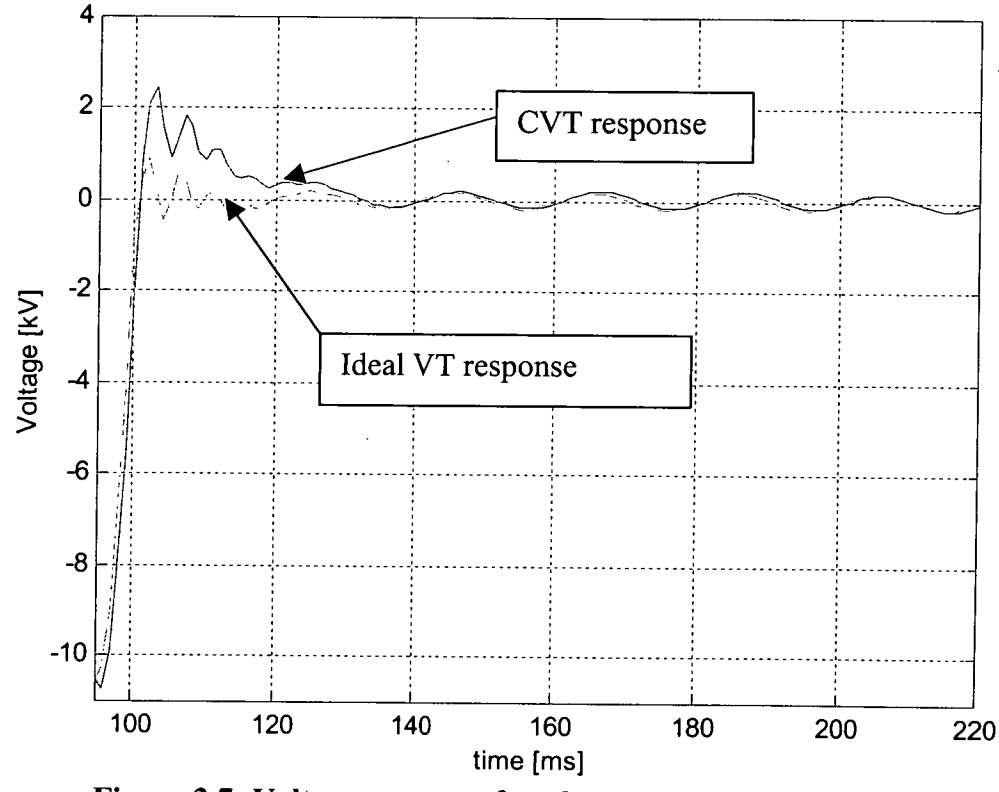

Figure 3.7: Voltage response for phase to ground fault. Fault location at 50 km from S-end busbar.

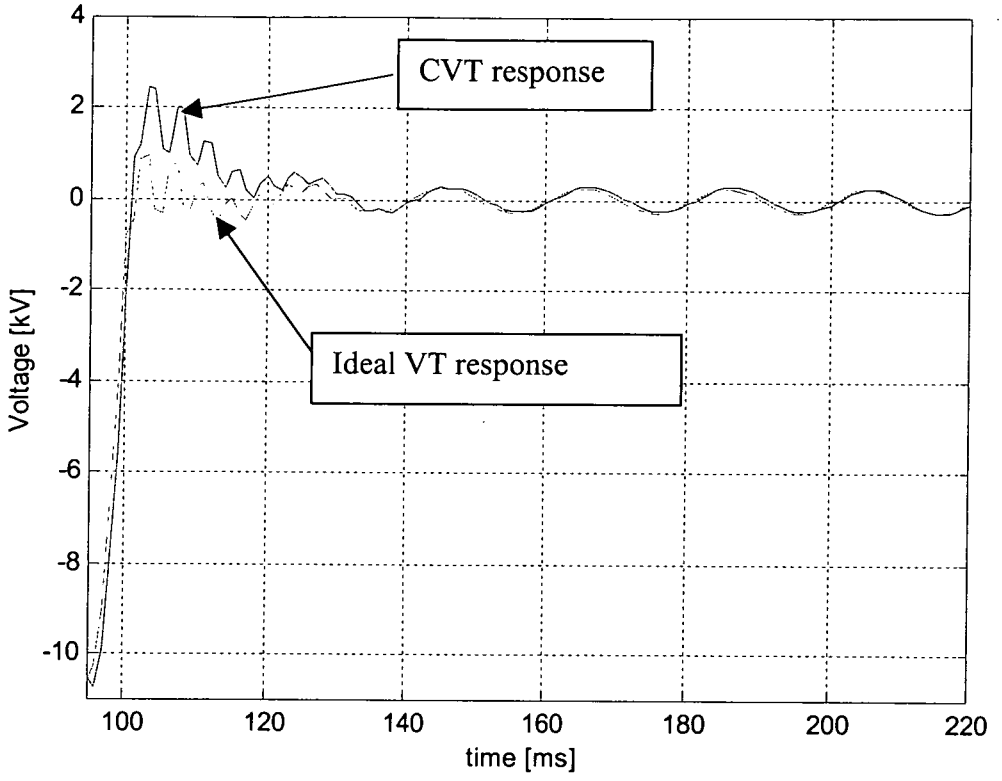

Figure 3.8: Voltage response for phase to ground fault. Fault location at 80 km from S-end busbar.

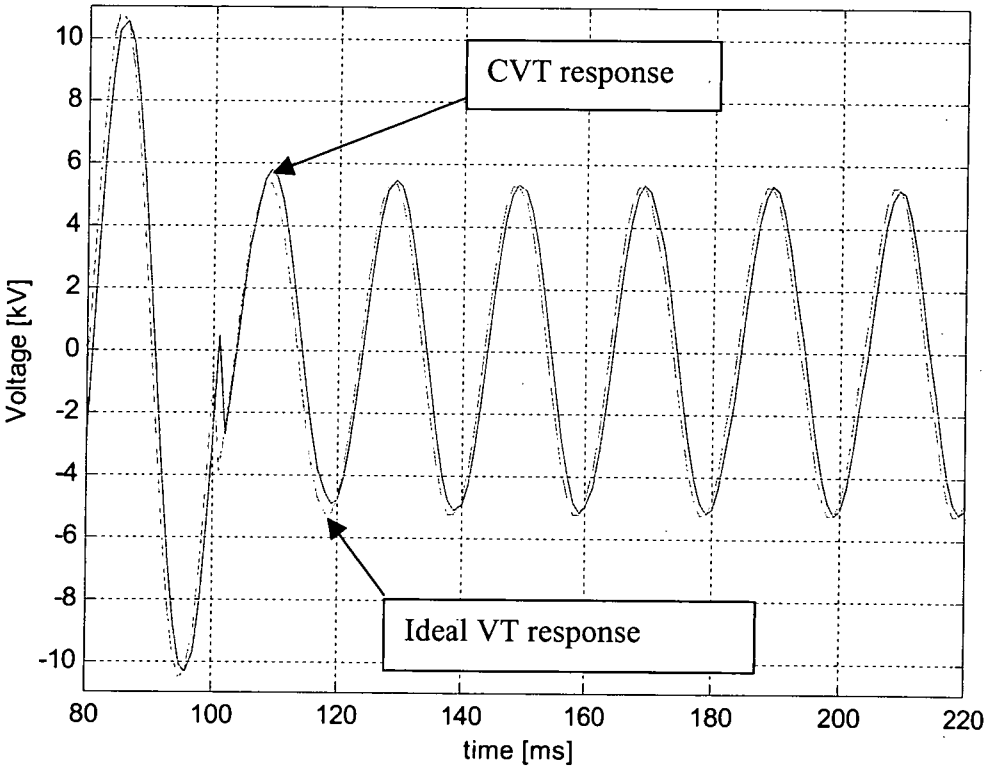

Figure 3.9: Voltage response for phase A-B fault. Fault location at 20 km from S-end busbar.

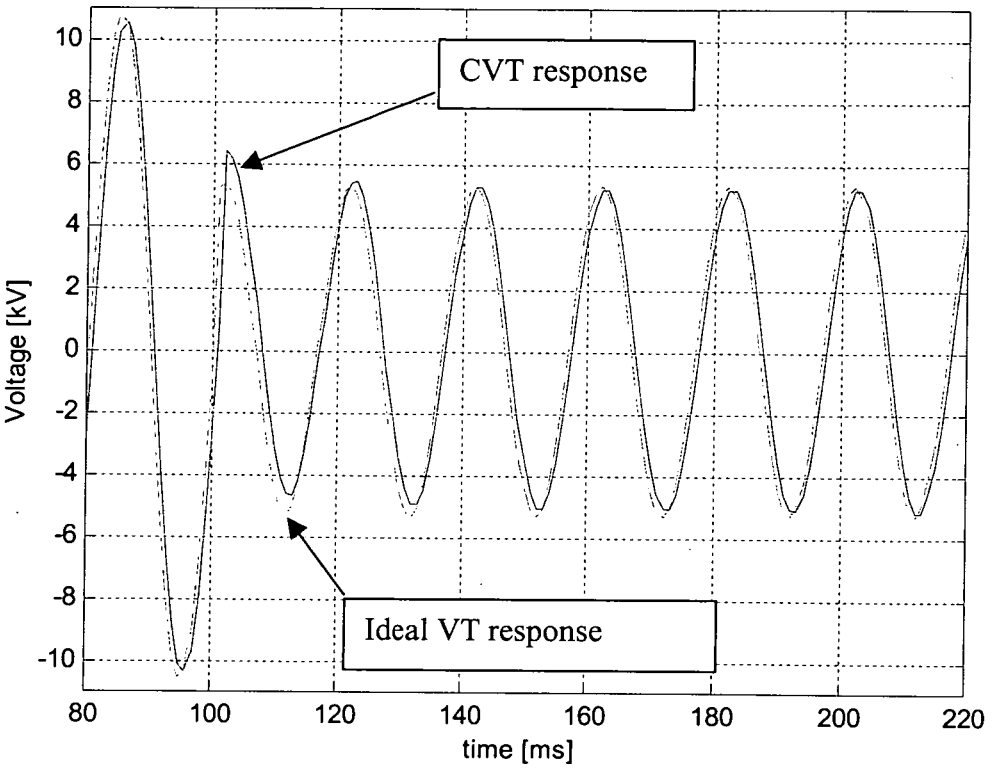

Figure 3.10: Voltage response for phase A-C fault. Fault location at 20 km from S-end busbar.

Figures 3.11 and 3.12 show the voltage response when a fault occurred 50 km from the S-end on faulted phases A-B and phases A-C respectively. Figures 3.13 and 3.14 show the response of voltage when a fault occurred 80 km away from S-end busbar for fault phase A-B and phase A-C respectively. The further the location of the fault, the noise becomes worst. This noise exists because of distributed parameter line model, which the noise is related to travelling waves propagating down line.

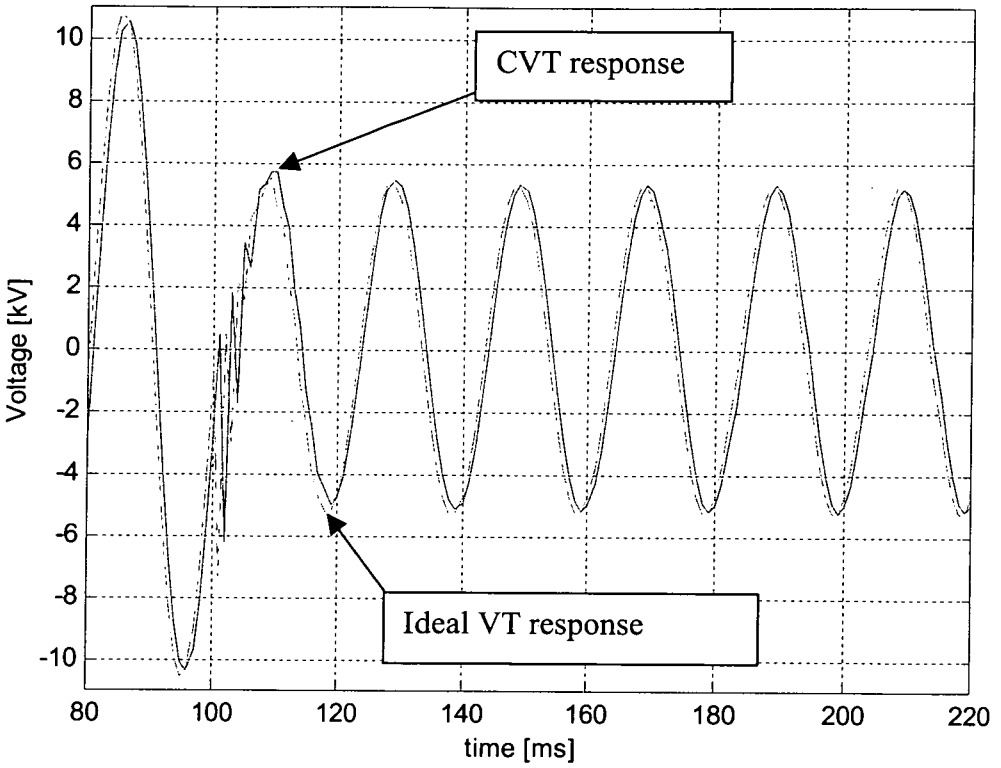

Figure 3.11: Voltage response for phase A-B fault. Fault location at 50 km from S-end busbar.

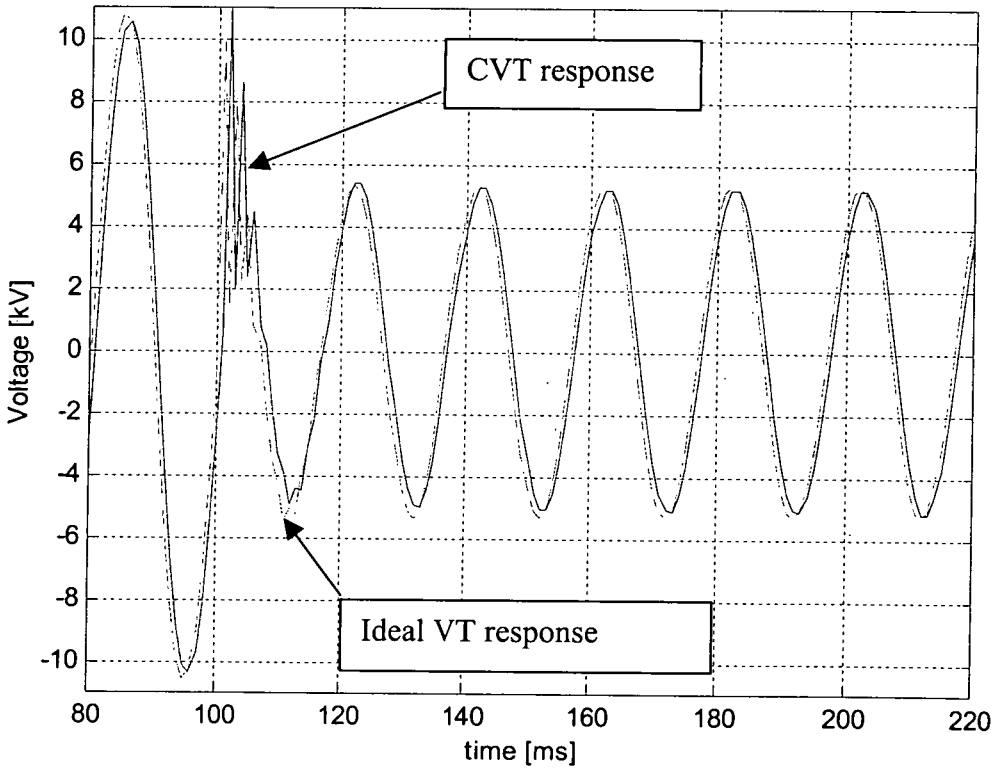

Figure 3.12: Voltage response for phase A-C fault. Fault location at 50 km from S-end busbar.

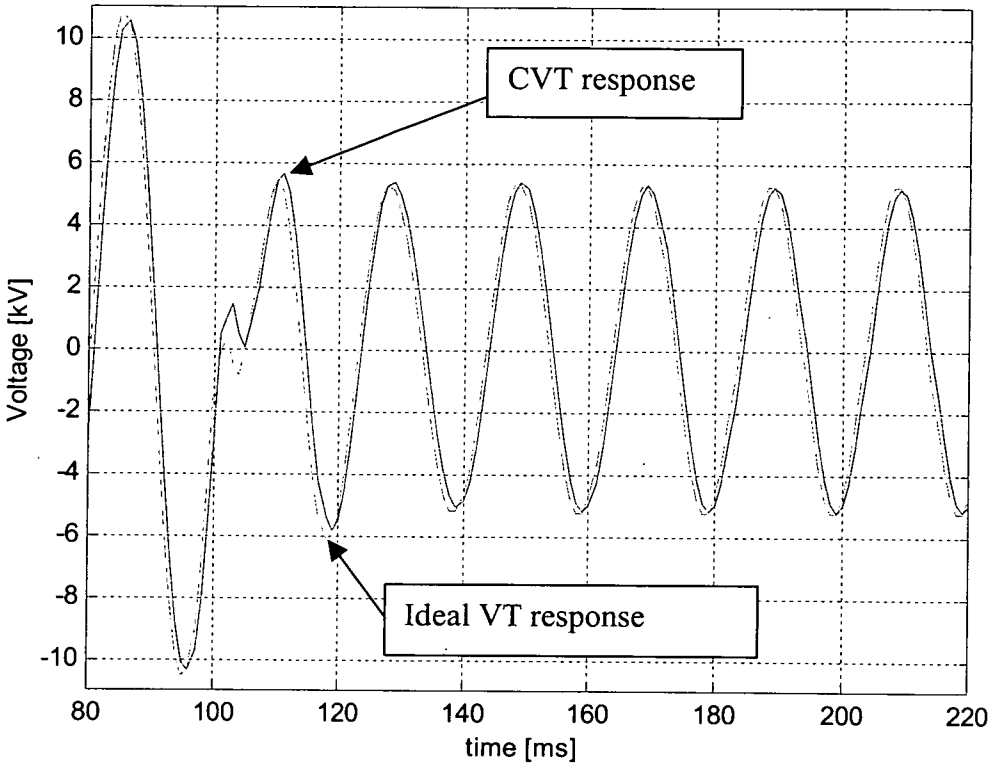

Figure 3.13: Voltage response for phase A-B fault. Fault location at 80 km from S-end busbar.

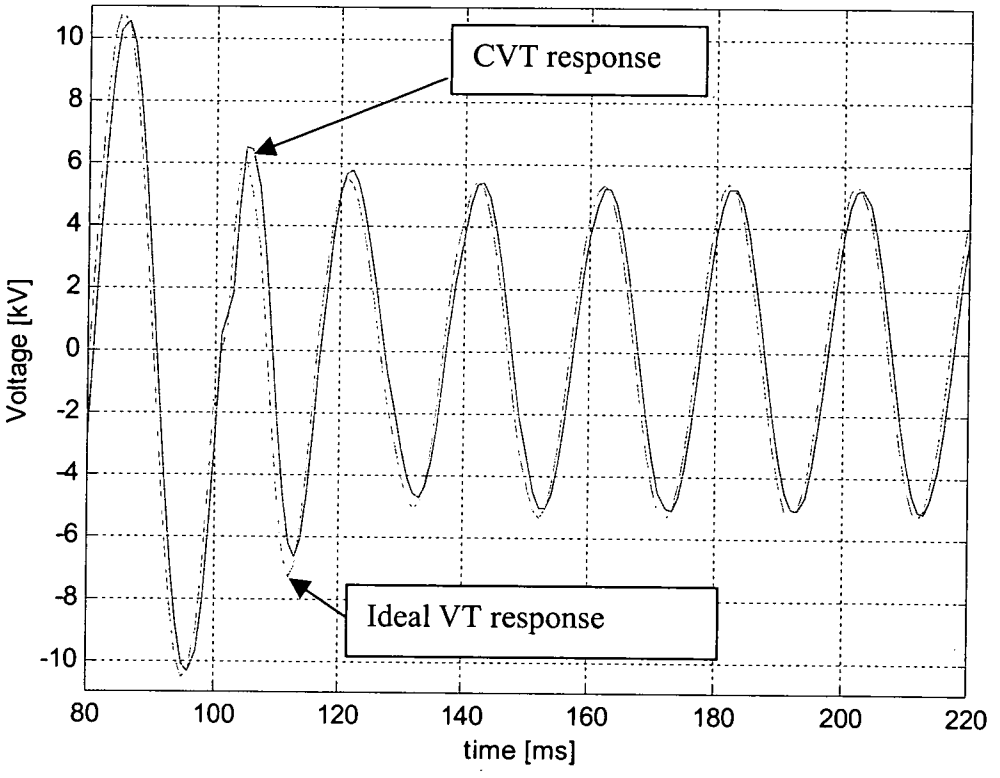

Figure 3.14: Voltage response for phase A-C fault. Fault location at 80 km from S-end busbar.

3.3.2.2 *With the Suppressing circuit connected.*

Figures 3.15 to 3.20 illustrate the response of voltage with the suppressing circuit connected. When compared with Figures 3.9 to 3.14 it is observed that by connecting the suppressing circuit, the magnitude of the voltages during fault initialisation increases. This due to the shape and parameters of the ferroresonance suppression circuit as explained in section 3.3.1.2.

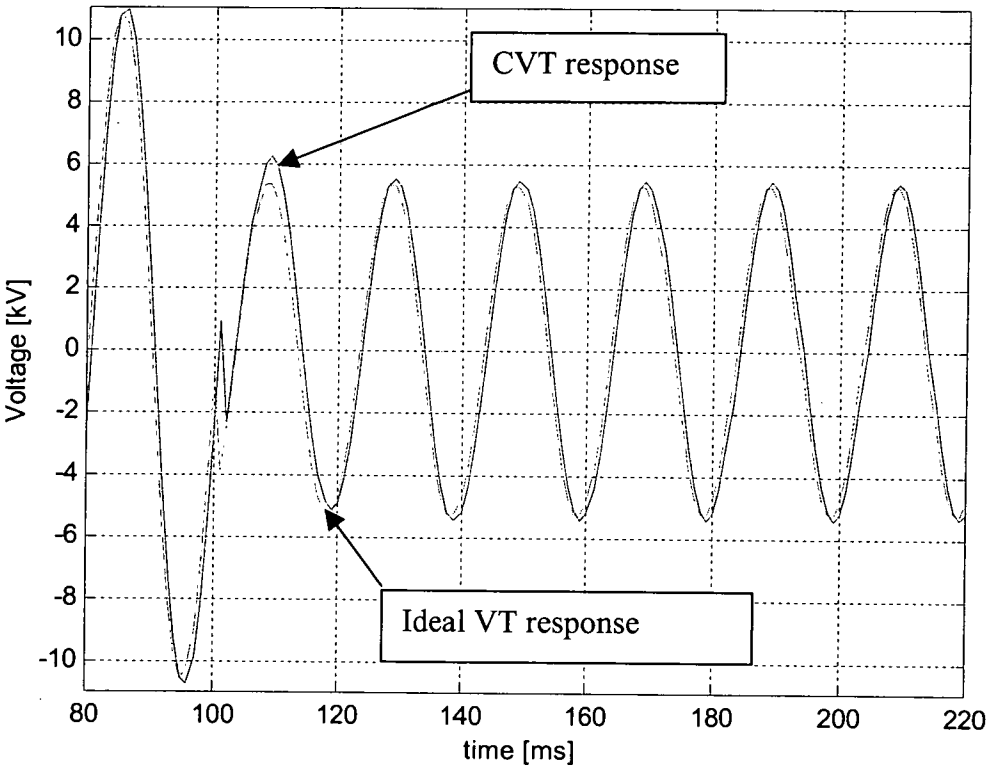

Figure 3.15: Voltage response for phase A-B fault. Fault location at 20 km from S-end busbar.

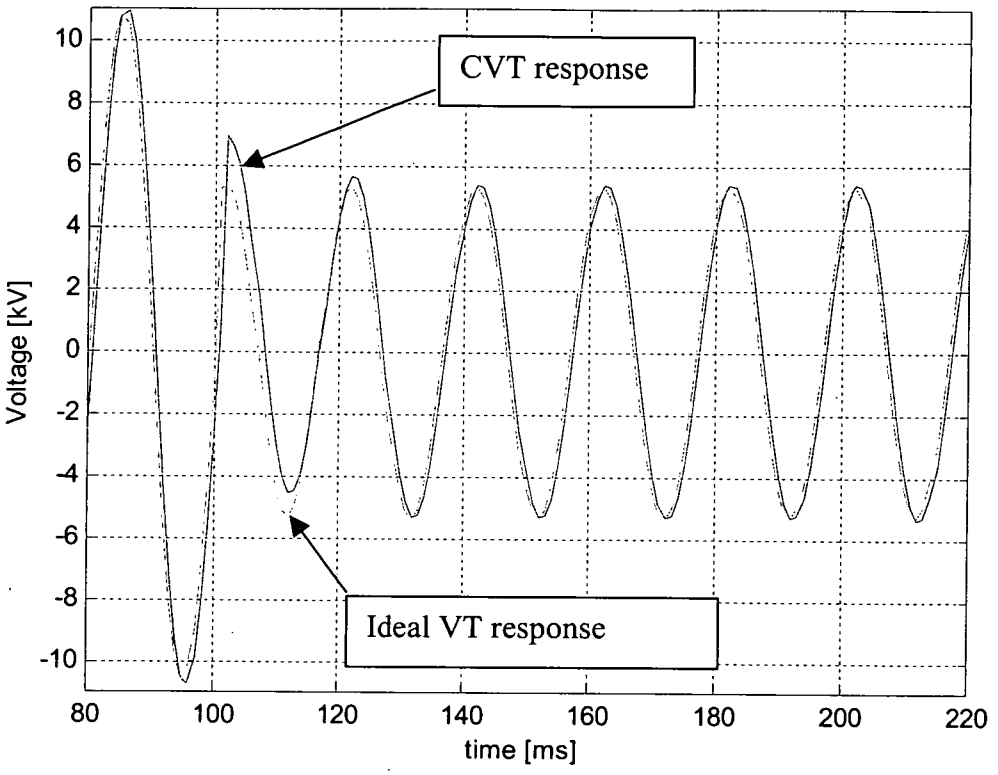

Figure 3.16: Voltage response for phase A-C fault. Fault location at 20 km from S-end busbar.

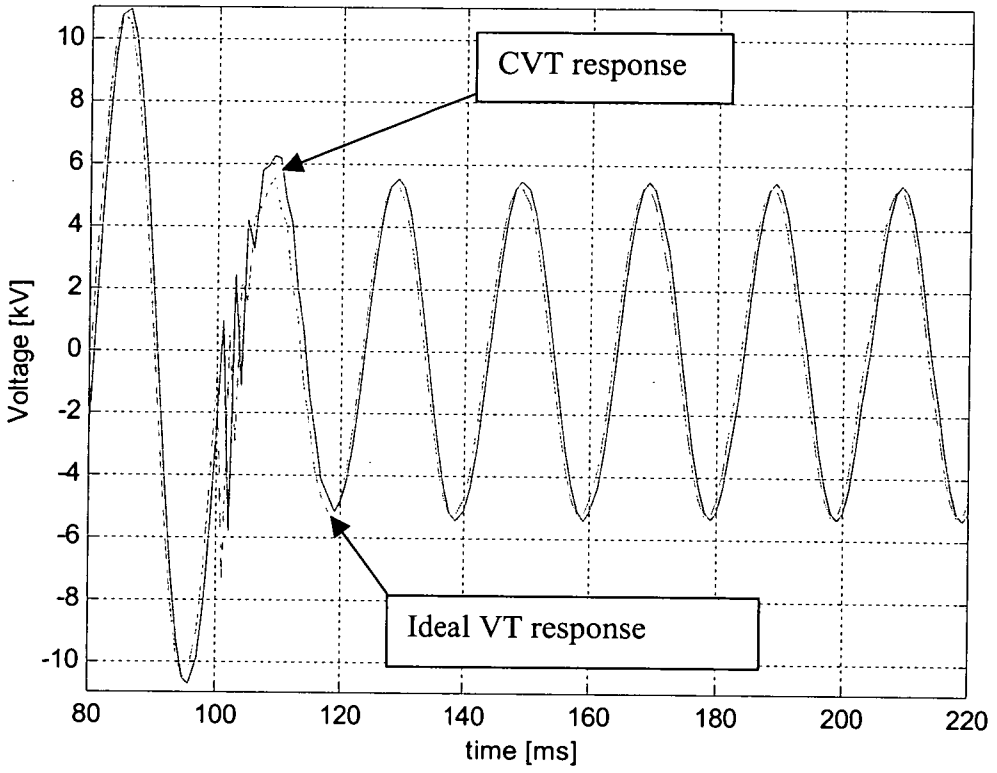

Figure 3.17: Voltage response for phase A-B fault. Fault location at 50 km from S-end busbar.

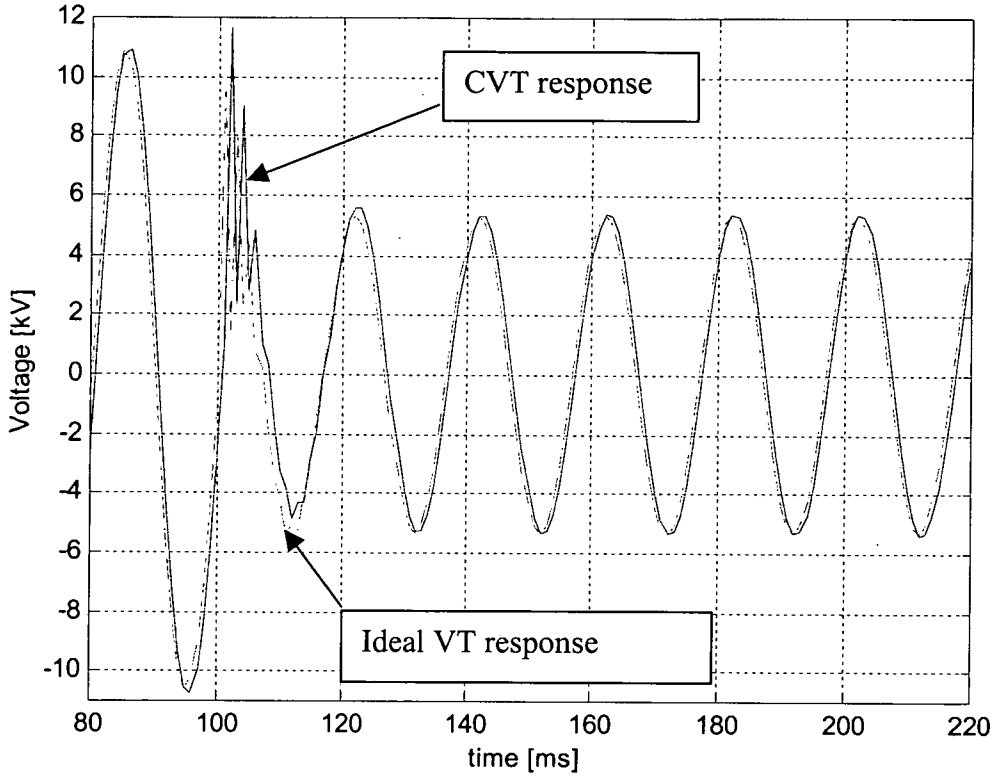

Figure 3.18: Voltage response for phase A-C fault. Fault location at 50 km from S-end busbar.

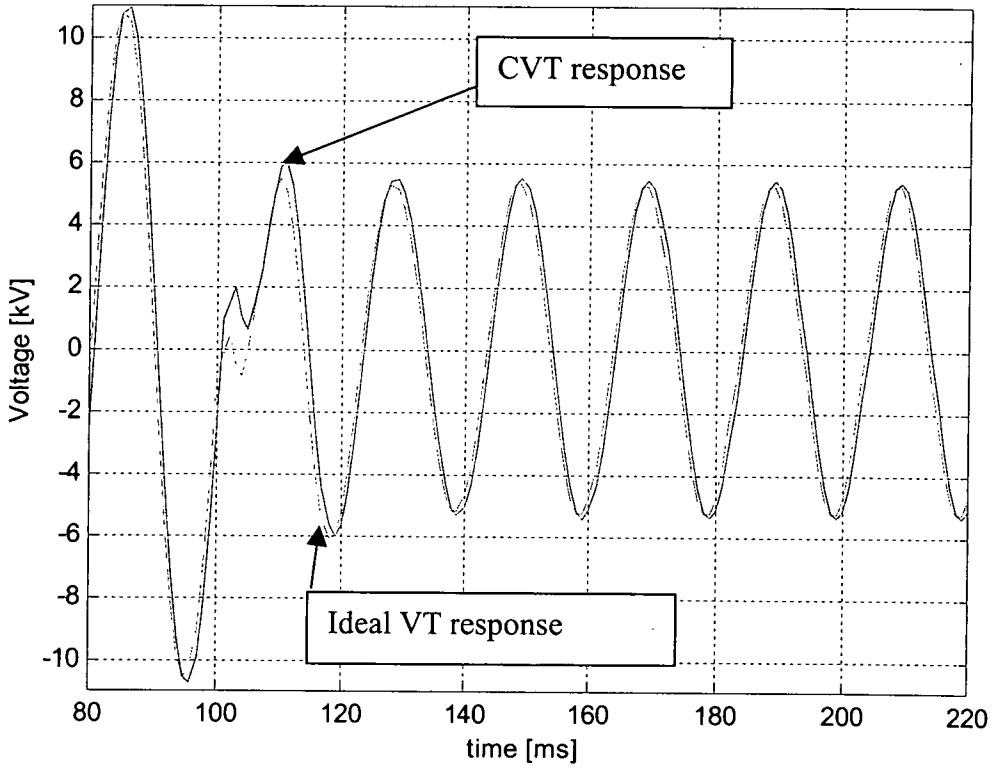

Figure 3.19: Voltage response for phase A-B fault. Fault location at 80 km from S-end busbar.

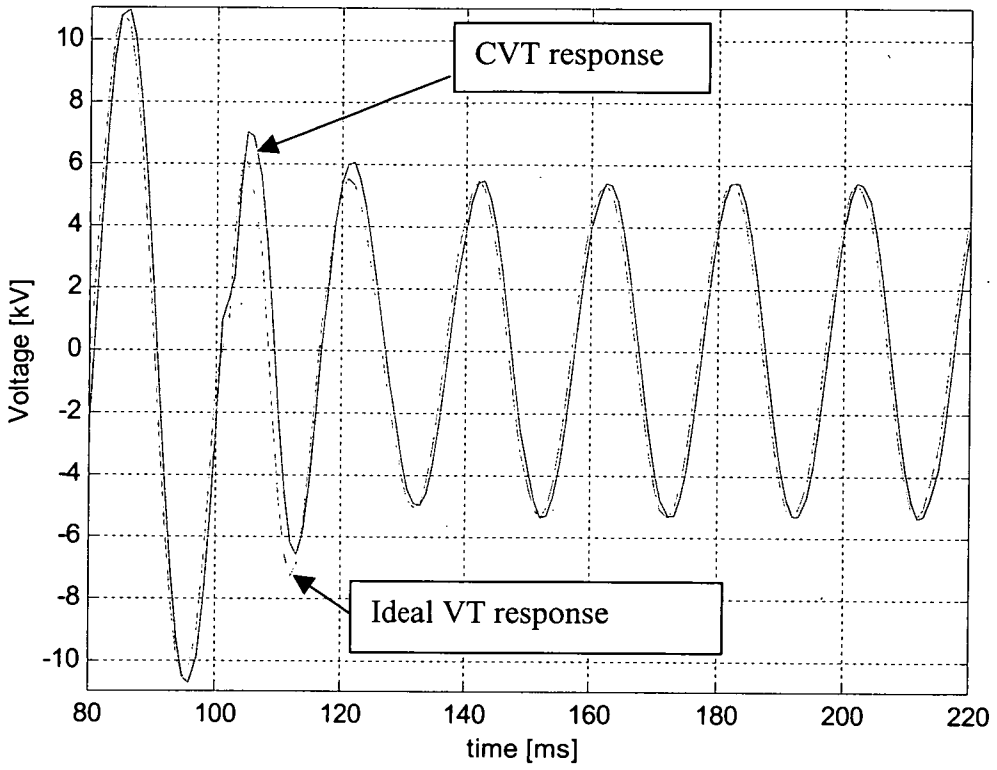

Figure 3.20: Voltage response for phase A-C fault. Fault location at 80 km from S-end busbar.

3.3.3 Phase angle fault.

This section examines the response of voltage signal when fault was initiated at zero voltage, i.e. angle is equal 0^0, at voltage maximum, i.e. angle is 90^0 and at mid voltage, i.e. angle is 45^0. For this, the fault was applied at 0.1005s, 0.105s and 0.102s respectively. Generally in a power system, the most common type of fault is the phase-to-ground fault. Thus, the latter type of fault will be used in order to simulate those phase angle faults mentioned above. The fault was applied at 20 km, 50 km and 80 km away from S-end busbar.

3.3.3.1 With the Suppressing circuit disconnected.

(a) Zero voltage: angle is equal to 0^0.

Figures 3.21 to 3.23 show the response of fault located at 20 km, 50 km and 80 km away from S-end busbar respectively. As seen from the Figure 3.21, the CVT transient can last for up to three cycles and reach the magnitude up 10%-20% of nominal voltage. As the fault location increases, the inductance of the line increasing too. Hence, as seen in Figures 3.22 and 3.23, the transient lasts more than six cycles.

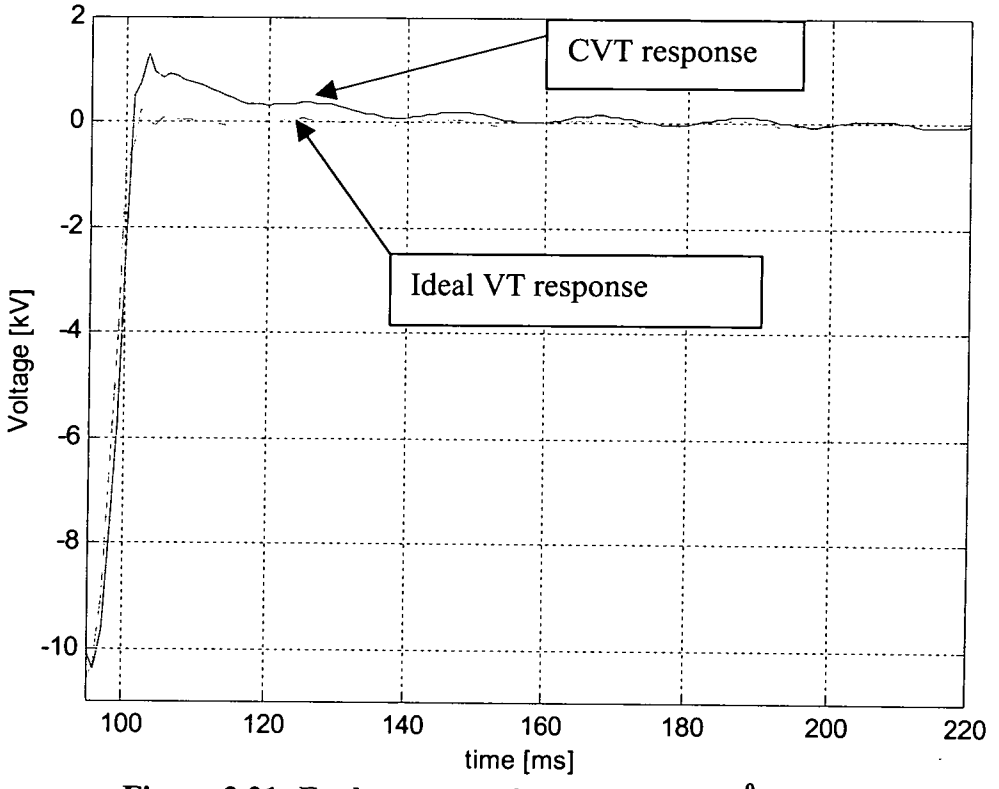

Figure 3.21: Fault at zero voltage, i.e. angle 0^0. Fault location at 20 km from S-end busbar.

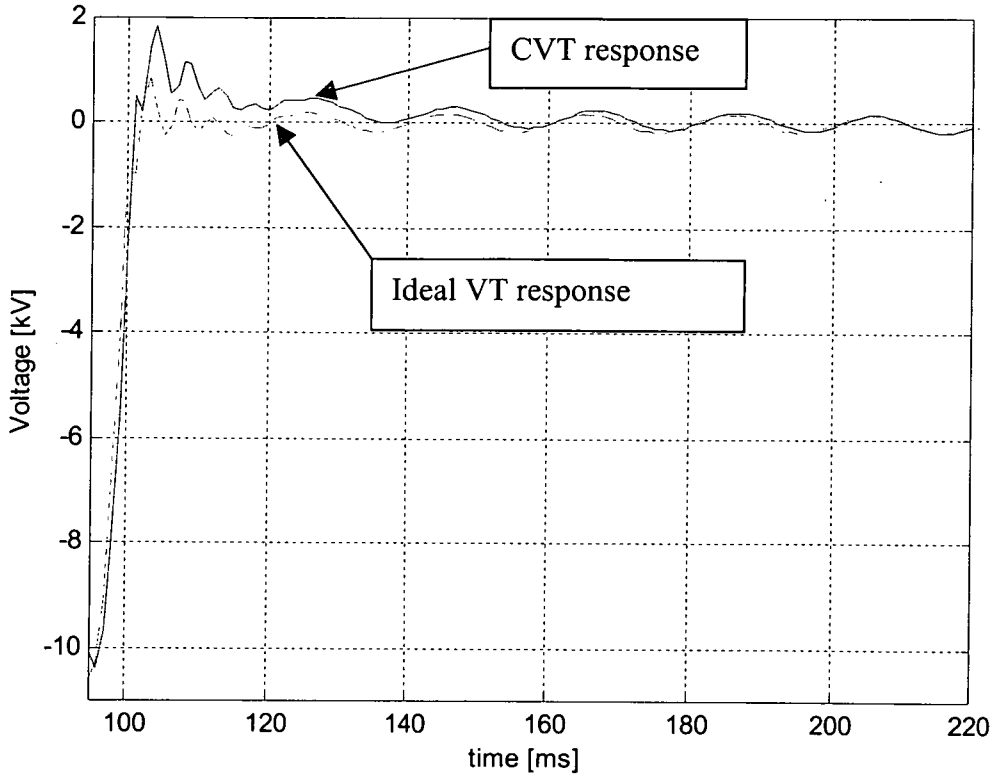

Figure 3.22: Fault at zero voltage, i.e. angle 0^0. Fault location at 50 km from S-end busbar.

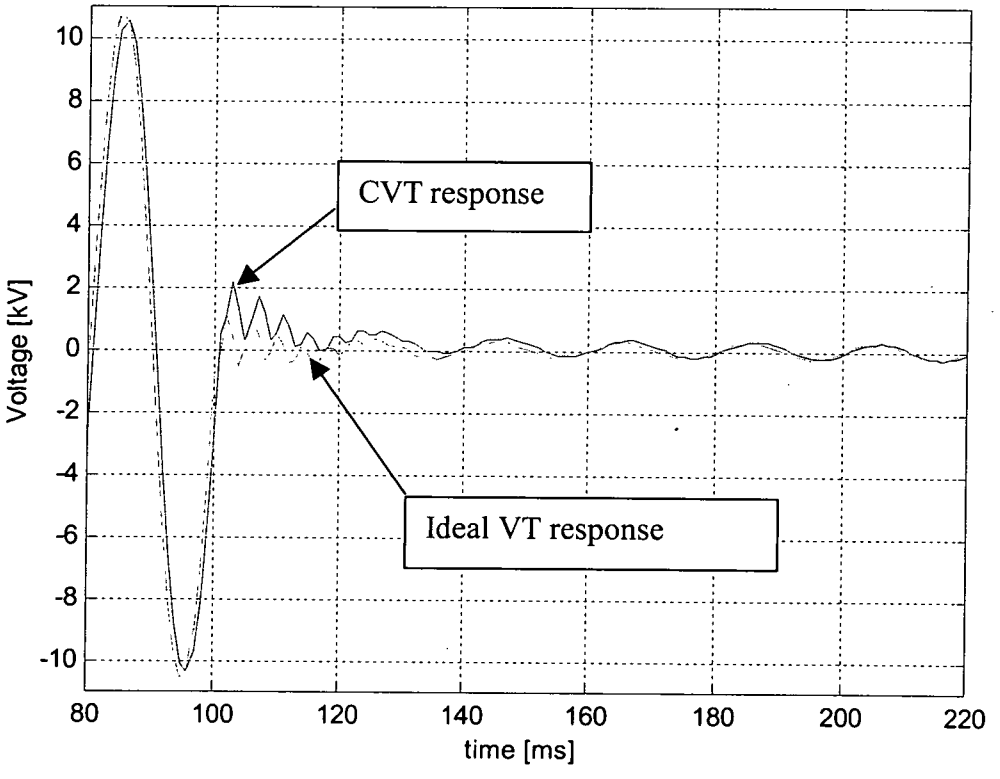

Figure 3.23: Fault at zero voltage, i.e. angle 0^0. Fault location at 80 km from S-end busbar.

(b) Voltage maximum: angle is equal to 90^0.

Figures 3.24 to 3.26 show the response of voltage when fault was applied at voltage maximum. Fewer cycles were required to reach steady state when compared with fault occurring at zero voltage. The CVT transient also decreases gradually compared with fault occurring at zero voltage. When comparing the CVT transient in Figure 3.24 and 3.21, it can be seen that the magnitude of voltage immediately reaches zero after fault occurred at voltage maximum.

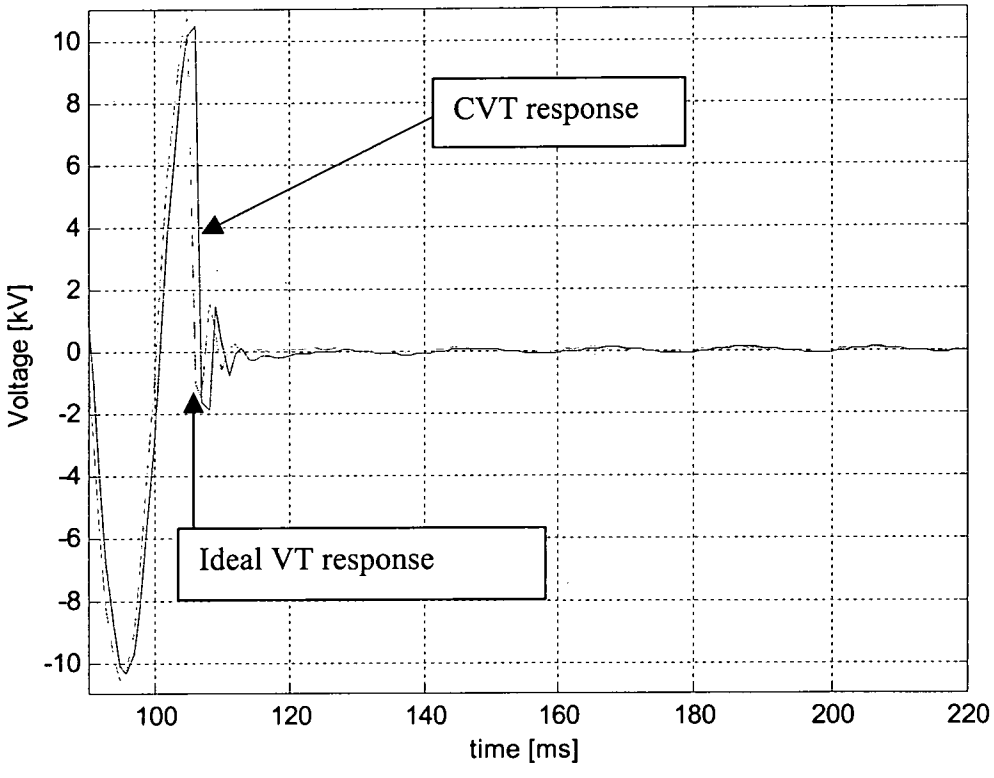

Figure 3.24: Fault at maximum voltage, i.e. angle 90^0. Fault location at 20 km from S-end busbar.

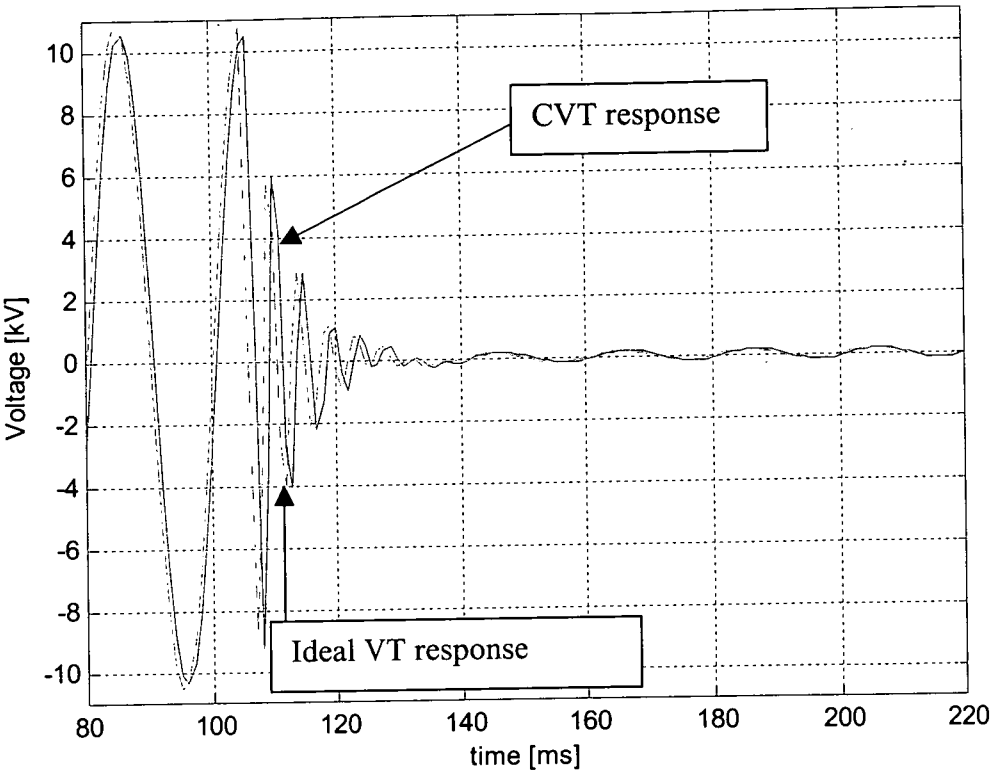

Figure 3.25: Fault at maximum voltage, i.e. angle 90^0. Fault location at 50 km from S-end busbar.

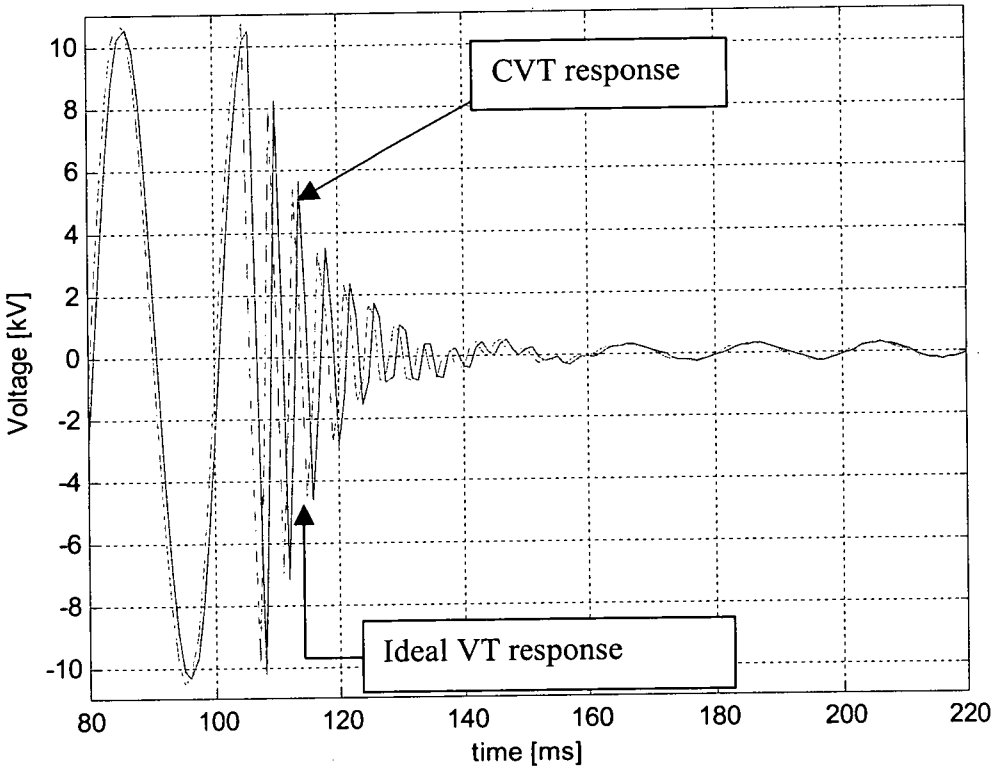

Figure 3.26: Fault at maximum voltage, i.e. angle 90^0. Fault location at 80 km from S-end busbar.

(c) Mid voltage: angle is equal to 45^0.

Figures 3.27 to 3.29 show the voltage response when fault was applied at mid voltage. It can be seen that it will take more cycles before reaching steady state when compared with fault occurring at maximum voltage. The point on wave when a fault occurs is another factor which determines the transient.

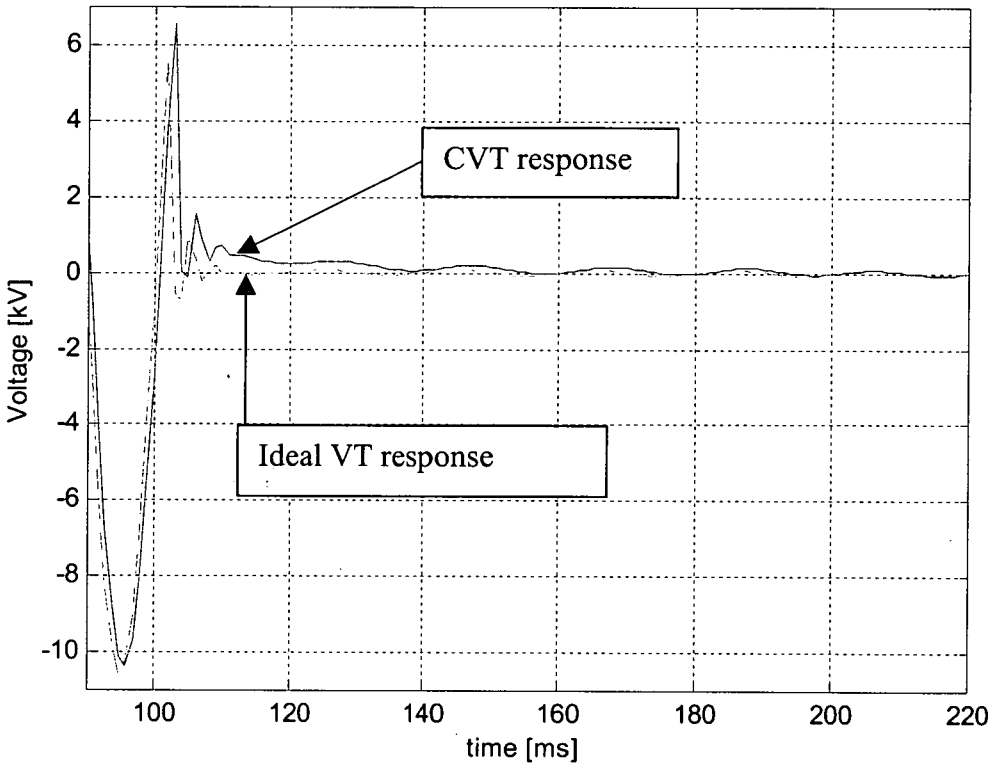

Figure 3.27: Fault at mid voltage, i.e. angle 45^v. Fault location at 20 km from S-end busbar.

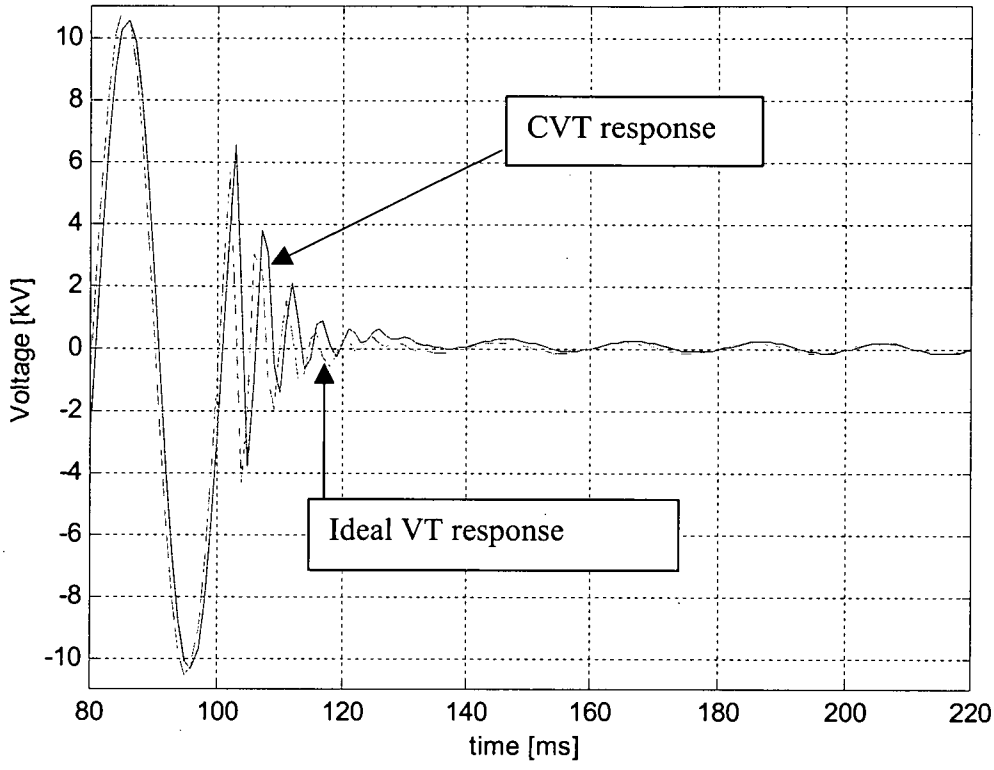

Figure 3.28: Fault at mid voltage, i.e. angle 45^{0}. Fault location at 50 km from S-end busbar.

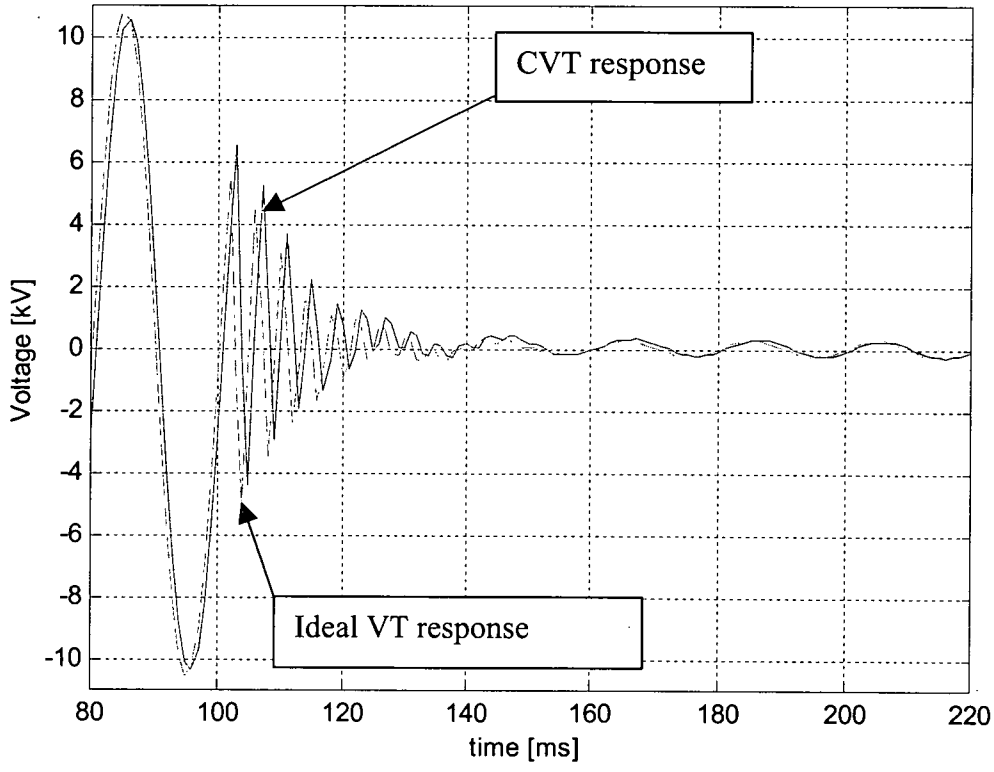

Figure 3.29: Fault at mid voltage, i.e. angle 45^{0}. Fault location at 80 km from S-end busbar.

3.3.3.2 With the Suppressing circuit connected.

(a) Zero voltage: angle is equal to 0^0.

As shown in Figures 3.30 to 3.32, the CVT transient is of a larger magnitude but shorter duration as compared with transient without the suppressing circuit. It can be seen that the oscillation of transient decreases and the magnitude increases compared with the results obtained in section 3.3.3.1 (a). This due to the shape and parameters of the ferroresonance suppression circuit as explained in section 3.3.1.2.

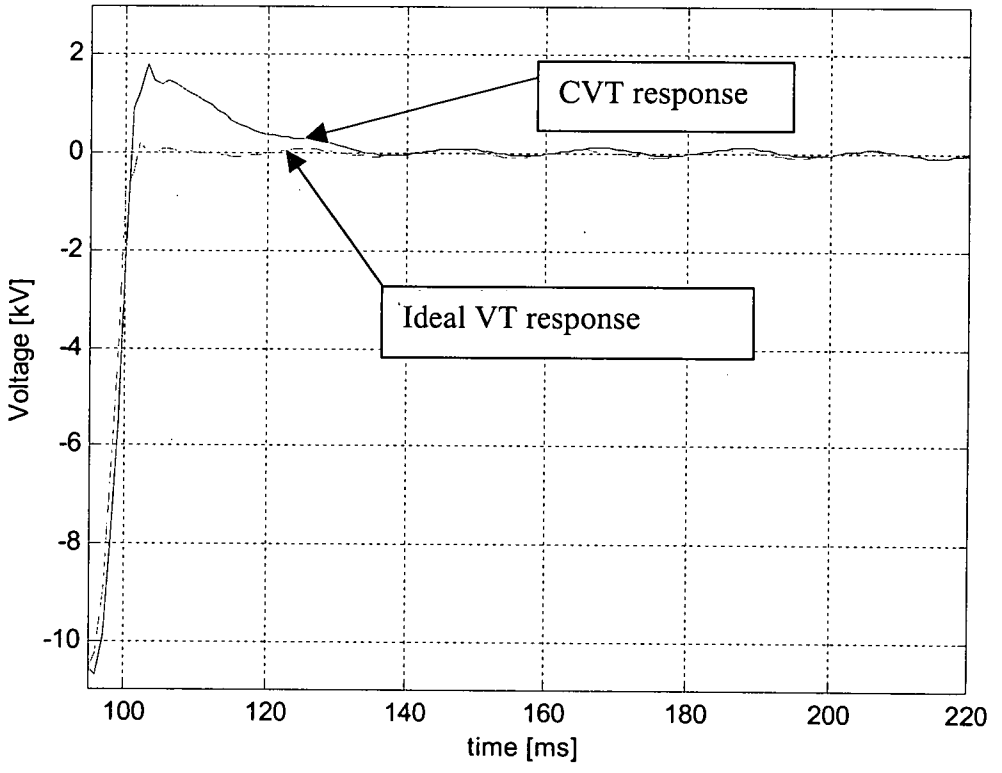

Figure 3.30: Fault at zero voltage, i.e. angle 0^0. Fault location at 20 km from S-end busbar.

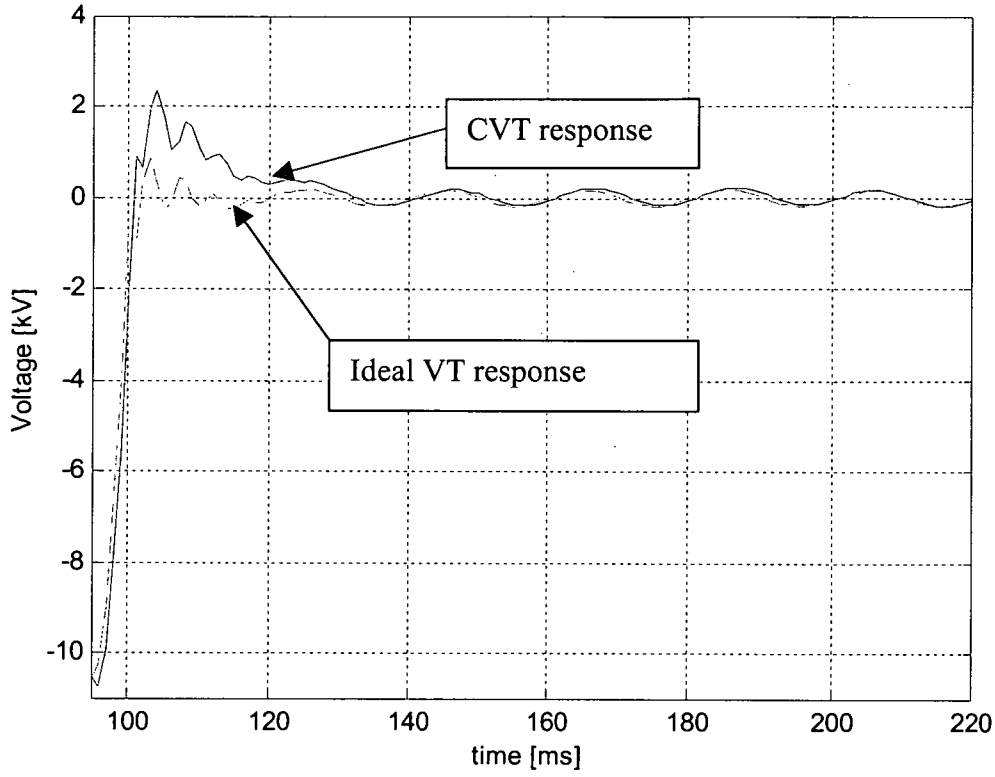

Figure 3.31: Fault at zero voltage, i.e. angle 0^0. Fault location at 50 km from S-end busbar.

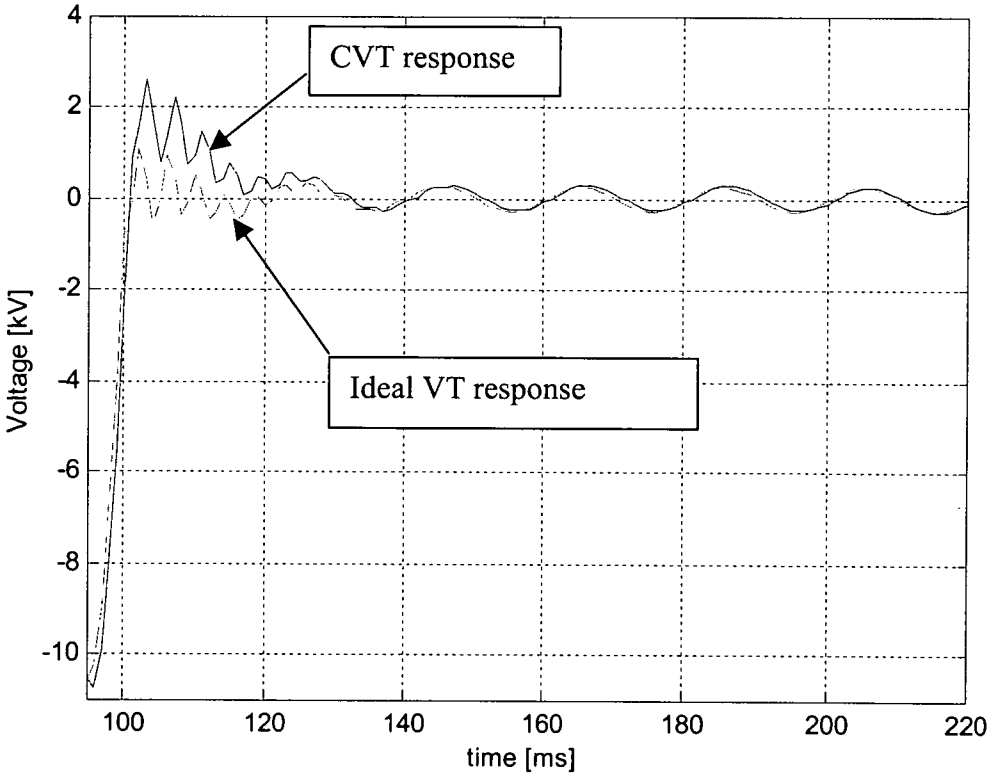

Figure 3.32: Fault at zero voltage, i.e. angle 0^0. Fault location at 80 km from S-end busbar.

(b) Voltage maximum: angle is equal to 90^0.

The voltage responses are shown in Figures 3.33 to 3.35. By introducing the suppressing circuit, the oscillation of transient reduces and magnitude increases for each fault location case.

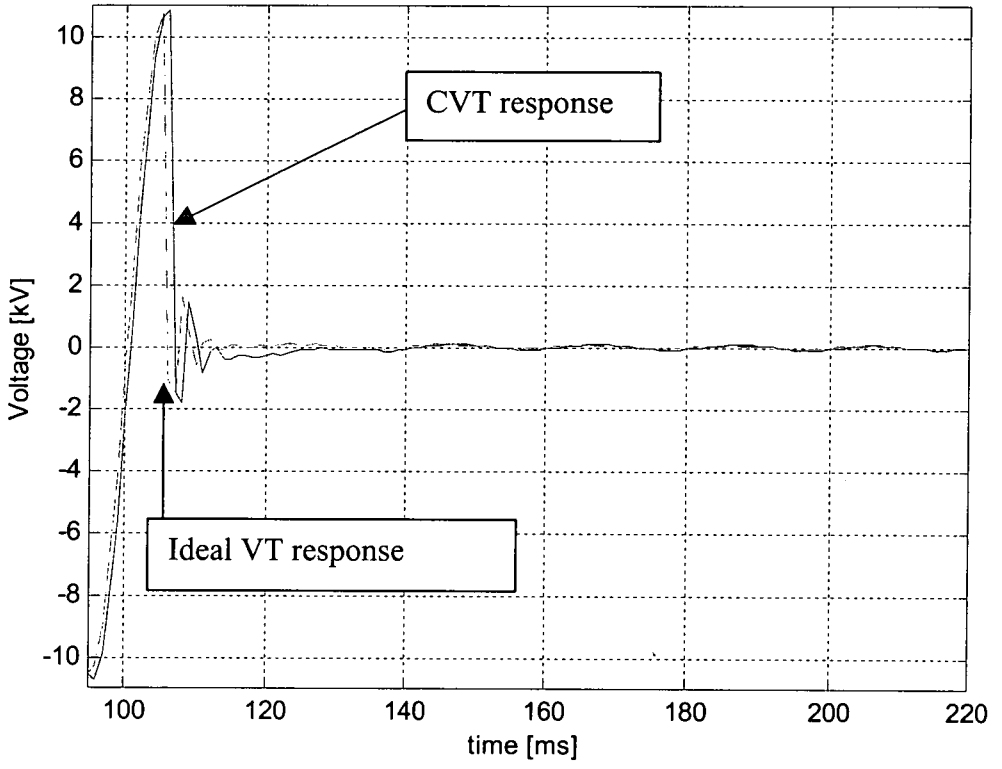

Figure 3.33: Fault at maximum voltage, i.e. angle 90^0. Fault location at 20 km from S-end busbar.

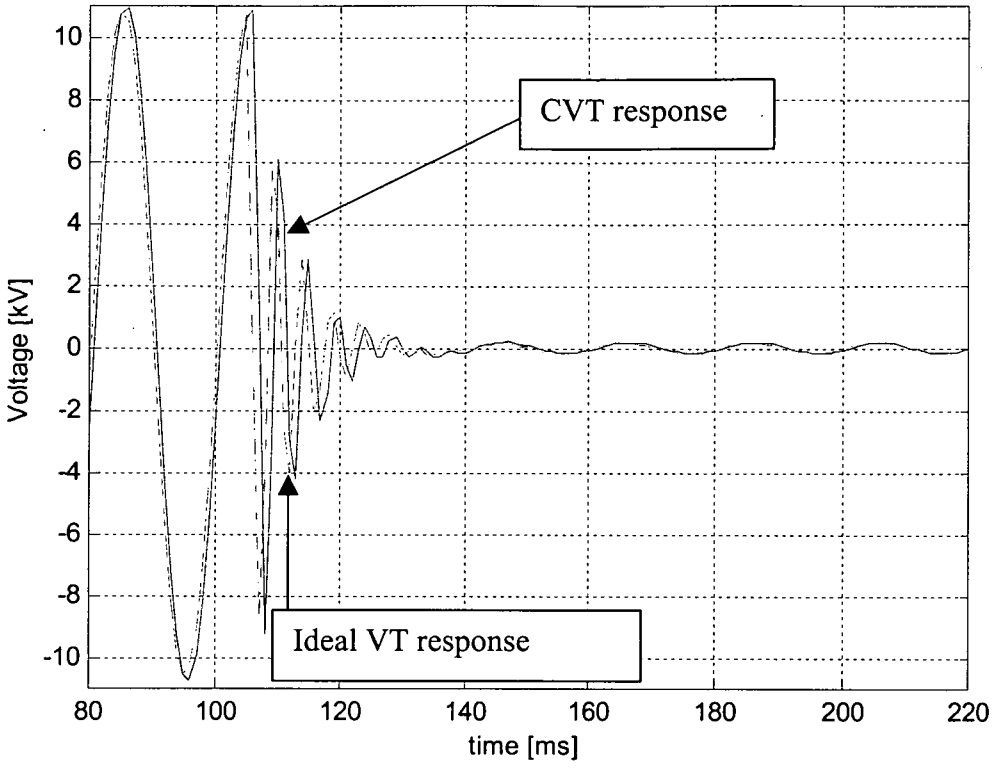

Figure 3.34: Fault at maximum voltage, i.e. angle 90^0. Fault location at 50 km from S-end busbar.

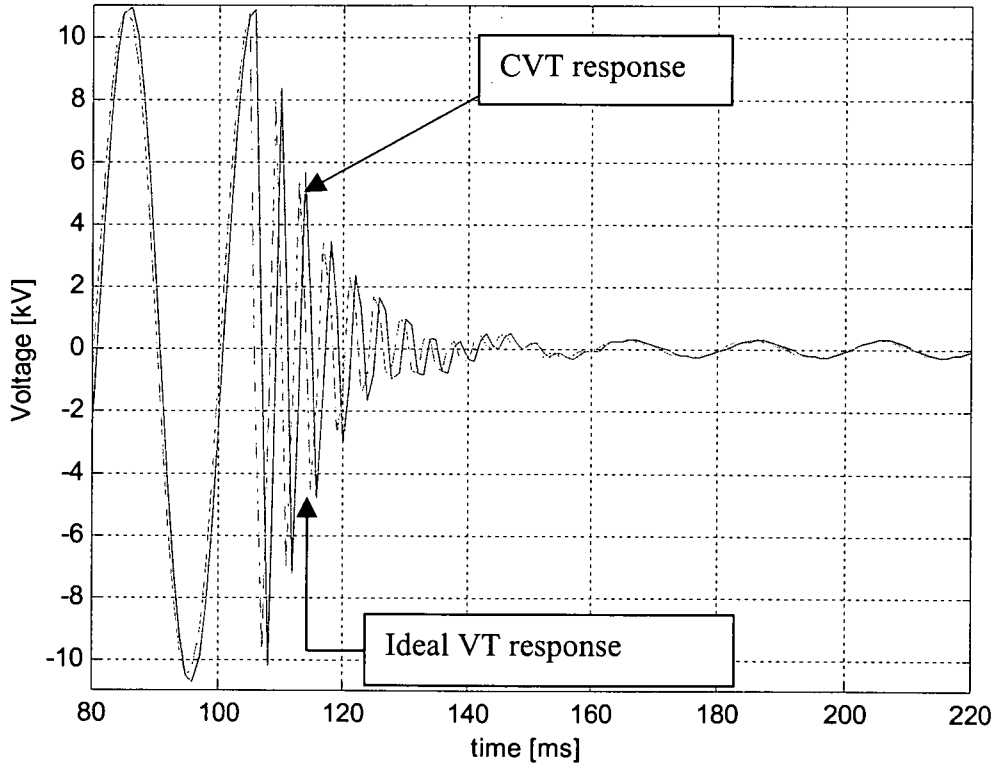

Figure 3.35: Fault at maximum voltage, i.e. angle 90^0. Fault location at 80 km from S-end busbar.

(c) Mid voltage: angle is equal to 45^0.

Figures 3.36 to 3.38 show the voltage response when fault was applied at mid voltage. The oscillation of transient is reduced and the magnitude is increased for each fault location case.

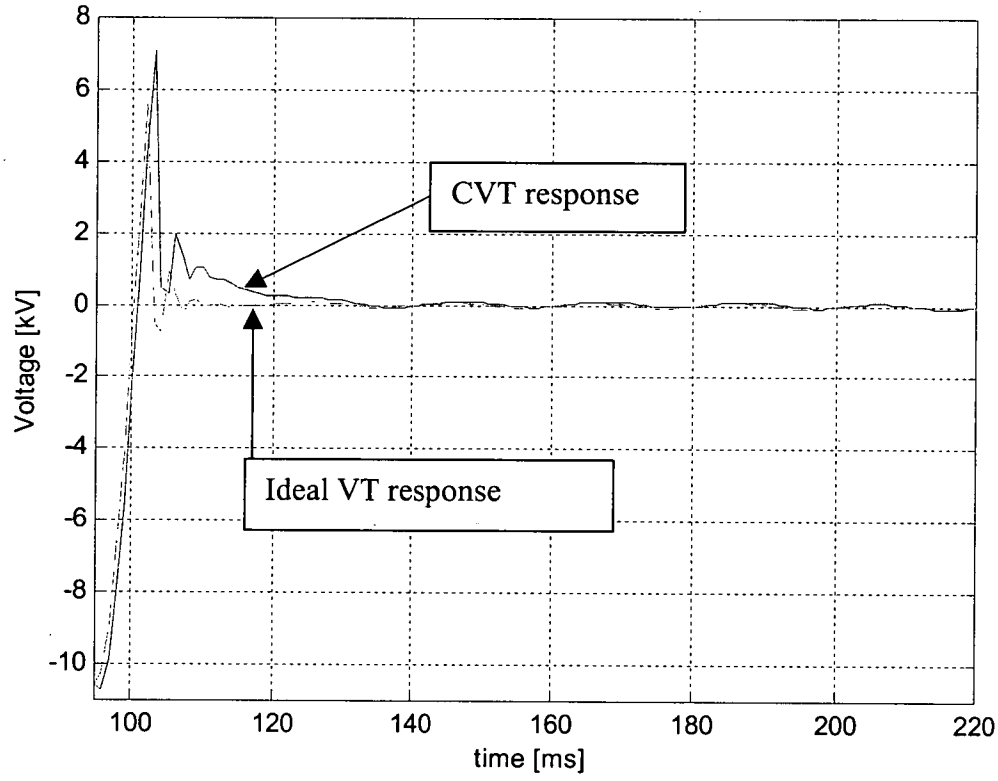

Figure 3.36: Fault at mid voltage, i.e. angle 45^0. Fault location at 20 km from S-end busbar.

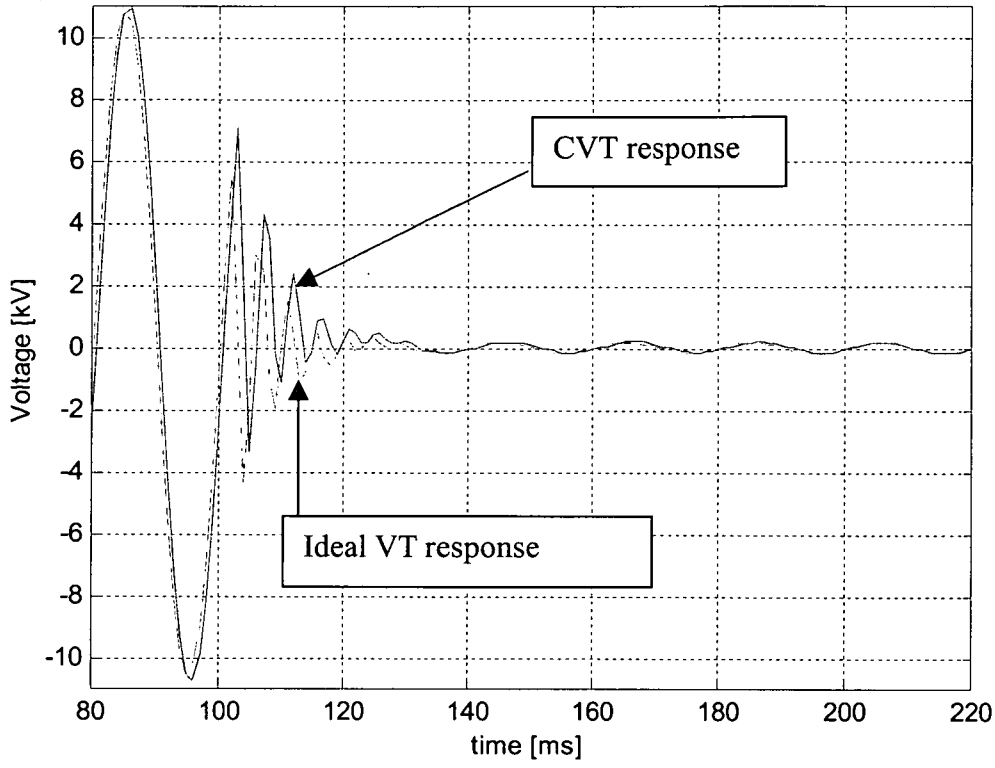

Figure 3.37: Fault at mid voltage, i.e. angle 45^0. Fault location at 50 km from S-end busbar.

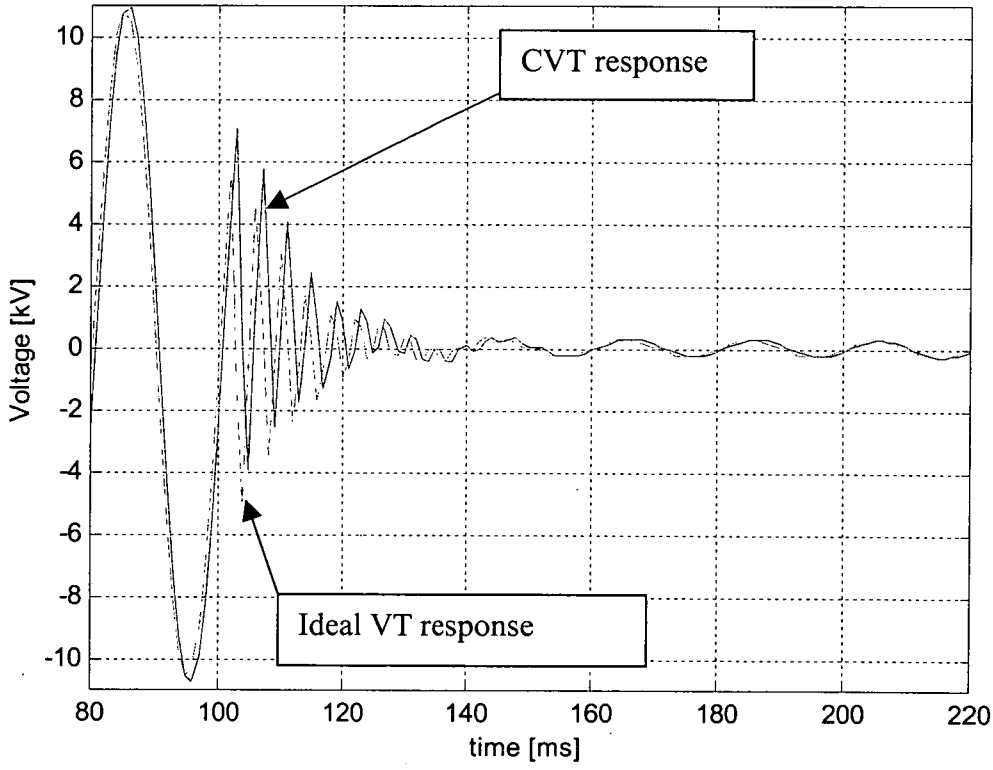

Figure 3.38: Fault at mid voltage, i.e. angle 45^0. Fault location at 80 km from S-end busbar.

3.3.4 *Impedance fault.*

Two values of ground fault resistance, 200 Ω and 50 Ω is used. The fault was applied at 0.1 second.

3.3.4.1 *With the Suppressing circuit disconnected.*

Figures 3.39 and 3.40 show the voltage response for 200 Ω and 50 Ω fault resistance respectively. It can be observed that as the fault resistance is increased, the amplitude of voltage after the fault occurred is increases too. Figure 3.5 in section 3.3.1.1 is used as a reference. Increasing R will affect Ex. Therefore it can be seen that the amplitude of the voltage after the fault occurred, Figure 3.39, is high compared with Figure 3.40.

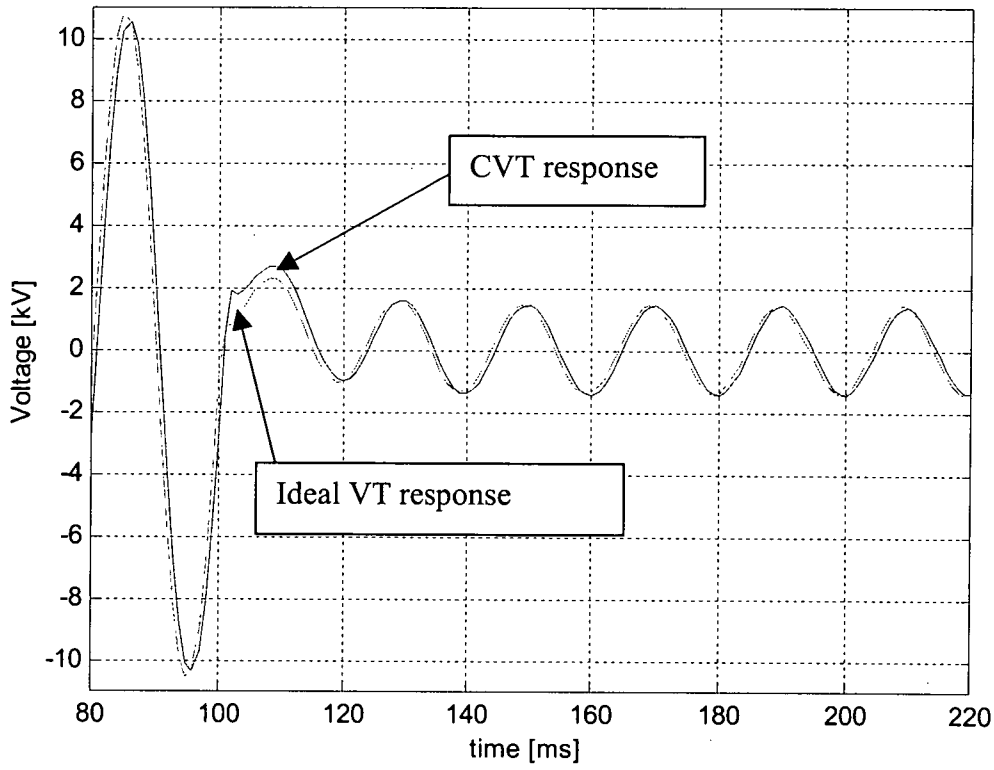

Figure 3.39: Voltage response for impedance fault, 200Ω. Fault location at 20 km from S-end busbar.

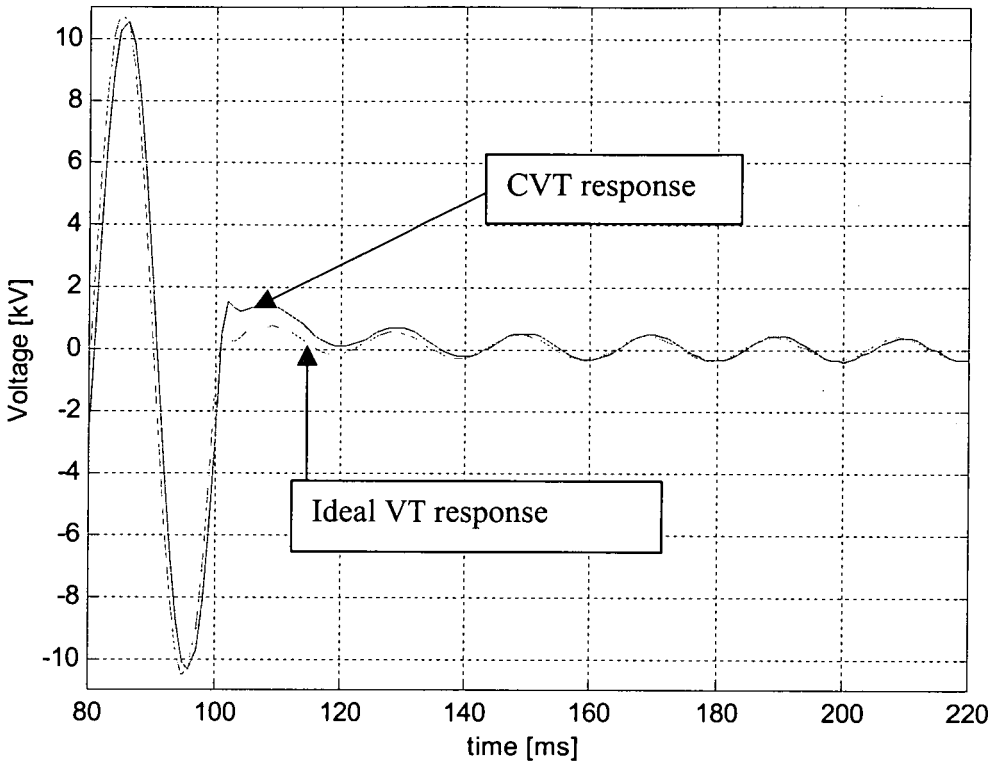

Figure 3.40: Voltage response for impedance fault, 50Ω. Fault location at 20 km from S-end busbar.

Figures 3.41 and 3.42 show the response of voltage signal for fault located at 50 km away from S-end busbar while Figures 3.43 and 3.44 show the response of voltage signal for fault at 80 km away from S-end busbar. It can be seen that as the fault resistance is increased, the amplitude of transient is increases as well.

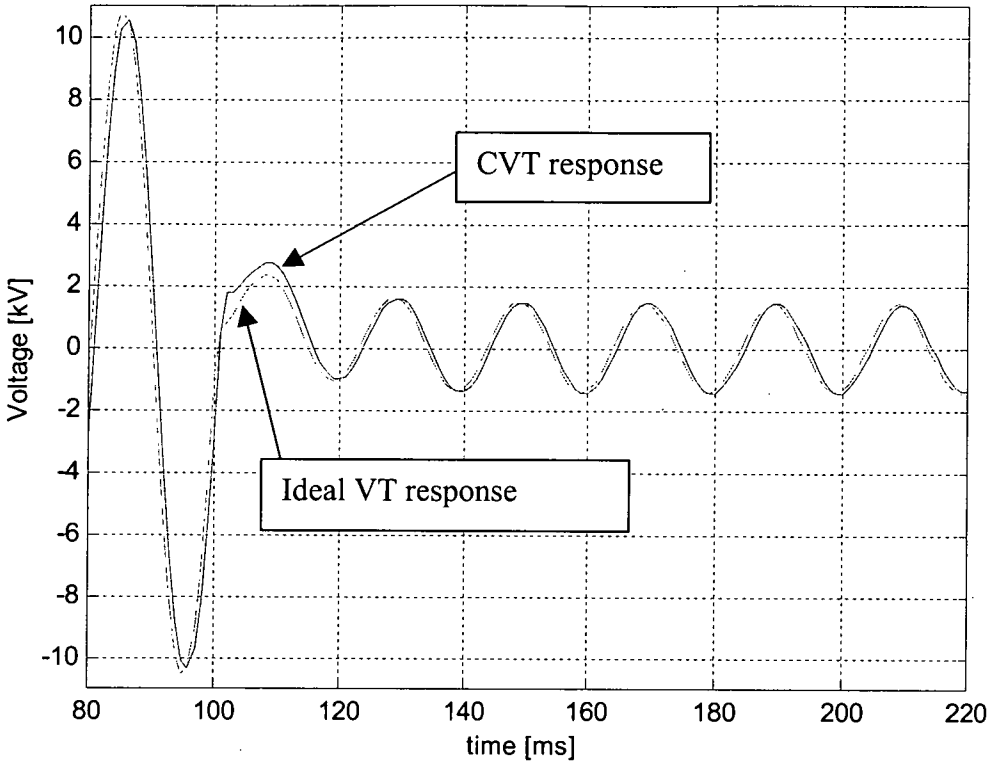

Figure 3.41: Voltage response for impedance fault, 200Ω. Fault location at 50 km from S-end busbar.

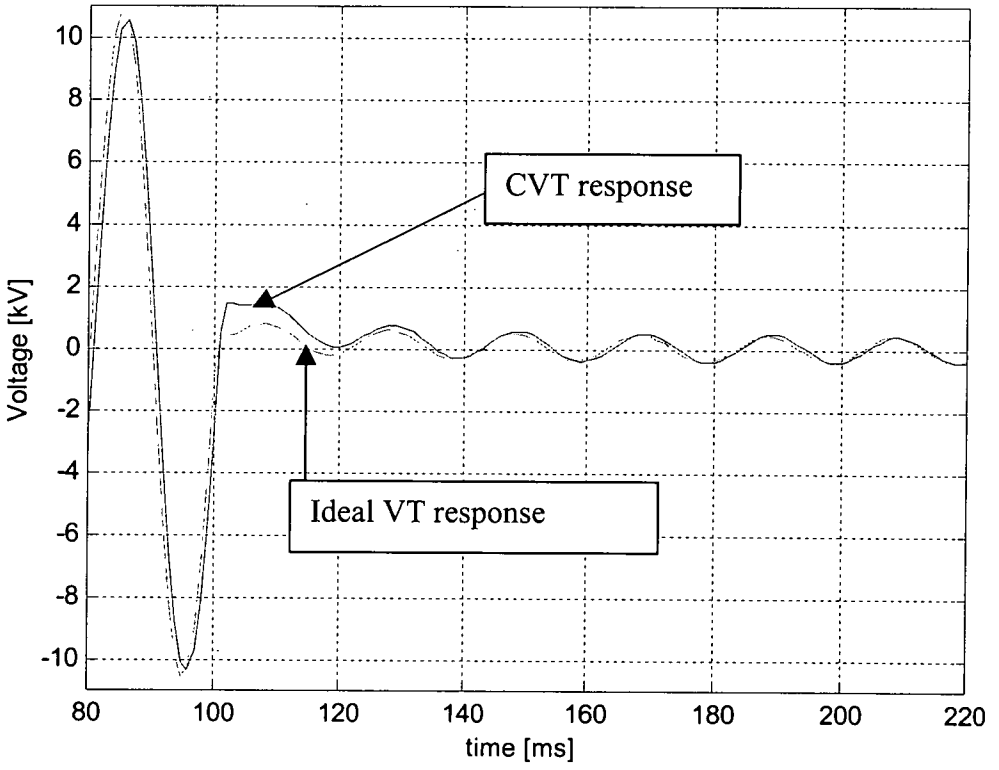

Figure 3.42: Voltage response for impedance fault, 50Ω. Fault location at 50 km from S-end busbar.

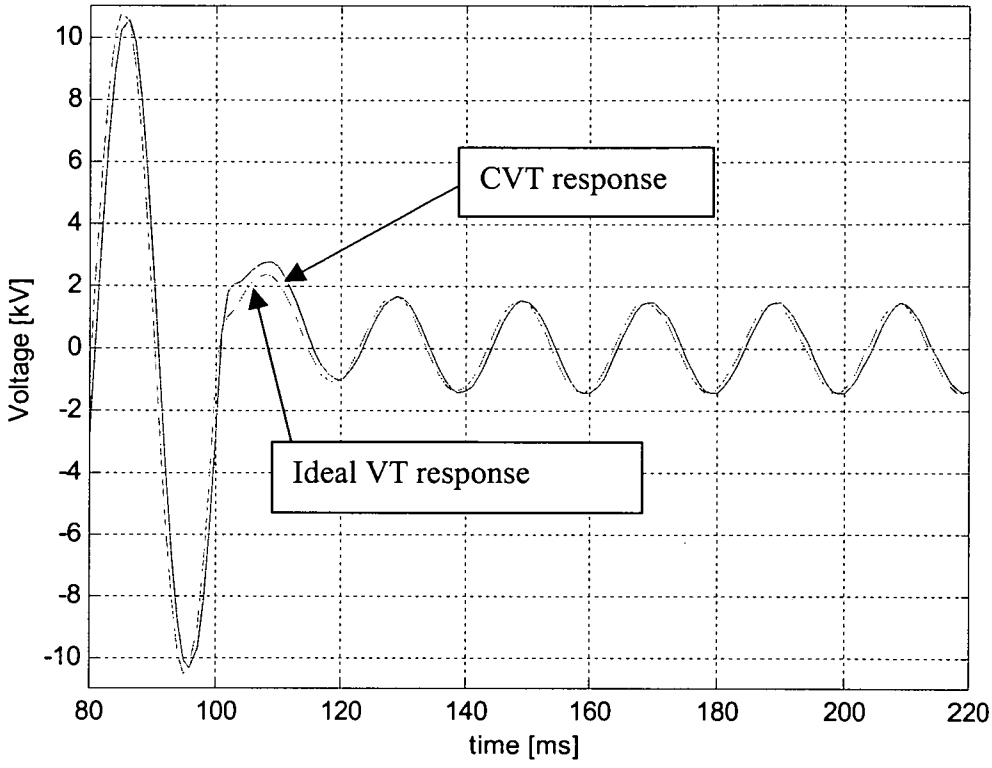

Figure 3.43: Voltage response for impedance fault, 200Ω. Fault location at 80 km from S-end busbar.

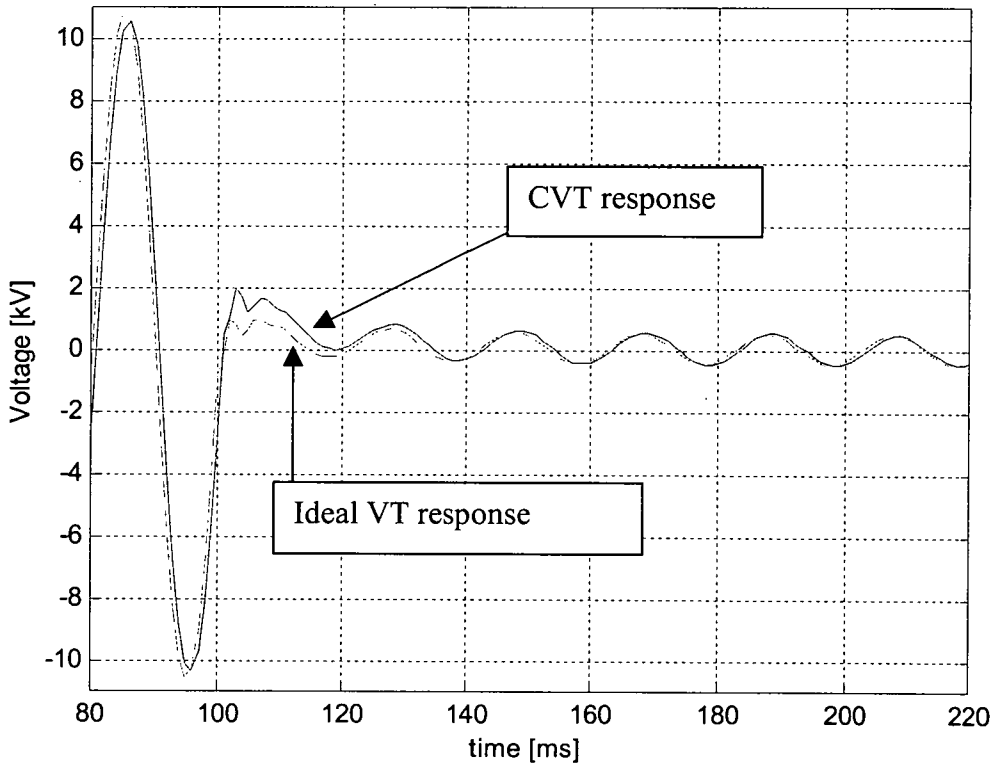

Figure 3.44: Voltage response for impedance fault, 50Ω. Fault location at 80 km from S-end busbar.

3.3.4.2 *With the Suppressing circuit connected.*

The amplitude of CVT transient increases when compared with response without the suppressing circuit as shown in Figures 3.45to 3.50. This due to the shape and parameters of the ferroresonance suppression circuit as explained in section 3.3.1.2.

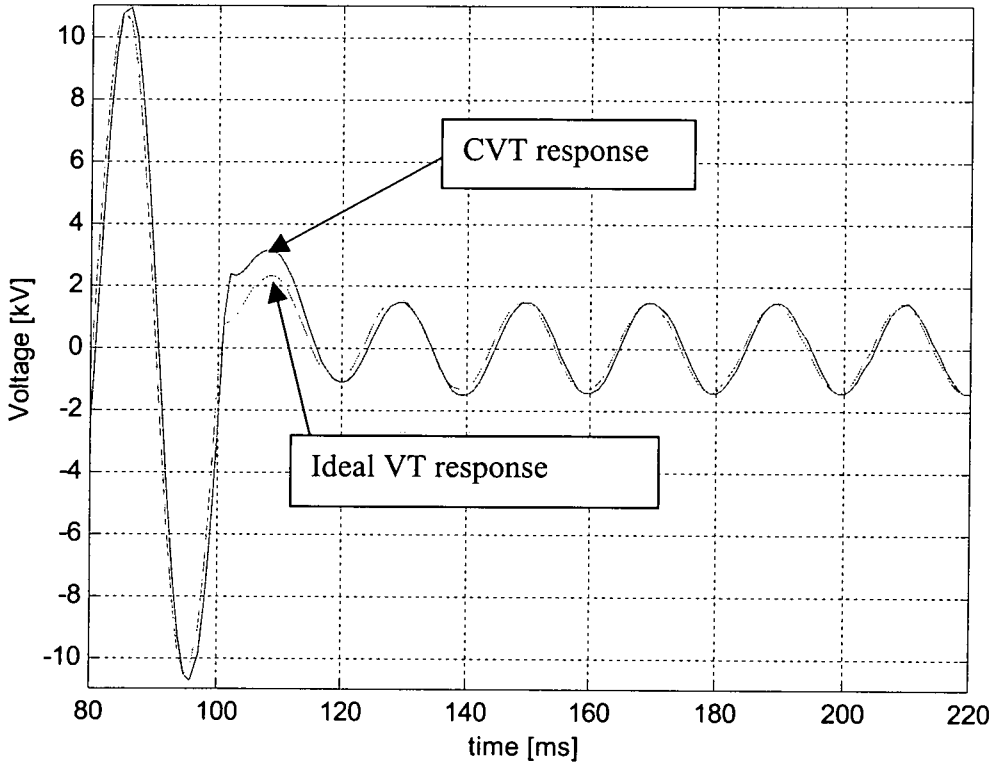

Figure 3.45: Voltage response for impedance fault, 200Ω. Fault location at 20 km from S-end busbar.

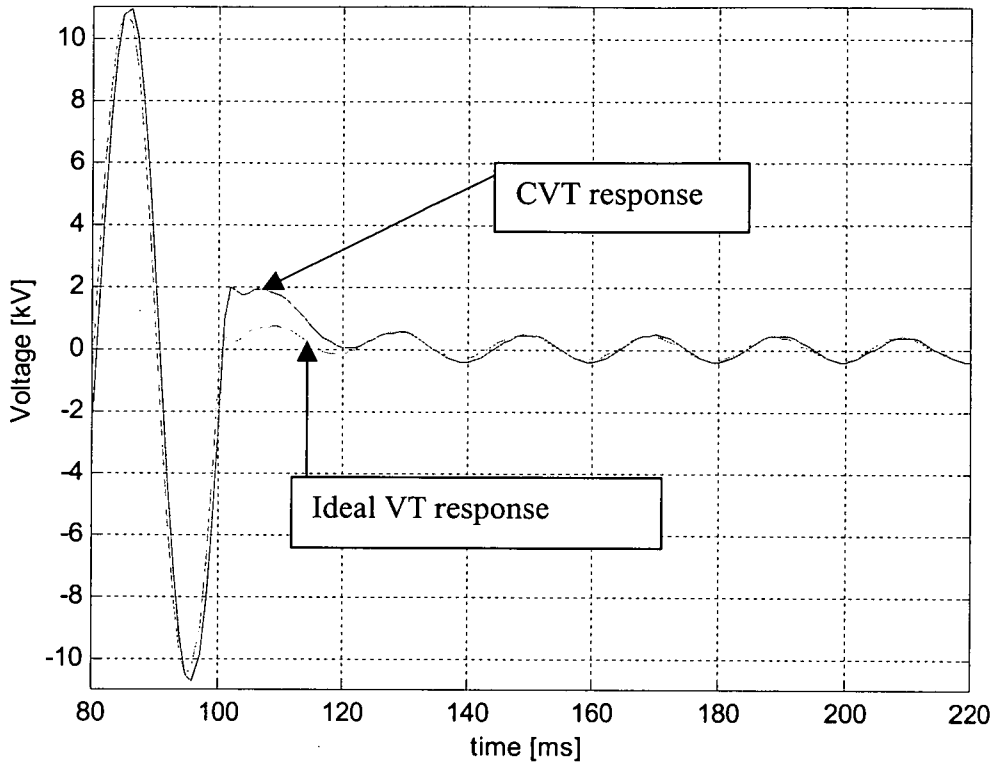

Figure 3.46: Voltage response for impedance fault, 50Ω. Fault location at 20 km from S-end busbar.

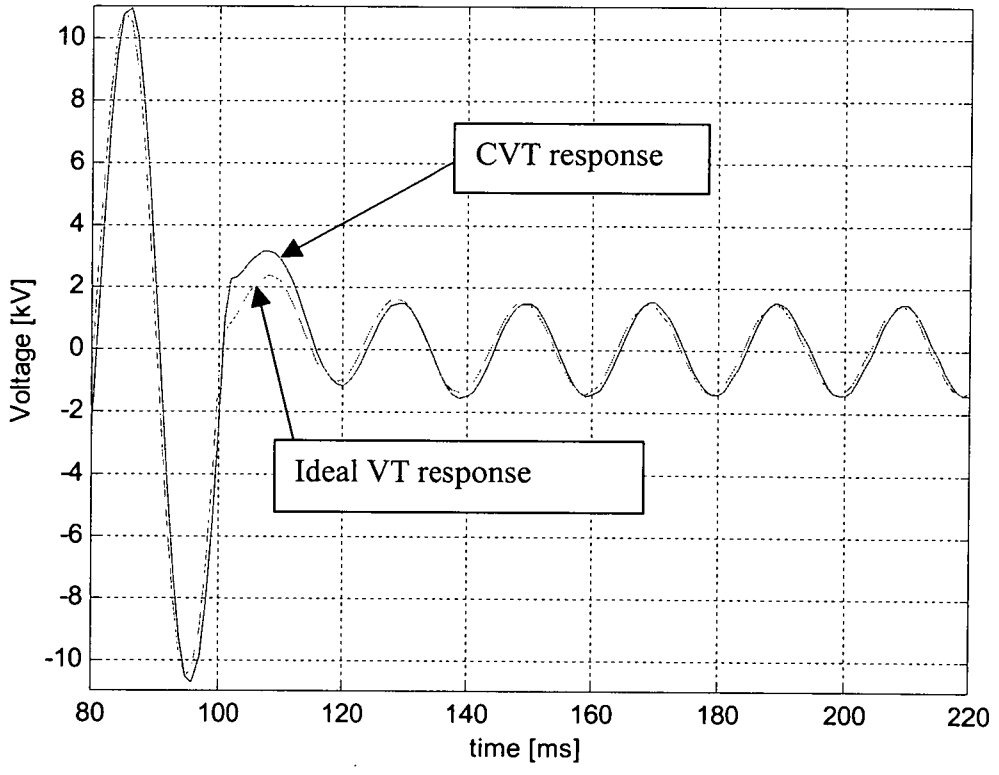

Figure 3.47: Voltage response for impedance fault, 200Ω. Fault location at 50 km from S-end busbar.

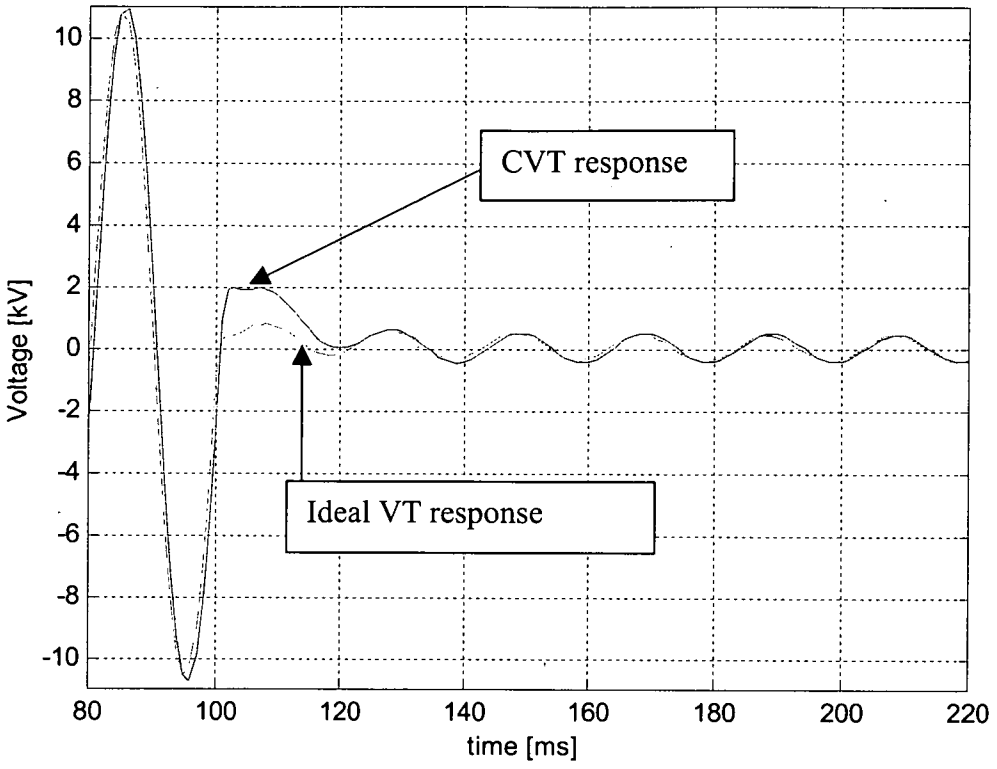

Figure 3.48: Voltage response for impedance fault, 50Ω. Fault location at 50 km from S-end busbar.

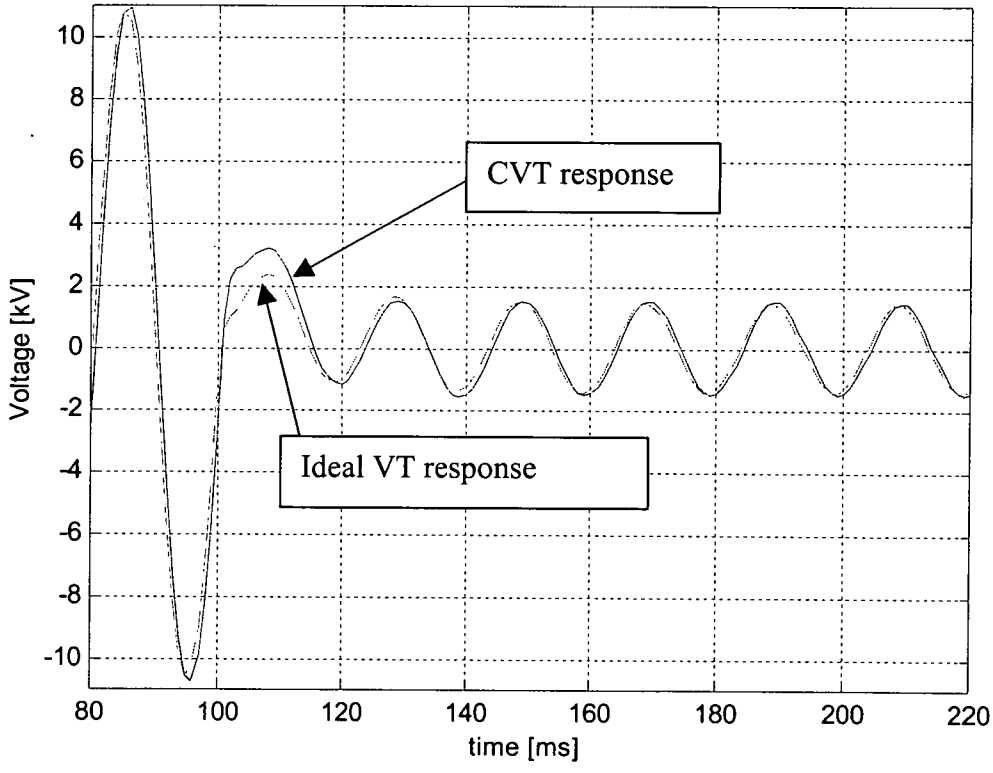

Figure 3.49: Voltage response for impedance fault, 200Ω. Fault location at 80 km from S-end busbar.

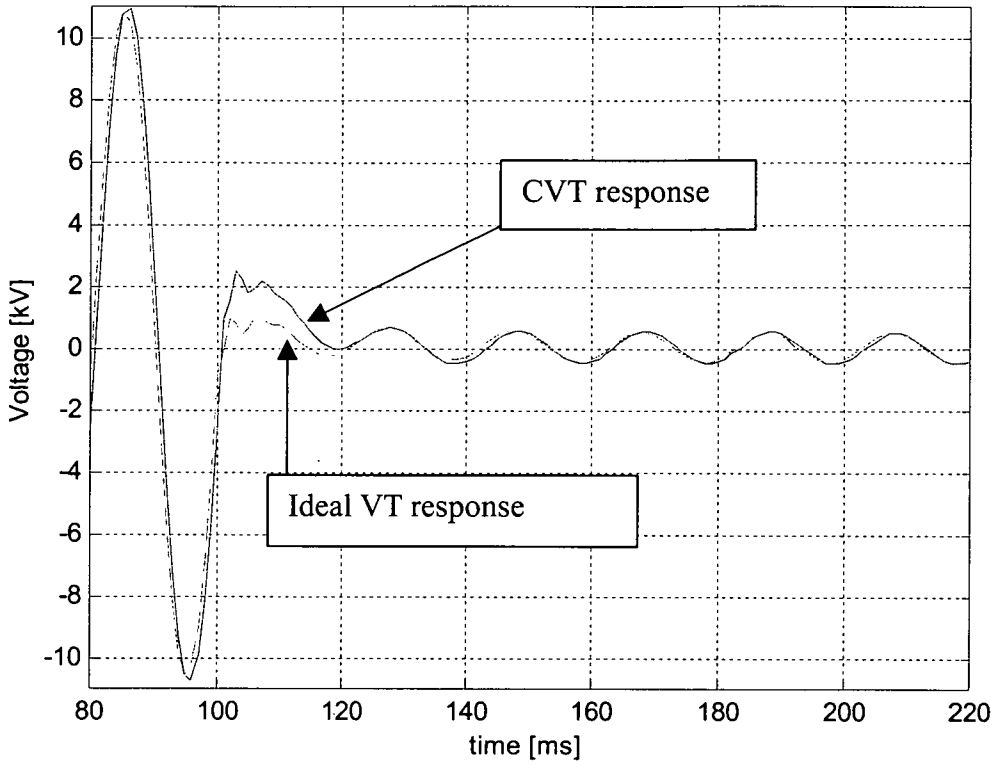

Figure 3.50: Voltage response for impedance fault, 50Ω. Fault location at 80 km from S-end busbar.

CHAPTER 4
EXPERIMENTAL

4.0 THE TEST BENCH

As mentioned in Chapter 1, to evaluate the effect on the performance of a Distance relay of a CVT, a test bench needs to be set up. The test bench comprises the following instruments:-

a) OMICRON CMC 56 Test Set.

b) OPTHIMO LFZP 111 Distance Relay.

c) Stabilised dc power supply to the distance relay at 48 Volts.

d) IBM-compatible PC with DOS or recently, Windows Operating System.

The software has been used in this project is CMC SW version 2.53. It has a hierarchical structure. It was designed in a tree-structure. Selecting a menu item indicated on a menu line allows us to

- move to another menu,
- execute an instruction, or
- move to a corresponding mask field.

The connection network of the test bench is illustrated in Figure 4.1.

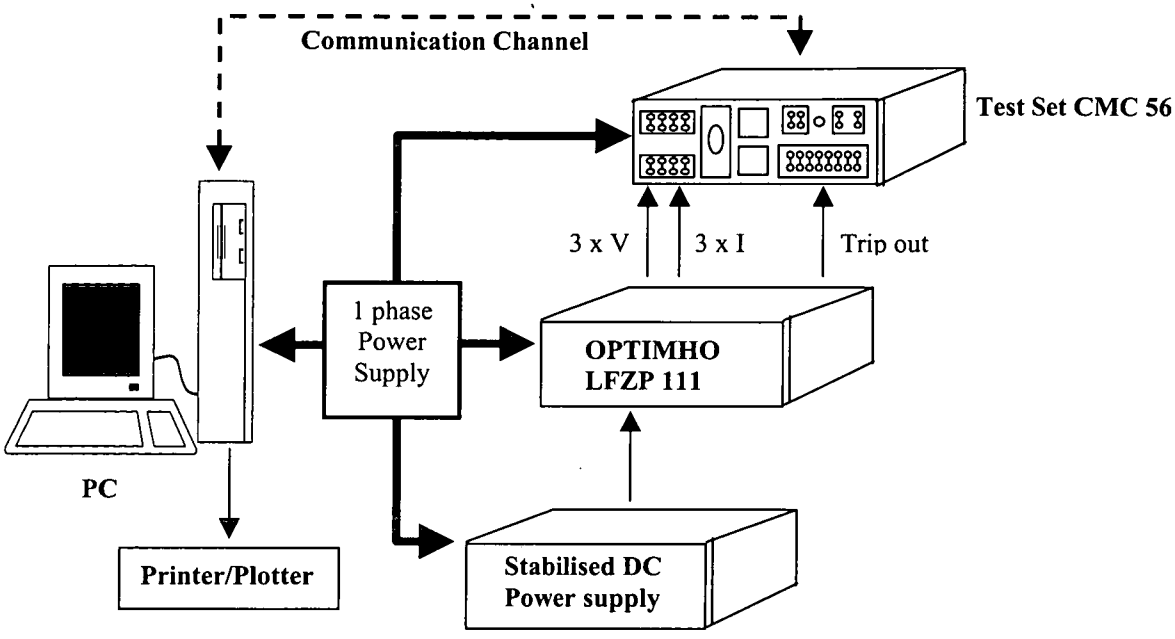

Figure 4.0: Connection network diagram of the test bench.

4.1 OMICRON CMC 56 Test Set.

OMICRON electronics is an international company that develops, manufactures, and markets state of the art test equipment for advanced testing of power system protection and measurement devices. The integration of lightweight and reliable hardware with flexible and user-friendly software is referred to as the OMICRON CMC Test Universe.

The CMC test system sets a new standard for versatility, accuracy, easy use and lightweight for the testing of power system protection and measuring devices. There are several types of CMC, e.g. CMC 56, CMC 156, CMC 156 EP, CMC 256-6 EP

and CMC 151. Type of CMC is used in this project is CMC 56, shown in Figure 4.1. While Figure 4.2 shows the front panel terminals of the unit.

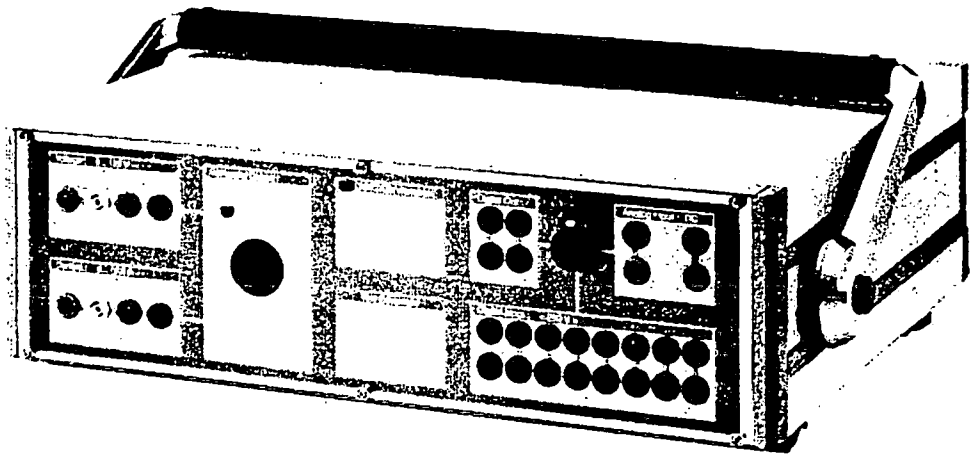

Figure 4.1: CMC 56 test set.

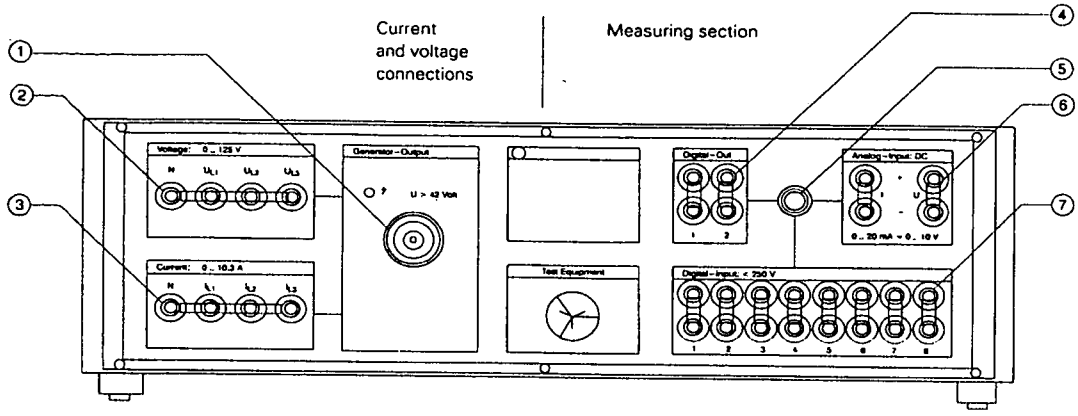

① Current and voltage group socket (parallel to the individual conenctions)

② Voltage connection U_{L1}, U_{L2}, U_{L3}

③ Current connection I_{L1}, I_{L2}, I_{L3}

④ Connection of the two internal potential-free contacts

⑤ Measuring component group socket
20-pole combination socket for the following connections (parallel to the individual connections)
- Current measurement input
- Voltage measurement inputs
- 10 contact inputs
- 2 outputs of internal isolated contacts

⑥ Analog current and voltage measurement inputs

⑦ Inputs 1 to 8

Figure 4.2: Front panel.

The CMC 56 test set is three-phase and software controlled. It is available to test Distance protection, overcurrent protection and differential protection equipment as well as monitoring relays, synchronising devices and measuring transducers. Steady state and dynamic tests, automatic program sequences and the playback of transient signals can all be performed from one uniform system in the CMC 56. The complete set of the CMC 56 test set is integration of the following items:

a) PC with DOS or Windows operating system.

b) Three-phase test unit in desktop design, incorporating current and voltage amplifiers, measurement sections and control electronics.

c) Software.

The operating software on a personal computer performs all control tasks and data acquisition, processing and recording of test results. The data exchange between the CMC and the PC is established via the parallel printer port available on every standard PC. The technical data of CMC 56 is attached in the Appendix C.

4.1.1 The software.

A mentioned in section 4.0, the version of CMC software has been used in this project is 2.53. This software offer the following advantages:

- User-friendly operation through a menu-driven user interface, mouse support and on-line help.
- Clear presentation of relevant data in graphical and tabular form
- Real time communication with the hardware, measured results are displayed on-line.
- No programming knowledge is required.
- No need for test files.
- Results are available in graphical and/or tabular form. Output options: printer, file or external analysis programs.
- Easy generation of key-macros.

4.2 OPTIMHO LFZP 111

The OPTIMHO LFZP 111, shown in Figure 4.3, is the model of Distance protection relay used in this project. It is full scheme static distance protection relay, in use for the main and backup protection of overhead (O/H) transmission, sub-transmission and distribution systems against phase and ground faults. This relay has the following characteristics:

- Voltage transformer supervision (VTS).
- Three independent zones with 18 measuring elements, one pair each for ground and phase faults for each zone.
- Optional fault locator with instrumentation.
- Selectable quadrilateral earth fault characteristic.
- Single or three phase tripping.
- Power swing blocking (PSB).
- Options of sensitive directional earth fault element with scheme options (DEF).
- Front panel is user interface, shown in Figure 4.4, for manual access to relay settings and fault records and has provision for remote communication via a modem.
- Available to store up to 8 independent groups of settings.

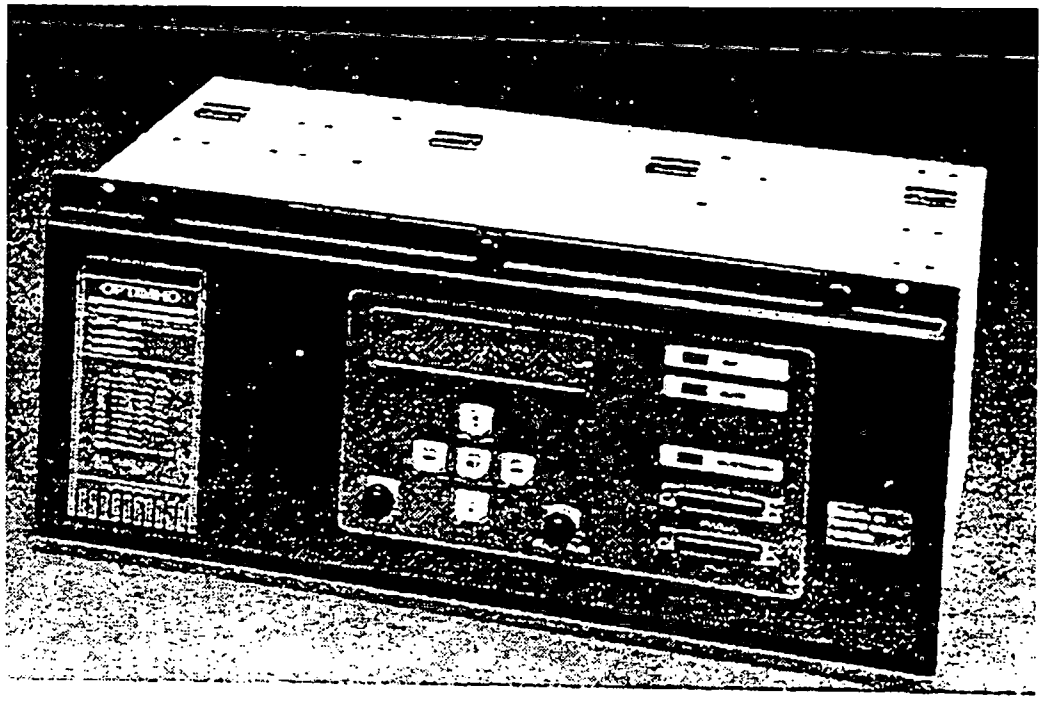

Figure 4.3: OPTIMHO LFZP 111.

4.2.1 Settings

The setting options allow the user to select functions to suit each application. However, the available options depend on the model of OPTIMHO. But usually include:

- Scheme type.
- Which distance zones are enabled (up to 5 zones).
- Whether ground fault time delayed zones are enabled.
- Direction of reach-stepped zones or of Zone 3.
- Whether start indications are required for remote faults which do not result in a trip.

- Eight independent groups of settings which are stored in the relay memory and are selectable from the menu.

In this experiment following setting has been set up:

- Zone 1, Zone 2 and Zone 3 are enabled.
- Distance characteristic is self-polarised mho.

4.2.2 Integral User Interface.

Figure 4.4 shows the user interface on front panel of OPTIMHO. All relay settings and records are accessible from this integral user interface. The records can be obtained by pressing READ button. After the indications have been read, pressing RESET button can clear them. The cursor and SET buttons are used for selection of menu options and for entering the relay settings.

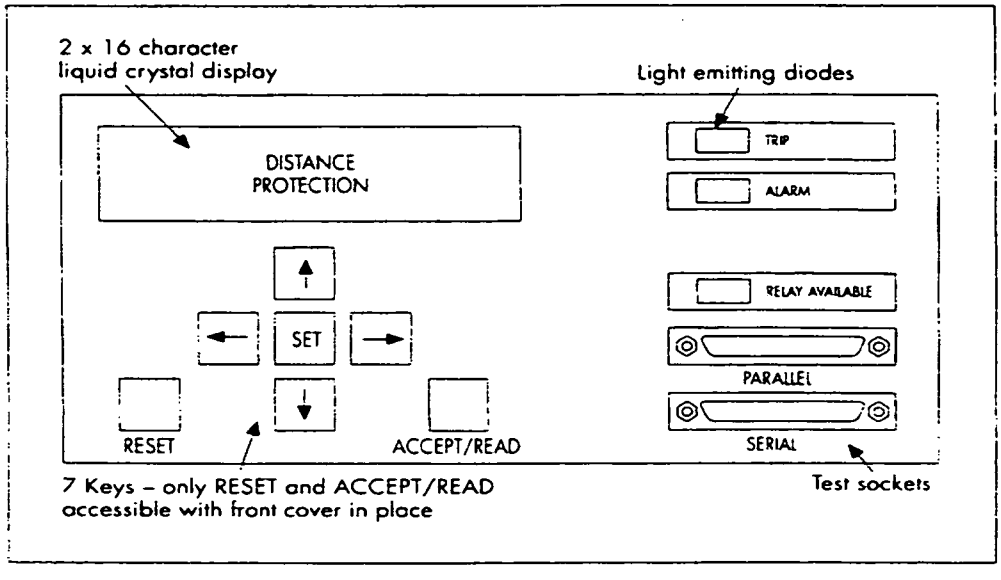

Figure 4.4: User interface on front panel.

The menu holds an extensive range of options, including:

- Viewing records of the LCD indications from the last four faults.
- Printing records or settings on a portable printer plugged into the parallel test socket.
- Entering a relay identification code for use on printouts.
- Comprehensive test options such as:
  - Blocking output contacts.
  - On load directional testing.
  - Monitoring test points on the parallel socket.
  - Closing selected output contacts for testing purposes.
- Setting up the baud rate and protocol for the serial communications.

4.2.3 Relay Setting Calculations.

In this project the forward and reverse zone settings are calculated as below:

Line impedances.

Positive sequence impedance $= Z_{L1} = 0.4216\angle 85.22^0$ (see Appendix D).

Zero sequence impedance $= Z_{L0} = 1.2068\angle 75^0$ (see Appendix D).

C.T. ratio = 1200/1

V.T. ratio = 400,000/110 (for the OPTIMHO V.T. ratio is 3635/1)

Therefore secondary to primary impedance ratio is equal to

C.T. ratio/V.T. ratio = 0.33

Length of line = 100 km

Zone 1 Reach Setting.

Zone 1 is set to 80% of protected line:

Zone 1 (secondary) = $0.8 \times 100 \times 0.4216\angle 85.22^0 \times 0.33$

$= 11.129\angle 85.22^0$ ohms.

For the OPTIMHO setting:

Zone 1 = $KZ_{ph} \times KZ1 \times 5 / In$

KZ_{ph} setting range is from 0.040 to 1.0 in steps of 0.001 (refer to Appendix E). To obtain maximum relay sensitivity KZ_{ph} should be set as high as possible as the current setting of the relay current level detector is inversely proportional to it. Therefore let KZ_{ph} is equal to 1.0. From the equation by OPTIMHO above, KZ1 therefore equal to 2.22.

The relay characteristics angle, θ_{ph}, has setting range of 50^0 to 85^0 in steps of 5^0 (refer to Appendix E). Hence $\theta_{ph} = 85^0$. Therefore the actual zone 1 settings for the OPTIMHO is $11.1\angle 85^0$ ohms.

Zone 2 Reach Setting.

Zone 2 is set to 120% of protected line:

Zone 2 (secondary) = $1.2 \times 100 \times 0.4216\angle 85.22^0 \times 0.33$

$= 16.695\angle 85.22^0$ ohms.

For the OPTIMHO setting:

$$\text{Zone 2} = KZ_{ph} \times KZ2 \times 5 / In$$

Same as zone 1 setting,

$$KZ_{ph} = 1.0.$$

Therefore KZ2 is equal to 3.34.

Actual zone 2 settings for the OPTIMHO is $16.7\angle 85^0$ ohms.

Zone 3 Reach Setting.

$$\text{Zone 3 (secondary)} = 1.2 \times (2 \times 100) \times 0.4216\angle 85.22^0 \times 0.33$$

$$= 33.391\angle 85.22^0 \text{ ohms.}$$

For the OPTIMHO setting:

$$\text{Zone 3} = KZ_{ph} \times KZ3 \times 5 / In$$

Same as zone 1 setting,

$$KZ_{ph} = 1.0.$$

Therefore KZ3 is equal to 6.68.

Actual zone 3 settings for the OPTIMHO is $33.4\angle 85^0$ ohms.

Zone 3 Reverse Reach Setting.

$$\text{Zone 3 (secondary)} = 0.2 \times (2 \times 100) \times 0.4216\angle 85.22^0 \times 0.33$$

$$= 2.783\angle 85.22^0 \text{ ohms.}$$

For the OPTIMHO setting:

$$Z3' = KZ_{ph} \times KZ3' \times 5 / In$$

Same as zone 1 setting,

$$KZ_{ph} = 1.0.$$

Therefore KZ3' is equal to 0.459. Possible settings for the reverse zone 3 multiplier factor has arrange of 0.2 to 49.9 in steps of 0.1 (refer to Appendix E). Hence,

KZ3' is equal to 0.6.

Actual reverse zone 3 settings for the OPTIMHO is $3.0\angle 85^0$ ohms.

Earth Fault Residual Compensation.

Residual compensation factor, $KN = (Z_{L0} - Z_{L1}) / (3 \times Z_{L1})$

$$= 0.6427\angle -15.62^0$$

Residual Compensation Setting, $KZN = KN \times KZ_{ph}$

$$= 0.6427\angle 69.6^0$$

The setting range for KZN is from 0 to 1.36 in steps of 0.001. Therefore KZN is equal to $0.64\angle 70^0$.

4.3 RELAY TESTS

To test the relay using the transient voltage and current signals obtained in Chapter 3, the menu option *Transient* is selected. This program section permits the reading, editing and outputting of signals of any wave shape, i.e. voltages and currents. Under this option transient faults from various simulation software can be replayed by the CMC 56 test device and fed to the relay to determine the relay response to these faults. The format that is available in this option is OMICRON format (TRF) or COMTRADE format (CFG).

In order to apply the transient fault signals obtained in Chapter 3 into the CMC 56 test device, PSCAD/EMTDC is used. In PSCAD/EMTDC the transient fault signals were recorded using 'real-time playback (rtp) recorder' component that available in the main library of the transient simulator. The rtp recorder can record analogue transient signals in digital formats of RTP, COMTRADE 91 and COMTRADE 97. The OMICRON software v2.53 supports COMTRADE 91.

4.3.1 Testing and results.

Table 3 show the test results for single phase fault with the CVT. Table 4 show the test results for single phase fault without the CVT. The report for all test results is shown in Appendix F. Figures 4.5 and 4.6 illustrate the graphical presentation of the data for single phase to ground fault in Table 3 and 4 respectively.

Table 3: Relay response for single phase to ground fault with CVT.

		Single phase to ground faults	
Fault Location (km)	Nominal Zone	Tripping Zone	Operating time (ms)
10	1	1	64
20	1	1	46
30	1	1	44
40	1	1	34
50	1	1	34
60	1	1	33
70	1	1	33
80	1	1	48
100	2	1	48
120	2	2	450
150	3	2	450
160	3	2	436
180	3	3	801
200	3	3	737

Table 4: Relay response for single phase to ground fault without CVT.

		Single phase to ground faults	
Fault Location (km)	Nominal Zone	Tripping Zone	Operating time (ms)
10	1	1	35
20	1	1	34
30	1	1	40
40	1	1	36
50	1	1	36
60	1	1	36
70	1	1	37
80	1	1	38
100	2	1	33
120	2	2	420
150	3	2	414
160	3	2	412
180	3	3	784
200	3	3	756

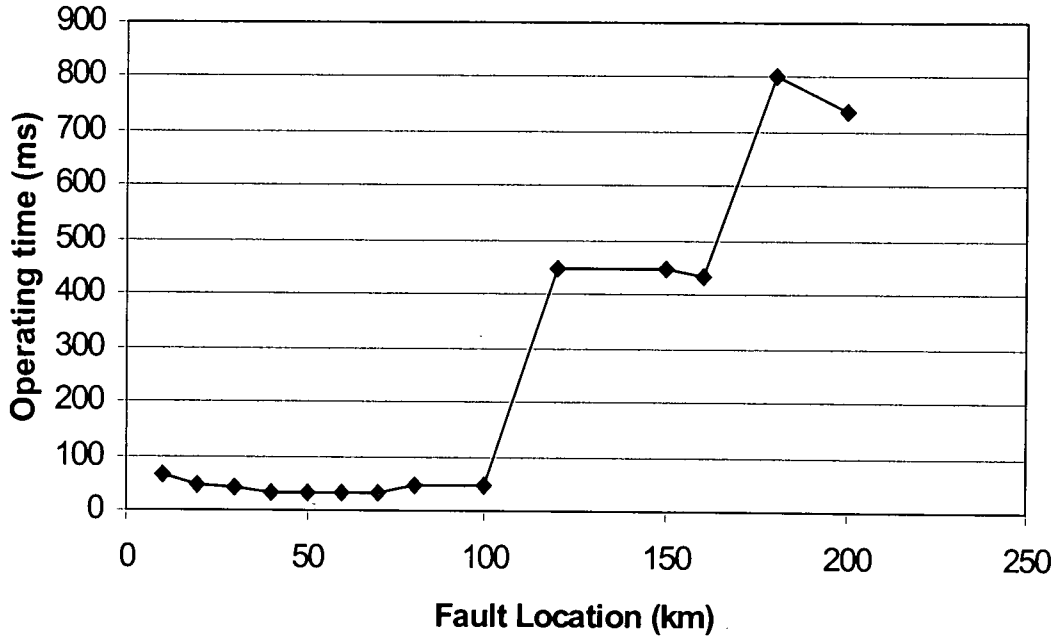

Figure 4.5: Single phase to ground fault with CVT.

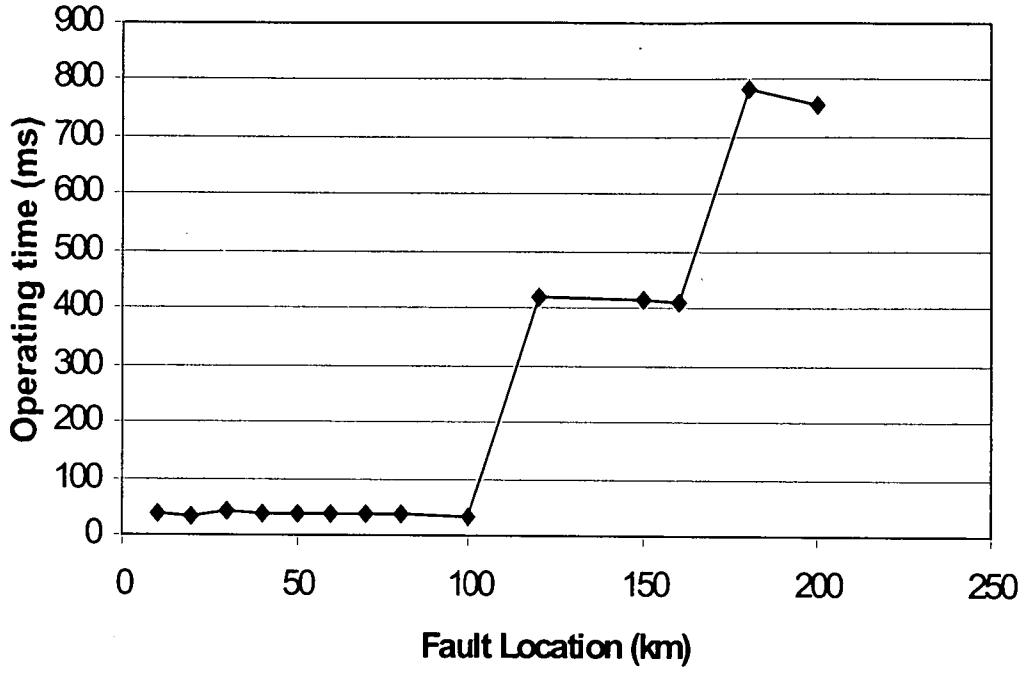

Figure 4.6: Single phase to ground fault without CVT.

From Figure 4.5 and 4.6 show slight differences between the operating time of the distance relay with and without CVT. Especially when fault occurred at 10 km of the line. This is due to the transients generated by CVT itself. For example, lets take an example given in [12] as a reference. The 50 Hz voltage signal carrying the information as to the fault location is buried beneath the CVT noise for a long time. If the faults occurred at 75% at reach, the relay must set apart the voltage of 3% x 0.75 =2.2% of the nominal (tripping) and 3% of the nominal (blocking). The difference of 0.8% of the nominal must be sensed in the situation when the noise assumes the level of 30% of the nominal. Normally a relay would not trip until the CVT transients die out and 50 Hz signal emerges from beneath the noise. As stated in [12], albeit phasor estimators with short data windows are used it will not improve the situation.

However it is not influenced at all the performance of the distance relay. We can see that the average of the operating time of the zone 1 (0-100%) with CVT is around 42 ms and without CVT is around 36 ms for single phase to ground fault. The zone 2 for both, i.e. with and without CVT, tripping for the single phase to ground fault occurred at 120% of the length which is equal to 120 km of the line. The zone 3 for both, i.e. with and without CVT, tripping for the single phase to ground fault occurred at 180% of the length which is equal to 180 km. Figure 4.7 and 4.8 show the differences between zones reach of nominal and experiment results. It can be seen that there are extended zones reach for experiment results compared with nominal zones reach. It most probably due to the noise contributed by distributed parameter line model.

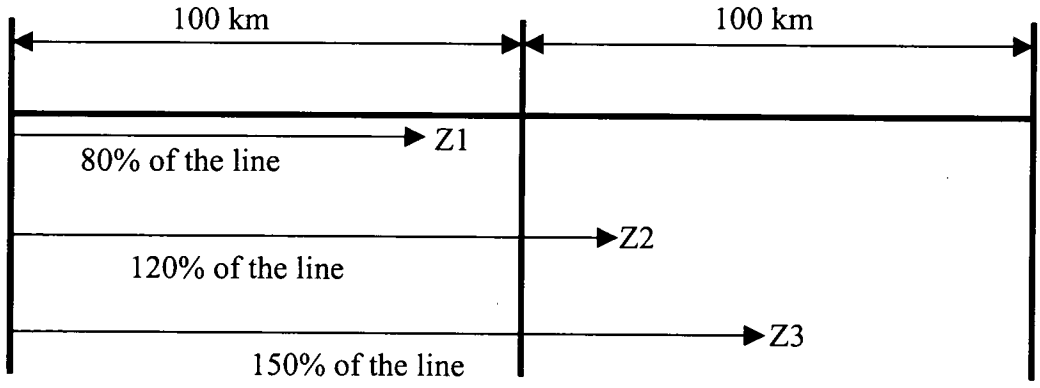

Figure 4.7: Nominal zones reach diagram.

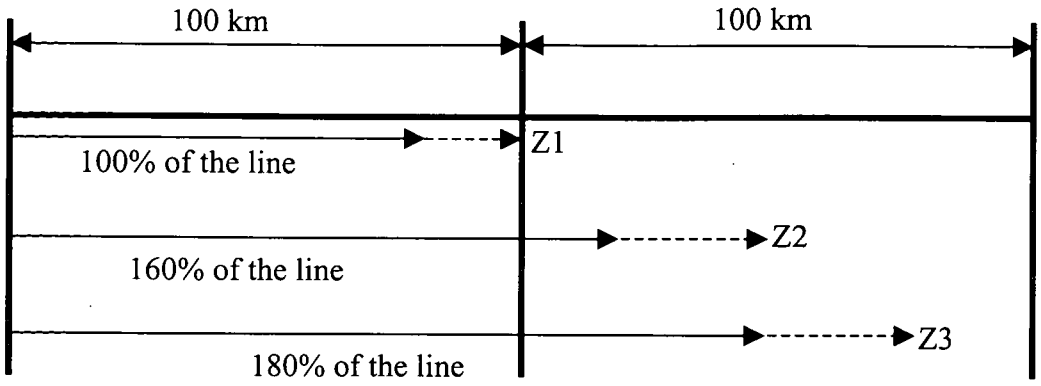

Figure 4.8: Experiment zones reach diagram.

CHAPTER 5
CONCLUSIONS

5.0 CONCLUSIONS AND DISCUSSIONS

Representing the CVT by an equivalent circuit and using the method of inverse Fourier transform to examine the transient generated by CVT is a very effective and efficient way to assess the performance of distance relay.

All the results obtained in Chapter 3 support the conclusion that the CVT transients basically controlled by the following factors:

- **Sum of the stack capacitances.**

The higher the sum of the stack capacitances, the lower the magnitude of the transients. Therefore, judging only from the magnitude of the CVT transient, one should recommend CVTs with higher sum of the stack capacitances to be used to feed distance relays with the voltage signals.

- **Shape and parameters of the ferroresonance suppression circuits.**

By introducing suppressing circuit, we can see that the magnitude of the transient of the CVT transient is increased. The transient also take extra cycles to reach steady state. It is because the suppressing circuit loads a CVT and creates an extra path for the dissipating energy. Therefore, the suppressing circuit has significant impact on the characteristic of the CVT transients.

- **Point on wave when fault occurs.**

The most severe transients are generated when a fault occurs at the zero crossing of the voltage. The accumulated energy is then at its maximum resulting in larger magnitudes of the transient components. The least severe transient occurs during faults initiated at the maximum wave point.

From results obtained in Chapter 4, we can conclude that the CVT transients influence the speed of the relay. It will slow down the relay for in zone faults as the fault location increases. However the results obtained in Chapter 4 are not quite consistent as we can see in Table 3 and 4. It will be more interesting if various type of faults such as phase to phase, phase to phase to ground and three phase to ground were applied in the experiment. Therefore from the results we can observe and analyse more information about the performance of the distance relay affected by CVT transients is required.

5.1 Future work.

Another factor that can be used to control the CVT transient is the total load of the CVT. It is possible to modify the total load of the CVT so as to avoid a transient voltage of a frequency or an amplitude particularly ill adapted to a given type of relay. Therefore in the future try to investigate the performances of the relays by modifying the total load of the CVT.

REFERENCES

[1] G.A.GERTSCH, *Capacitive Voltage Transformers And Their Operation In Conjunction With System Protection Relays*, CIGRE 1960, Report 318.

[2] G.A. GERTSCH, F.ANTOLIC, F.GYGAX, *Capacitor Voltage Transformers And Protective Relays*, CIGRE 1968, Report 31-14.

[3] WONG CHEE WEE, *The Simulation of Capacitor Voltage Transformer Using MATLAB,* Bachelor Degree, UMIST.

[4] G.R.JONES, M.A.LAUGHTON, M.G.SAY, *Electrical Engineer's Reference Book*, Butterworth Heinemann Ltd.,15th Edition, 1993, pp 3/32-3/34.

[5] M.S. NAIDU, V. KAMARAJU, *High Voltage Engineering*, McGaw-Hill, Second Edition, 1995, pp 191-194.

[6] LJ. KOJOVIC, M.KEZUNOVIC, C.W.FROMEN, *A New Method For The CCVT Performance Analysis Using Field Measurements, Signal Processing And EMTP Modelling*, IEEE Transactions on Power Delivery Vol-9, No. 4, October 1994, pp 1907-1914.

[7] ADRIAN BIRAN, MOSHE BREINER, *MATLAB for Engineers,* Addison-Wesley Publishing Company, 1996.

[8] THE ELECTRICITY COUNCIL, *Power System Protection, Volume 1,* Macdonald & Co. (Publishers) Ltd, 1969, page 32-37.

[9] KO YU MING, *Transient Response of CVT,* MSc Dissertation, UMIST.

[10] STANLEY H. HOROWITZ, ARUN G. PHADKE, *Power System Relaying, Second Edition,* Research Studies Press Ltd., 1995, Chapter 3 and Chapter 11.

[11] MUHAMMAD SHAHID KHAN, *An Investigation Into The Effects o FACTS Devices on Distance Relays,* MSc Dissertation, UMIST.

[12] BOGDAN KASZTENNY, DAVE SHARPLES, VINCE ASARO, MARZIO POZZUOLI, *Distance Relays And Capacitive Voltage Transformers – Balancing Speed And Transient Overreach*, 53rd Annual Conference for Protective Relay Engineers.

[13] PSCAD/ EMTDC User's Guide/ Manual version 3.1.

[14] User Manual CMC Software Version 2.53.

[15] Siemens Information Brochure, R2.13.1994: Three-Phase Portable Test Set 7VP151 (OMICRON CMC 56).

[16] Instruction Manual for Opthimo LFZP Distance Relays.

[17] The MathWorks, Inc., *MATLAB for Windows User's Guide,* December 1991.

APPENDIX A

```
%******************CVT without ferroresonance cct.***********
global R1 R2 L1 Lm C1 C2 f w Z1 Z2 H Rf If RR II HH ht hht
%*********************************************************

%Value of CVT's components simplified circuit
R1=3289;
R2=1.03997e+5; %represent load resistance(Ro)
C1=86e-9; %represent the total capacitance(C)
C2=1.06e-9;
L1=1.136; %represent the total inductance(L)
Lm=2.705e+4;


f=1:2:2000;
w=2*pi*f;
Z1 =R1+i*(w*L1-1./(w*C1));
Z2=(i*w*Lm)./(1-w.^2*C2*Lm);
H=(Z2*R2)./(Z1.*Z2+Z1.*R2+Z2.*R2);

Rf=real(H);
If=imag(H);
c=1:500;
RR(c)=Rf(c);
c=501:1000;
RR(c)=Rf(1001-c);
subplot(2,1,1),plot(f,Rf);xlabel('freq');ylabel('Amplitude');
title('Real part of H(w) function');grid;
subplot(2,1,2),plot(f,RR);xlabel('freq');ylabel('Amplitude');
title('Sampled Real frequency function');grid;
figure;

c=1:500;
II(c)=If(c);
c=501:1000;
II(c)=-If(1001-c);
subplot(2,1,1),plot(f,If);xlabel('freq');ylabel('Amplitude');
title('Imaginary part of H(w) function');grid;
subplot(2,1,2),plot(f,II);xlabel('freq');ylabel('Amplitude');
title('Sampled Imaginary frequency function');grid;
figure;

figure(3);
semilogx(f,20*log10(abs(H)));
grid
xlabel('frequency');ylabel('degree');
```

```
figure(4);
semilogx(f,20*log10(angle(H)));
grid
xlabel('frequency');ylabel('degree');

HH=RR+i*II;
ht=IFFT(HH);
c=1:100;
hht(c)=ht(c);

figure(5);
plot(c,hht);
grid
xlabel('n');ylabel('Amplitude');
print -dmeta;


%*************CVT with ferroresonance cct.*******************
global R1 R2 Rf L1 Lm Lf C1 C2 Cf f w Z1 Za Zb Zc Z2 H Rw Iw
RR II HH ht hht
%************************************************************

%Value of CVT's components simplified circuit
R1=3289;
R2=1.03997e+5; %represent load resistance(Ro)
Rf=77379;
C1=86e-9; %represent the total capacitance(C)
C2=1.06e-9;
Cf=0.285e-9;
L1=76.136; %represent the total inductance(L)
Lm=2.705e+4;
Lf=315.3;

f=1:2:2000;
w=2*pi*f;
Z1 =R1+i*(w*L1-1./(w*C1));
Za=Rf+(i*w*Lf)./(1-w.^2*Lf*Cf);
Zb=(i*w*Lm.*Za)./(i*w*Lm+Za);
Zc=Zb./(1+i*w*C2.*Zb);
Z2=(Zc*R2)./(Zc+R2);
H=Z2./(Z1+Z2);

Rw=real(H);
Iw=imag(H);
```

```
c=1:500;
RR(c)=Rw(c);
c=501:1000;
RR(c)=Rw(1001-c);
subplot(2,1,1),plot(f,Rw);xlabel('freq');ylabel('Amplitude');
title('Real part of H(w) function');grid;
subplot(2,1,2),plot(f,RR);xlabel('freq');ylabel('Amplitude');
title('Sampled Real frequency function');grid;
figure;

c=1:500;
II(c)=Iw(c);
c=501:1000;
II(c)=-Iw(1001-c);
subplot(2,1,1),plot(f,Iw);xlabel('freq');ylabel('Amplitude');
title('Imaginary part of H(w) function');grid;
subplot(2,1,2),plot(f,II);xlabel('freq');ylabel('Amplitude');
title('Sampled Imaginary frequency function');grid;
figure;

figure(3);
semilogx(f,20*log10(abs(H)));
grid
xlabel('frequency');ylabel('db');

HH=RR+i*II;
ht=IFFT(HH);
c=1:100;
hht(c)=ht(c);

figure(4);
plot(c,hht);
grid
xlabel('n');ylabel('Amplitude');
print -dmeta;
```

APPENDIX B

```
%****************CVT without ferroresonance cct.***********
%Value of CVT's components simplified circuit
R1=3289;
R2=1.03997e+5; %represent load resistance(Ro)
C1=86e-9; %represent the total capacitance(C)
C2=1.06e-9;
L1=1.136; %represent the total inductance(L)
Lm=2.705e+4;

f=1:2:2000;
w=2*pi*f;
Z1 =R1+i*(w*L1-1./(w*C1));
Z2=(i*w*Lm)./(1-w.^2*C2*Lm);
H=(Z2*R2)./(Z1.*Z2+Z1.*R2+Z2.*R2);

X=load ('C:\nur\cs.txt');
t=X(:,1);
v=X(:,2);
t1=t*1000;
figure(1);
plot (t1,v,'r--');
xlabel ('time [ms]');ylabel('Voltage [kV]');
hold

ht=IFFT(H);
c=1:100;
hht(c)=ht(c);

figure(2);
plot(c,hht);
grid
xlabel('n');ylabel('Amplitude');
print -dmeta;

N=conv(v,hht);
t2=1:220;
M(t2)=N(t2);
figure (1);
plot (t2,M)
grid
```

```
%**************CVT with ferroresonance cct.****************
%Value of CVT's components simplified circuit
R1=3289;
R2=1.03997e+5; %represent load resistance(Ro)
Rf=77379;
C1=86e-9; %represent the total capacitance(C)
C2=1.06e-9;
Cf=0.285e-9;
L1=1.136; %represent the total inductance(L)
Lm=2.705e+4;
Lf=315.3;

f=1:2:2000;
w=2*pi*f;
Z1 =R1+i*(w*L1-1./(w*C1));
Za=Rf+(i*w*Lf)./(1-w.^2*Lf*Cf);
Zb=(i*w*Lm.*Za)./(i*w*Lm+Za);
Zc=Zb./(1+i*w*C2.*Zb);
Z2=(Zc*R2)./(Zc+R2);
H=Z2./(Z1+Z2);

X=load ('C:\nur\cs7.txt');
t=X(:,1);
v=X(:,2);
t1=t*1000;
v1=v/1000;

figure(1);
figure(1);
plot (t1,v,'r--');
xlabel ('time [ms]');ylabel('Voltage [kV]');
hold

ht=IFFT(H);
c=1:100;
hht(c)=ht(c);

figure(2);
plot(c,hht,'b');
grid
xlabel('time [ms]');ylabel('Amplitude');
print -dmeta;


t2=1:220;
N=conv(v,hht);
M(t2)=N(t2);
```

```
figure (1);
plot (t2,M)
grid
```

Sample of the data from EMTDC.

0	0
1.00E-03	0.195383936
2.00E-03	1.143614152
3.00E-03	3.124877396
4.00E-03	5.933020254
5.00E-03	8.925639182
6.00E-03	11.23603145
7.00E-03	12.04828203
8.00E-03	10.86716971
9.00E-03	7.678384949
1.00E-02	2.970540885
1.10E-02	-2.3947055
1.20E-02	-7.408552483
1.30E-02	-11.1724759
1.40E-02	-13.10677053
1.50E-02	-13.05773398
1.60E-02	-11.28167002
1.70E-02	-8.323793054
1.80E-02	-4.839394436
1.90E-02	-1.415682634
2.00E-02	1.552751719
2.10E-02	3.906303978
2.20E-02	5.679546835
2.30E-02	7.004388282
2.40E-02	7.998314106
2.50E-02	8.680419934
2.60E-02	8.943669003
2.70E-02	8.590644384
2.80E-02	7.417128099
2.90E-02	5.312163943
3.00E-02	2.338458942
3.10E-02	-1.235637731
3.20E-02	-4.96506634
3.30E-02	-8.310954932
3.40E-02	-10.75406465
3.50E-02	-11.90699572
3.60E-02	-11.59489766
3.70E-02	-9.884944136
3.80E-02	-7.060282912
3.90E-02	-3.549707403
4.00E-02	0.164872803
4.10E-02	3.637651987
4.20E-02	6.523668077
4.30E-02	8.607842608
4.40E-02	9.799067223
4.50E-02	10.10015632
4.60E-02	9.569755069
4.70E-02	8.291645346
4.80E-02	6.361190114
4.90E-02	3.890312022
5.00E-02	1.024441826
5.10E-02	-2.040040568
5.20E-02	-5.049772342
5.30E-02	-7.70772616
5.40E-02	-9.707033955
5.50E-02	-10.77919836
5.60E-02	-10.74520907
5.70E-02	-9.556272122
5.80E-02	-7.313060796
5.90E-02	-4.257800919
6.00E-02	-0.740380384
6.10E-02	2.834039927
6.20E-02	6.064482457
6.30E-02	8.608548757
6.40E-02	10.22208434
6.50E-02	10.77904144
6.60E-02	10.27167906
6.70E-02	8.795521963
6.80E-02	6.525774827
6.90E-02	3.691814444
7.00E-02	0.554389791
7.10E-02	-2.612776325
7.20E-02	-5.538009006
7.30E-02	-7.965904153
7.40E-02	-9.673269376
7.50E-02	-10.48778382
7.60E-02	-10.30807274
7.70E-02	-9.121715987
7.80E-02	-7.016510236
7.90E-02	-4.180587433
8.00E-02	-0.888764044
8.10E-02	2.524713209

APPENDIX C

TECHNICAL DATA FOR OMICRON CMC 56 TEST SET

Three-phase portable test set 7VP151 (Omicron CMC 56)

7VP151 test facility specifications

Power supply	Nominal voltage	AC 230 V (optional 115 V), ± 15 %, single phase
	Power consumption	<500 VA
	Frequency	45 to 65 Hz
Outputs	3 Current outputs	
	Power	3 x 23 VA [1]
	Setting range	continuous from 0 to 10.3 A_{rms}
	Resolution	500 µA
	Accuracy	typ. 0.01 % error (guaranteed: <0.1 %)[2]
	Distortion	typ. 0.025 % (guaranteed: <0.07 %)[3]
	3 Voltage outputs	
	Power	3 x 30 VA (optional: 1 x 100 VA, 2 x 10 VA)
	Setting range	continuous from 0 to 125 V_{rms} (optional: 0 to 250 V_{rms})
	Resolution	6 mV (optional: 12 mV)
	Accuracy	typ. 0.025 % error (guaranteed: <0.1 %)[2]
	Distortion	typ. 0.015 % (guaranteed: <0.05 %)[3]
	The following applies for all current and voltage outputs:	
	Frequency range	
	Continuous sine signals	10 to 1000 Hz
	Transient signals	0 to 3.1 kHz
	Frequency resolution	5 µHz
	Frequency accuracy	1 ppm (0 to 50 °C, 1 year)
	Phase angle φ	−360 to +360°
	Phase resolution	0.001°
	Phase error	typ. 0.02° (guaranteed: <0.1°)[2]
	Binary outputs	
	Number	2
	Loadability	AC 250 V/1 A, DC 30 V/1 A
	Activation	via operational software
Inputs	Binary inputs	
	Number	10 (8 accessible via banana sockets)
	Time resolution	100 µs
	Trigger criterion	Switching of a potential-free contact or connection of a DC voltage up to 250 V. Threshold value configurable.
	Analog measurement inputs	
	DC measurement input	
	Measurement range	0 to ±20 mA
	Accuracy	Error typ. 0.01 % (guaranteed: < 0.05 %)[2]
	DC voltage measurement input	
	Measurement range	0 to ±10 V
	Accuracy	Error typ. 0.01 % (guaranteed: < 0.05 %)[2]
Device particulars	Weight	15 kg
	Dimensions W x H x D	450 x 145 x 390 mm (without handle)

1) For higher current or power requirements the addition of a voltage amplifier is possible (e.g. 7VP153).
2) Typical values apply over 24 hours and within 23 °C ± 1 °C at rated output power.
Guaranteed values apply over 1 year and within 23 °C ± 1 °C at rated output power.
3) THD + N: Values at 10 to 70 Hz and 20 kHz bandwidth.

APPENDIX D

POSITIVE AND ZERO SEQUENCE IMPEDANCE CALCULATION.

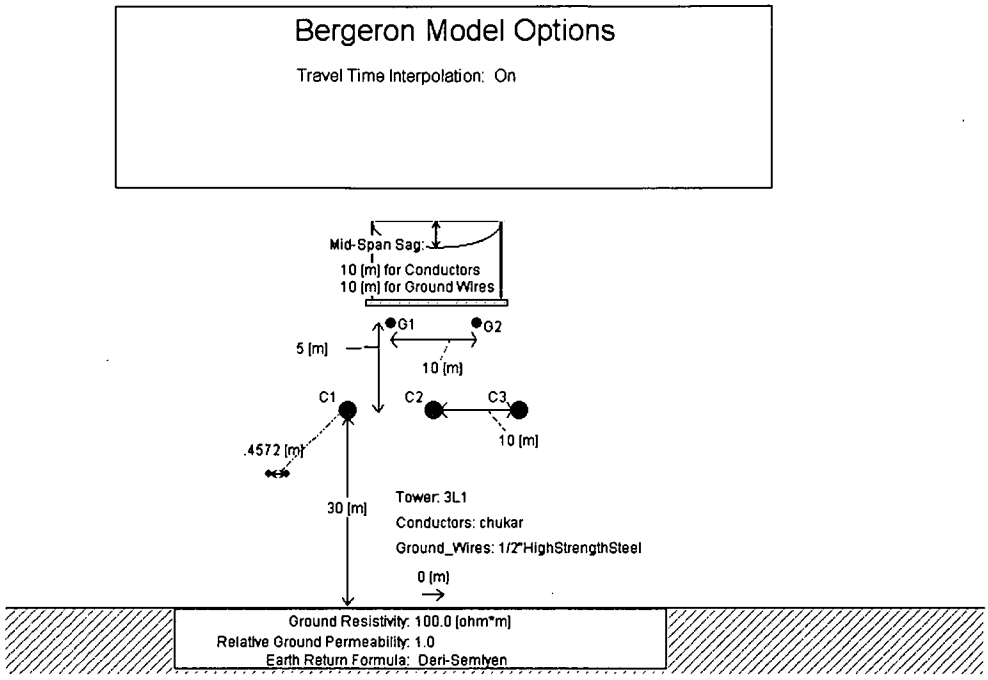

Transmission Line model

From a data file of the transmission line:-

Line length = 20 km

Total Positive Sequence Travel Time = 0.06849768 ms

Positive Sequence Surge Impedance = 390.4566 Ω

Positive Sequence resistance = 0.3506455e-04 Ω/m

Total Zero Sequence Travel Time = 0.09663007 ms

Zero Sequence Surge Impedance = 767.9808 Ω

Zero Sequence resistance = 0.3124661e-03 Ω/m

From the above data the **positive** and **zero** sequence impedances can be calculated as below:

Let τ = Travel time per unit length of line = $1/v = \sqrt{LC}$

Where **v** is the velocity of a wave on the transmission line.

Surge Impedance = $Z = \sqrt{L/C}$

From where it follows that

$L = Z \times \tau$

Hence,

$L_1 = 390.4566 \times 0.06849768e\text{-}03 / 20$

$= 1.337$ mH/km

$X_{L1} = 2 \times \pi \times 50 \times 1.337e\text{-}03$

$= 0.4201\ \Omega$/km

Therefore $Z_1 = R_1 + jX_1$

$= 0.03506455 \times j0.4201$

$= \mathbf{0.4216\angle 85.22^0}$

$L_0 = 767.9808 \times 0.09663007e\text{-}03 / 20$

$= 3.7105$ mH/km

$X_{L0} = 2 \times \pi \times 50 \times 3.7105e\text{-}03$

$= 1.1657\ \Omega$/km

Therefore $Z_0 = R_0 + jX_0$

$= 0.3124661 \times j1.1657$

$= \mathbf{1.2068\angle 75^0}$

APPENDIX E

TECHNICAL DATA FOR OPTIMHO LFZP 111.

Technical Data

Ratings

AC voltage V_n: 100 to 120V rms phase-phase

AC current I_n: 1A or 5A rms per phase

Frequency I_n: 50Hz or 60Hz

Operating frequency range: 47 to 51Hz or 56.4 to 61.2 Hz

DC Supply $V_x(1)$: For switched mode dc/ac/dc power supply unit, available in three versions:

Nominal range	Operative withstand	Maximum
48/54V	37.5 to 60V	64.8V
110/125V	87.5 to 137.5V	150V
220/250V	175 to 275V	300V

There is negligible change of accuracy with change of voltage within the operative range of the relay.

DC supply $V_x(2)$: For optically coupled isolators. Supply options are the same as $V_x(1)$. External resistor box provided for 220/250V version (see Figure 15).

Maximum overload ratings

AC voltage: $1.2V_n$ for measuring accuracy
$1.5V_n$ continuous withstand
$2.5V_n$ withstand for 10s.

AC current: $2.4I_n$ continuous withstand
$100I_n$ withstand for 1s (I_n = 1A)
$80I_n$ withstand for 1s (I_n = 5A)

Burdens

AC voltage circuits: 0.1 VA per phase at Vn

AC current circuits: 0.08 VA per phase (I_n = 1A)
0.5 VA per phase (I_n = 5A)

DC supply (1): 18W under healthy live line conditions at $V_x(1)$ 28W maximum

DC supply (2): 10mA per energised optically coupled isolator at $V_x(2)$.

Distance Elements

Range of positive sequence settings referred to line VT and CT secondaries:

All employed zones except reverse Zone 3:

Overhead line models	0.2	to 250Ω (I_n = 1A)
	0.04	to 50Ω (I_n = 5A)
Underground cable models	0.1	to 125Ω (I_n = 1A)
	0.02	to 25Ω (I_n = 5A)

Reverse Zone3

Overhead line models	0.04	to 250Ω (I_n = 1A)]
	0.008	to 50Ω (I_n = 5A)
Underground cable models and LFZP 151	0.02	to 125Ω (I_n = 1A)
	0.004	to 25Ω (I_n = 5A)

Reach setting method is by digitally controlled analogue attenuators. Attenuation factors KZPh and KZN operate on current signals and are common to all zones.

Attenuation factors KZ1, KZ1X, KZ1Y, KZ2, KZ3 and KZ3' operate on voltage signals and are specific to Zone 1, Zone 1X, Zone 1Y, Zone 2, Zone 3 forward and Zone 3 reverse respectively. The positive sequence reach for Zone 1 is given by:

Zone 1 = KZ1. KZPh.5/In for overhead line models.

Zone 1 = KZ1. KZPh. 5/21n for underground cable models.

Either KZ1 or KZPh is set to 1.000. To obtain the formula for each of the other zones employed, replace KZ1 by the appropriate attenuation factor for the zone.

Extra settings for ground fault distance:

Residual compensation factor:

$$\frac{KZN}{KZPh} = \frac{Z_{L0} \cdot Z_{L1}}{3Z_{L1}}$$

Where Z_{L0} and Z_{L1} are the phasor values of zero and positive sequence impedance of the protected line.

Quadrilateral resistive reach settings:

Right hand reach = $KR.5/I_n$
Left-hand reach = $KR.6/I_n$ (LFZP 111)
Left-hand reach = $KR.5/I_n$ (LFZP 121)

Range of factors:		
	KZPh	0.040 to 1.000 in steps of 0.001
	KZN	0.000 to 1.360 in steps of 0.001
	KZ1 KZ1X KZ1Y KZ2 KZ3	1.00 to 49.98 steps of 0.02
	KZ3'	0.2 to 49.9 in steps of 0.1
	KR	1 to 30 in steps of 1

Range of setting of Zone 3 lenticular aspect ratio:

a/b = 1.00, 0.67 or 0.41

Characteristic angle settings:

θ Ph - arg Z_{L1} to nearest available setting.
θ Ph = 50° to 85° in 5° steps (overhead line models)
θ Ph = 45° to 80° in 5° steps (LFZP 113 only)
θ Ph = 20°, 25°, 30°, 35°, 40°, 50°, 60° or 70° (LFZP 123 only)

Vectorial residual compensation for ground fault distance:

θ N = arg $(Z_{L0} - Z_{L1})$ to nearest available setting
θ N = 50° to 85° in 5° steps (overhead line models)
θ N = -45°, -35° and -25° to 80° in 5° steps (LFZP 113 and 123 only)

Note: LFZP 113 is not designed to be used with a ground fault loop setting $(2Z_{L1} + Z_{L0})/3$ with an argument less than 30°.

15

Minimum operating values of the distance measuring elements for all types of fault:

Voltage: zero

Current: $0.05I_n/KZ\Phi$.

Accuracy: Reach: ±5% at $2I_n$ and 20°C

Dynamic range: up to $25I_n$ for fault locator and instrumentation up to $56I_n$ for distance protection

Characteristic angle: ±2°

Resetting ratio: 105%

Timer ranges: Zone 1X timer, Zone 1Y timer, Zone 2 timer, Zone 3 timer — each timer 0.10s to 9.98s in steps of 0.02s

Scheme co-ordination timers used in permissive overreach, unblocking and blocking schemes:

TP

TD — 0 to 98ms in steps of 2ms

TDW

Timer accuracy: ±1% of setting and ±3ms.

Operating time: Typical relay operating times for Zone 1 are shown in Figures 9 to 12.

Mho characteristic (type m, f or c) — 50Hz minimum: 14ms, typical: 18ms; 60Hz minimum: 12ms, typical: 16ms

Quadrilateral characteristic (type q) — 50Hz minimum: 16ms, typical: 23ms; 60Hz minimum: 15ms, typical: 20ms

Reset time: The trip contacts are sealed in for 60ms following the initial contact closure. Thereafter, the maximum reset time is 35ms.

Power swing blocking

Power swing detected by transit time of impedance between Zone 6 and either Zone 2 or Zone 3 as selected. Zone 6 is offset mho or offset lenticular, with the same range of forward and reverse reach settings and aspect ratios as Zone 3.

Zone 6 timer range: 20ms to 90ms in steps of 5ms

Power swing detection regimes:

(i) detection disabled.

(ii) detection indicated only.

(iii) indication plus blocking of any one or more selected zones.

Blocking disabled if a ground fault or (if DEF fitted) a phase fault occurs during a power swing.

APPENDIX F

RESULTS.

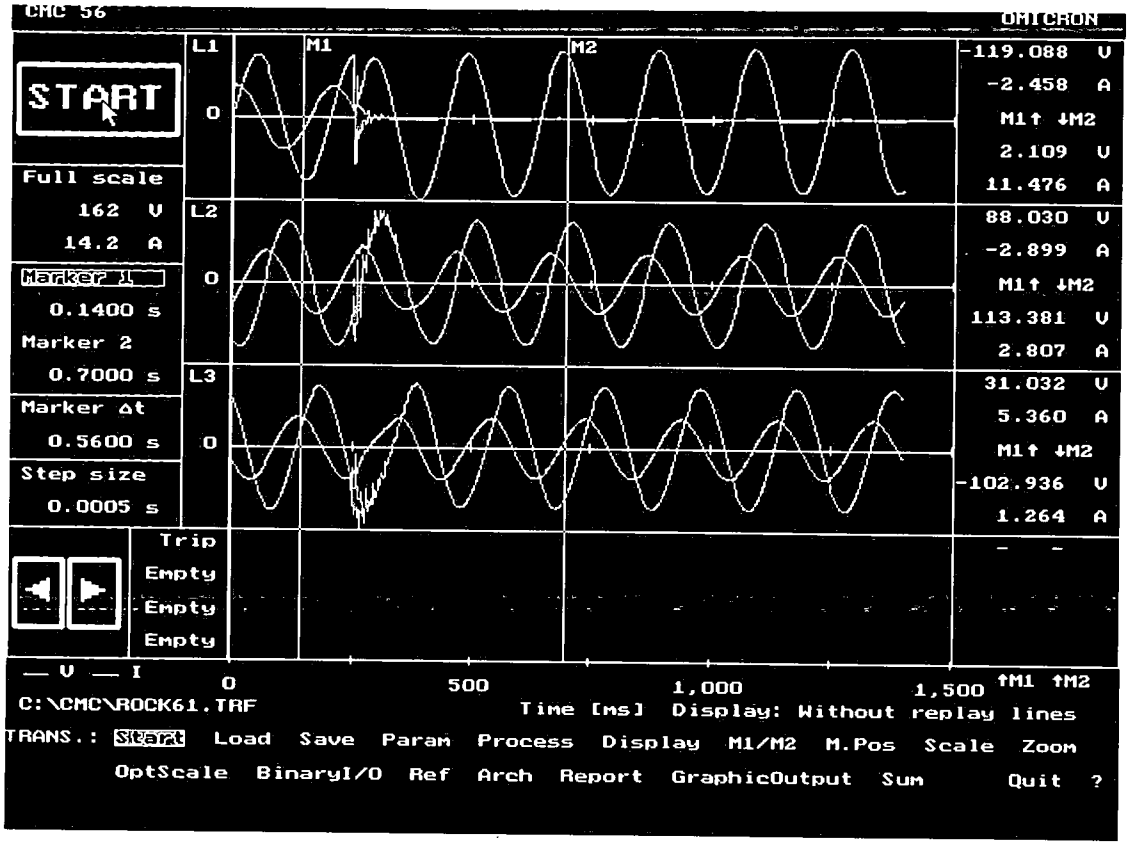

Sample of voltage response has been downloading from EMTDC model. It is single phase to ground fault with point of view at voltage maximum.

OMICRON electronics CMC 56 BK22
6C
UMIST

Test object: OPTIMHO LFZP 111
B26/FERRANTI BLDG
Location : 10 km (with CVT)
Date : 2001-09-11 08:46:24
Test person: Nursyarizal Mohd Nor
Comment : Phase to ground fault

Table of switching times of binary inputs:

Trip

State	Time	Difference
0->1	0.3570 s	
1->0	0.4210 s	0.0640 s

OMICRON electronics CMC 56 BK22
6C
UMIST

Test object: OPTIMHO LFZP 111
B26/FERRANTI BLDG
Location : 20 km (with CVT)
Date : 2001-09-11 08:48:41
Test person: Nursyarizal Mohd Nor
Comment : Phase to ground fault

Table of switching times of binary inputs:

Trip

State	Time	Difference
0->1	0.3550 s	
1->0	0.4010 s	0.0460 s

OMICRON electronics CMC 56 BK22
6C
UMIST

Test object: OPTIMHO LFZP 111
B26/FERRANTI BLDG
Location : 30 km (with CVT)
Date : 2001-09-11 08:50:45
Test person: Nursyarizal Mohd Nor
Comment : Phase to ground fault

Table of switching times of binary inputs:

Trip

State	Time	Difference
0->1	0.3570 s	
1->0	0.4010 s	0.0440 s

OMICRON electronics CMC 56 BK22
6C
UMIST

Test object: OPTIMHO LFZP 111
B26/FERRANTI BLDG
Location : 40 km (with CVT)
Date : 2001-09-11 08:54:12
Test person: Nursyarizal Mohd Nor
Comment : Phase to ground fault

Table of switching times of binary inputs:

Trip

State	Time	Difference
0->1	0.3670 s	
1->0	0.4010 s	0.0340 s

OMICRON electronics CMC 56 BK22
6C
UMIST

Test object: OPTIMHO LFZP 111
B26/FERRANTI BLDG
Location : 50 km (with CVT)
Date : 2001-09-11 09:01:10
Test person: Nursyarizal Mohd Nor
Comment : Phase to ground fault

Table of switching times of binary inputs:

Trip

State	Time	Difference
0->1	0.3670 s	
1->0	0.4010 s	0.0340 s

OMICRON electronics CMC 56 BK22
6C
UMIST

Test object: OPTIMHO LFZP 111
B26/FERRANTI BLDG
Location : 60 km (with CVT)
Date : 2001-09-11 09:06:32
Test person: Nursyarizal Mohd Nor
Comment : Phase to ground fault

Table of switching times of binary inputs:

Trip

State	Time	Difference
0->1	0.3680 s	
1->0	0.4010 s	0.0330 s

OMICRON electronics CMC 56 BK22
6C
UMIST

Test object: OPTIMHO LFZP 111
B26/FERRANTI BLDG
Location : 70 km (with CVT)
Date : 2001-09-11 09:11:38
Test person: Nursyarizal Mohd Nor
Comment : Phase to ground fault

Table of switching times of binary inputs:

Trip

State	Time	Difference
0->1	0.3680 s	
1->0	0.4010 s	0.0330 s

OMICRON electronics CMC 56 BK22
6C
UMIST

Test object: OPTIMHO LFZP 111
B26/FERRANTI BLDG
Location : 80 km (with CVT)
Date : 2001-09-11 09:16:12
Test person: Nursyarizal Mohd Nor
Comment : Phase to ground fault

Table of switching times of binary inputs:

Trip

State	Time	Difference
0->1	0.3610 s	
1->0	0.4090 s	0.0480 s

OMICRON electronics CMC 56 BK22
6C
UMIST

Test object: OPTIMHO LFZP 111
B26/FERRANTI BLDG
Location : 100 km (with CVT)
Date : 2001-09-11 09:20:02
Test person: Nursyarizal Mohd Nor
Comment : Phase to ground fault

Table of switching times of binary inputs:

Trip

State	Time	Difference
0->1	0.3610 s	
1->0	0.4090 s	0.0480 s

OMICRON electronics CMC 56 BK22
6C
UMIST

Test object: OPTIMHO LFZP 111
B26/FERRANTI BLDG
Location : 120 km (with CVT)
Date : 2001-09-11 09:24:52
Test person: Nursyarizal Mohd Nor
Comment : Phase to ground fault

Table of switching times of binary inputs:

Trip

State	Time	Difference
0->1	0.9110 s	
1->0	1.3610 s	0.4500 s

OMICRON electronics CMC 56 BK22
6C
UMIST

Test object: OPTIMHO LFZP 111
B26/FERRANTI BLDG
Location : 150 km (with CVT)
Date : 2001-09-11 09:30:30
Test person: Nursyarizal Mohd Nor
Comment : Phase to ground fault

Table of switching times of binary inputs:

Trip

State	Time	Difference
0->1	0.9110 s	
1->0	1.3610 s	0.4500 s

OMICRON electronics CMC 56 BK22
6C
UMIST

Test object: OPTIMHO LFZP 111
B26/FERRANTI BLDG
Location : 160 km (with CVT)
Date : 2001-09-11 09:33:29
Test person: Nursyarizal Mohd Nor
Comment : Phase to ground fault

Table of switching times of binary inputs:

Trip

State	Time	Difference
0->1	0.9350 s	
1->0	1.3710 s	0.4360 s

OMICRON electronics CMC 56 BK22
6C
UMIST

Test object: OPTIMHO LFZP 111
B26/FERRANTI BLDG
Location : 180 km (with CVT)
Date : 2001-09-11 09:38:09
Test person: Nursyarizal Mohd Nor
Comment : Phase to ground fault

Table of switching times of binary inputs:

Trip

State	Time	Difference
0->1	1.0250 s	
1->0	1.8260 s	0.8010 s

OMICRON electronics CMC 56 BK22
6C
UMIST

Test object: OPTIMHO LFZP 111
B26/FERRANTI BLDG
Location : 200 km (with CVT)
Date : 2001-09-11 09:44:13
Test person: Nursyarizal Mohd Nor
Comment : Phase to ground fault

Table of switching times of binary inputs:

Trip

State	Time	Difference
0->1	1.0170 s	
1->0	1.7540 s	0.7370 s

OMICRON electronics CMC 56 BK22
6C
UMIST

Test object: OPTIMHO LFZP 111
B26/FERRANTI BLDG
Location : 10 km (without CVT)
Date : 2001-09-11 10:20:33
Test person: Nursyarizal Mohd Nor
Comment : Phase to ground fault

Table of switching times of binary inputs:

Trip

State	Time	Difference
0->1	0.3310 s	
1->0	0.3660 s	0.0350 s

OMICRON electronics CMC 56 BK22
6C
UMIST

Test object: OPTIMHO LFZP 111
B26/FERRANTI BLDG
Location : 20 km (without CVT)
Date : 2001-09-11 10:25:07
Test person: Nursyarizal Mohd Nor
Comment : Phase to ground fault

Table of switching times of binary inputs:

Trip

State	Time	Difference
0->1	0.3610 s	
1->0	0.3950 s	0.0340 s

OMICRON electronics CMC 56 BK22
6C
UMIST

Test object: OPTIMHO LFZP 111
B26/FERRANTI BLDG
Location : 30 km (without CVT)
Date : 2001-09-11 10:31:10
Test person: Nursyarizal Mohd Nor
Comment : Phase to ground fault

Table of switching times of binary inputs:

Trip

State	Time	Difference
0->1	0.3580 s	
1->0	0.3980 s	0.0400 s

OMICRON electronics CMC 56 BK22
6C
UMIST

Test object: OPTIMHO LFZP 111
B26/FERRANTI BLDG
Location : 40 km (without CVT)
Date : 2001-09-11 10:43:03
Test person: Nursyarizal Mohd Nor
Comment : Phase to ground fault

Table of switching times of binary inputs:

Trip

State	Time	Difference
0->1	0.3710 s	
1->0	0.4070 s	0.0360 s

OMICRON electronics CMC 56 BK22
6C
UMIST

Test object: OPTIMHO LFZP 111
B26/FERRANTI BLDG
Location : 50 km (without CVT)
Date : 2001-09-11 10:51:15
Test person: Nursyarizal Mohd Nor
Comment : Phase to ground fault

Table of switching times of binary inputs:

Trip

State	Time	Difference
0->1	0.3710 s	
1->0	0.4070 s	0.0360 s

OMICRON electronics CMC 56 BK22
6C
UMIST

Test object: OPTIMHO LFZP 111
B26/FERRANTI BLDG
Location : 60 km (without CVT)
Date : 2001-09-11 10:59:56
Test person: Nursyarizal Mohd Nor
Comment : Phase to ground fault

Table of switching times of binary inputs:

Trip

State	Time	Difference
0->1	0.3710 s	
1->0	0.4070 s	0.0360 s

OMICRON electronics CMC 56 BK22
6C
UMIST

Test object: OPTIMHO LFZP 111
B26/FERRANTI BLDG
Location : 70 km (without CVT)
Date : 2001-09-11 11:07:14
Test person: Nursyarizal Mohd Nor
Comment : Phase to ground fault

Table of switching times of binary inputs:

Trip

State	Time	Difference
0->1	0.3710 s	
1->0	0.4080 s	0.0370 s

OMICRON electronics CMC 56 BK22
6C
UMIST

Test object: OPTIMHO LFZP 111
B26/FERRANTI BLDG
Location : 80 km (without CVT)
Date : 2001-09-11 11:14:43
Test person: Nursyarizal Mohd Nor
Comment : Phase to ground fault

Table of switching times of binary inputs:

Trip

State	Time	Difference
0->1	0.3710 s	
1->0	0.4090 s	0.0380 s

OMICRON electronics CMC 56 BK22
6C
UMIST

Test object: OPTIMHO LFZP 111
B26/FERRANTI BLDG
Location : 100 km (without CVT)
Date : 2001-09-11 11:22:39
Test person: Nursyarizal Mohd Nor
Comment : Phase to ground fault

Table of switching times of binary inputs:

Trip

State	Time	Difference
0->1	0.3640 s	
1->0	0.3970 s	0.0330 s

OMICRON electronics CMC 56 BK22
6C
UMIST

Test object: OPTIMHO LFZP 111
B26/FERRANTI BLDG
Location : 120 km (without CVT)
Date : 2001-09-11 11:30:30
Test person: Nursyarizal Mohd Nor
Comment : Phase to ground fault

Table of switching times of binary inputs:

Trip

State	Time	Difference
0->1	0.9320 s	
1->0	1.3520 s	0.4200 s

OMICRON electronics CMC 56 BK22
6C
UMIST

Test object: OPTIMHO LFZP 111
B26/FERRANTI BLDG
Location : 160 km (without CVT)
Date : 2001-09-11 11:48:55
Test person: Nursyarizal Mohd Nor
Comment : Phase to ground fault

Table of switching times of binary inputs:

Trip

State	Time	Difference
0->1	0.9300 s	
1->0	1.3420 s	0.4120 s

OMICRON electronics CMC 56 BK22
6C
UMIST

Test object: OPTIMHO LFZP 111
B26/FERRANTI BLDG
Location : 200 km (without CVT)
Date : 2001-09-11 12:04:27
Test person: Nursyarizal Mohd Nor
Comment : Phase to ground fault

Table of switching times of binary inputs:

Trip

State	Time	Difference
0->1	1.0210 s	
1->0	1.7770 s	0.7560 s